PHYSICAL PROPERTIES OF THE NATURAL SATELLITES*

DAVID MORRISON and DALE P. CRUIKSHANK
Institute for Astronomy, University of Hawaii, Honolulu, HI 96822, U.S.A.

(Received 18 November, 1973)

Abstract. This paper reviews the physical nature of the satellites of the planets, excluding the Moon but including the rings of Saturn. Emphasis is placed on the best studied objects: Titan, Phobos and Deimos, the four Galilean satellites (Io, Europa, Ganymede, and Callisto), and the rings of Saturn.

1. Introduction

There are 32 known natural satellites accompanying 6 of the major planets. At least three important groups are evident: 7 objects only slightly smaller and less dense than the terrestrial planets, 8 comparable in size to the largest asteroids but probably of lower density, and 17 small, irregular satellites, some of which may be captured asteroids. Like the asteroids, at least some of these bodies probably preserve some of the most primitive and unaltered material in the solar system. The composition and physical properties of the satellites and asteroids are essential clues to an understanding of the chemical origin and development of the solar system.

Except for determinations of mass, measurements of radius, a spectroscopic survey, and relatively routine photometry, the natural satellites were largely neglected until the late 1960's. The modern surge of interest in these objects stems from: (1) the development of new observational and theoretical approaches; (2) the remarkable explosion of interest in, and knowledge of, the Moon; and (3) a recent extension of interest from the terrestrial to the outer planets, which have more satellites. To these we may add the prospect of flyby reconnaissance of several satellites in the next decade. It is therefore appropriate at this time to review our knowledge of the physical properties of the natural satellites.

No comprehensive review of the physical properties of the satellites exists, although several authors have recently reviewed particular aspects of satellite studies, as in a number of papers in *Surfaces and Interiors of Planets and Satellites* (1970) and in the special issue of *Space Science Reviews* (March/May 1973) entitled *Outer Solar System Exploration – An Overview*. The satellites of the major planets were also discussed briefly by Newburn and Gulkis (1973) as part of their survey of the outer planets. Most of the material used in the present paper, however, is derived from individual research papers, the majority of which have been published within the past three years, and while we include some historical material, our emphasis is upon the most

* The authors dedicate this paper to the memory of Gerard P. Kuiper, who died on 24 December 1973. It was his pioneering research begun in the early 1940's that opened the era of physical studies of the satellites. That work, together with his lifelong study of the origin of the system of planets and satellites, provided the foundation upon which much of the work reviewed in this paper is based.

Space Science Reviews **15** (1974) 641–739.

recent work. The literature survey for this review was completed in November 1973.*

In the paper we discuss all of the known satellites except the Moon. Several review articles would be required to treat adequately the Earth's satellite, and reference is made to it here only as an object of comparison. Emphasis is placed on the best studied satellites: Titan, Phobos and Deimos, and the 4 Galilean satellites of Jupiter. We also include a brief review of current work on the rings of Saturn. In the following sections we review first the nature of the satellite systems, the basic data of size, mass, and density, and models for composition and structure. We then examine in turn the satellites of Mars, the Galilean satellites, Titan, the other satellites of Saturn, the rings of Saturn, and the remaining objects, with emphasis on studies of their surfaces by imaging, photometry, spectrophotometry, polarimetry, and radiometry.

2. The Nature of Satellite Systems

2.1. Introduction

On the basis of their orbits, the satellites are conveniently separated into two classes. The 19 *regular* satellites move prograde in nearly circular orbits in the equatorial plane of the parent body. The 12 *irregular* satellites move either prograde (6) or retrograde (6) in orbits that may be eccentric and inclined to the equatorial plane at a considerable angle. Our own satellite is sometimes also included among the irregular satellites because of its anomalously large mass ratio to the Earth.

Satellites can exist only within a certain range of distance from their primaries. The inner limit, usually called the Roche limit, is determined by tidal forces. The outer limit has been defined by Kuiper (1951, 1961) in terms of a radius of action around a planet. If $\mu \equiv M_p/(M_\odot + M_p)$, the radius of action R_A is given by

$$\log R_A/a = 0.318 \log \mu - 0.327, \tag{1}$$

where a is the distance of the planet from the Sun in astronomical units. The practical limit for satellites in near-circular orbits is 0.5 R_A, while some irregular retrograde satellites of Jupiter slightly exceed this value. Table I lists the values of R_A and of the Roche limit for the planets.

Within the range of distances from the Roche limit to R_A, many searches for satellites have been carried out, and the list of discoveries continues to grow. The most extensive recent search for satellites both interior and exterior to the known systems was made by Kuiper (1961), who also reviewed earlier surveys. Since that time, additional unsuccessful searches have been made for new satellites of Uranus by Sinton (1972) and of Mars by Pollack *et al.* (1972), and one additional satellite of Saturn

* The 195 references cited in the bibliography clearly show the rapid increase in publications in the field of satellite studies in the past three years: 39% are dated 1973 or 74; 16% are 1972; 14% are 1971, and all previous years contribute only 31%. Of these references, 84% are journal publications, with two journals clearly dominating: *Icarus*, with 37% of the journal citations, and *The Astrophysical Journal* with 16%. Finally, we note that we obtained 35% of these papers in preprint form before they appeared in print.

TABLE I

Inner and outer radii of field in which satellites can occur[a]

Planet	Inner radius (AU)	Outer radius (AU)
Mercury	0.000057	0.00063
Venus	0.00014	0.0028
Earth	0.00015	0.0041
Mars	0.000072	0.0031
Jupiter	0.0010	0.134
Saturn	0.00069	0.167
Uranus	0.00037	0.185
Neptune	0.00039	0.307
Pluto	0.00014	0.162

[a] The inner radius is calculated from the Roche condition and is the minimum distance at which a satellite of density 1.0 g cm^{-3}, having no tensile strength, can hold itself together by mutual attraction. The outer radius is one-half the radius of action (Kuiper, 1961) for the stability of satellite orbits. For large orbits (i.e., the outer satellites of Jupiter), retrograde motion is more stable than prograde, so satellites in retrograde eccentric orbits can exist a bit beyond the maximum given in this table.

has been found by Dollfus (1967). The known satellites with some details of their discoveries are listed in Table II.

We now consider briefly the geometrical aspects of each of the satellite systems following the excellent treatment by Porter (1960), who gives extensive references on the mechanisms of the satellite motions.

2.2. Mars

Asaph Hall began his search for a satellite of Mars in August 1877 and described his discovery of Phobos and Deimos the next year. The motion of both satellites is prograde, but the period of Phobos is less than the rotation period of Mars. The orbital parameters are given in Table III together with those of the other satellites. Kuiper (1961) used special photographic techniques to search for fainter satellites in 1954 and 1956, setting an upper limit for the diameter of any object outside the orbit of Phobos of about 1.5 km for an assumed albedo of 0.05. An additional search for new satellites, primarily near the orbit of Phobos, was made by Pollack *et al.* (1973a) on 19 pre-insertion television images from Mariner 9. The upper limit in diameter for satellites of albedo 0.05 ranges from 1.6 to 0.25 km for the first to last picture, respectively, although only a fraction of the possible space-time domain of an unknown satellite was surveyed, particularly near the lower limit of size.

2.3. Jupiter

The extensive system of Jupiter has been a profitable hunting ground for 5 satellite searchers, including Galileo and Nicholson, who each discovered 4. The innermost

TABLE II

Satellite discoveries[a]

Year	Satellite		Discoverer	Country	Mean opposition visual magnitude
1610	J1	Io	Galileo	Italy	5.0
1610	J2	Europa	Galileo	Italy	5.3
1610	J3	Ganymede	Galileo	Italy	4.6
1610	J4	Callisto	Galileo	Italy	5.6
1655	S6	Titan	Huygens	Holland	8.4
1671	S8	Iapetus	Cassini	France	10.2–11.9
1672	S5	Rhea	Cassini	France	9.7
1684	S3	Tethys	Cassini	France	10.3
1684	S4	Dione	Cassini	France	10.4
1787	U3	Titania	Herschel	England	14.0
1787	U4	Oberon	Herschel	England	14.2
1789	S1	Mimas	Herschel	England	12.1
1789	S2	Enceladus	Herschel	England	11.8
1846	N1	Triton	Lassell	England	13.6
1848	S7	Hyperion	Bond/Lassell	U.S./England	14.2
1851	U1	Ariel	Lassell	England	14.4
1851	U2	Umbriel	Lassell	England	15.3
1877	M1	Phobos	Hall	U.S.	11.6
1877	M2	Deimos	Hall	U.S.	12.7
1892	J5	Amalthea	Barnard	U.S.	13
1898	S9	Phoebe	Pickering	U.S. (Peru)	16.5
1904/5	J6		Perrine	U.S.	14.7
1904/5	J7		Perrine	U.S.	16.0
1908	J8		Melotte	England	18.8
1914	J9		Nicholson	U.S.	18.3
1938	J10		Nicholson	U.S.	18.6
1938	J11		Nicholson	U.S.	18.1
1948	U5	Miranda	Kuiper	U.S.	16.5
1949	N2	Nereid	Kuiper	U.S.	18.7
1951	J12		Nicholson	U.S.	18.8
1966	S10	Janus	Dollfus	France	14

[a] After Porter (1960), with revision and additions.

five satellites move prograde in nearly circular orbits. The four Galilean satellites are Moon-size objects whose masses are sufficient to induce substantial mutual perturbations in the orbital motions. These satellites have received more attention than any others (except our Moon) since their discovery in 1610, and a substantial fraction of this review paper will be devoted to their physical characteristics. The Galilean satellites are known by their numerical designations and by names from mythology: J1, Io; J2, Europa; J3, Ganymede; J4, Callisto.

The innermost satellite, J5 (sometimes known as Amalthea), is very close to the oblate planet, and as a result the line of nodes regresses rapidly. The seven outer satellites of Jupiter, known only by their numerical designations, are all irregular but fall into two distinct groups in terms of distance from the primary. The members

TABLE III

Orbital data for the satellites[a]

Planet	Satellite	Orbit radius (10^3 km)	Period (days)	Eccentricity	Inclination to planet's equator (°)
Earth	Moon	384.4	27.3217	0.05490	5.1453
Mars	1 Phobos	9.37	0.3189	0.0210	1.1
	2 Deimos	23.52	1.262	0.0028	0.9–2.7
Jupiter	5 Amalthea	181.3	0.489	0.003	0.4
	1 Io	421.6	1.769	0	0.0
	2 Europa	670.9	3.551	0	0.0
	3 Ganymede	1070	7.155	0	0.0
	4 Callisto	1880	16.689	0	0.0
	6	11470	250.6	0.158	27.6
	10	11710	260	0.130	29.0
	7	11740	260.1	0.207	24.8
	12	20700	617	0.17	147
	11	22350	692	0.21	164
	8	23300	735	0.38	145
	9	23700	758	0.28	153
Saturn	10 Janus	159.5	0.74896	0	0
	1 Mimas	186	0.942	0.0201	1.5
	2 Enceladus	238	1.370	0.0044	0.0
	3 Tethys	295	1.888	0.0000	1.1
	4 Dione	377	2.737	0.0022	0.0
	5 Rhea	527	4.518	0.0010	0.4
	6 Titan	1222	15.95	0.0289	0.3
	7 Hyperion	1481	21.28	0.1042	0.4
	8 Iapetus	3560	79.33	0.0283	14.7
	9 Phoebe	12930	550.4	0.1633	150
Uranus	5 Miranda	130	1.4135	0.017	3.4
	1 Ariel	192	2.520	0.0028	0
	2 Umbriel	267	4.144	0.0035	0
	3 Titania	438	8.706	0.0024	0
	4 Oberon	586	13.46	0.0007	0
Neptune	1 Triton	354	5.877	0.00	160.0
	2 Nereid	5570	359.4	0.76	27.5

[a] The orbital data are taken from Gondolatsch (1965), except for Janus (Dollfus, 1967) and Miranda (Whitaker and Greenberg, 1973). The orbital eccentricities for the Galilean satellites of Jupiter are small and variable.

of the inner group, consisting of J6, J7, and J10, have prograde motions, while J8, J9, J11, and J12, comprising the outer group, all have retrograde motion. The grouping by distance has led to the suggestion that these satellites were captured (cf. Kuiper, 1956). Bailey (1971) has shown that Jupiter can capture satellites through the inner Lagrangian point when at perihelion and at aphelion, the former case resulting in prograde orbits of radius comparable to that of the inner group, and the latter case yielding retrograde orbits of radius similar to that of the outer group.

2.4. Saturn

The satellite system of Saturn also consists of a regular and an irregular group, of which the seven inner satellites comprise the former. Their nearly circular orbits lie close to the ring plane, and the attractions of the satellite masses appear to affect the ring particles dynamically, causing the well-known gap and regions of low particle density. All of the satellites of Saturn have names, and Janus, the innermost, is the most recently discovered satellite in the solar system (Dollfus, 1967). Titan, the largest of all and the outermost of the regular group, has an atmosphere and has in recent years received great attention as a possible object for study by automated space probes.

The irregular group, consisting of three satellites, is quite mixed. Hyperion has very close orbital commensurabilities with Titan, resulting, in part, in a variable orbital inclination. Iapetus has a large and nearly circular orbit of high inclination. This satellite is apparently the second largest of the Saturn system and has peculiar photometric properties which we consider in some detail below. The outermost, Phoebe, moves retrograde in a very large circular orbit, also at high inclination.

2.5. Uranus and Neptune

Moving retrograde in circular orbits in the equatorial plane of their retrograde rotating primary, the companions of Uranus, with the exception of Miranda, form the most regular satellite system in the solar system. By comparison, the two satellites of Neptune are irregular. Triton, the largest, has a highly inclined circular retrograde orbit, while Nereid moves prograde in the most eccentric orbit of any satellite in the solar system. Sinton (1972) has searched for satellites of Uranus interior to Miranda and down to the Roche limit by taking photographs through a filter centered on the strong methane absorption band at 0.89 μm, thereby greatly reducing the glare from the planet, but he found no satellites brighter than mag. 17. The same technique can be applied to Neptune, because the planet's atmosphere has similar strong methane absorptions.

3. Radii, Masses and Densities

3.1. Introduction

One of the most fundamental bulk properties of a satellite is its mean density, which can be calculated only when the radius and mass are known. Masses have been measured for ten of the regular satellites from their mutual perturbations; these will be discussed later in this chapter, and all of the data on radii, masses and densities are summarized in Table V. First, however, we address the problem of determining satellite radii. Since only the Galilean satellites and Titan are large and near enough to present measurable disks, a number of indirect techniques have been applied recently to obtain radii.

3.2. CLASSICAL MEASUREMENTS OF RADII

The direct measurements of the disks of the larger satellites have been reviewed by Dollfus (1970); this discussion is derived largely from his comprehensive work. Three instruments have been used to determine the angular diameters: (1) the filar micrometer, used in the second half of the 19th century with telescopes up to 100-cm aperture; (2) the double-image micrometer, used by Dollfus and his collaborators, largely at the Pic-du-Midi 60-cm refractor; and (3) the diskmeter, developed by Camichel and used by him at the same 60-cm telescope and subsequently by Kuiper at the Hale 5-m telescope. Each of these instruments is capable, with care, of yielding diameters reproducible to within between 0.05 and 0.10″. Systematic errors of at least 0.1″ are possible, however, and these errors can be expected to depend on the size of the satellite, the size of the telescope, and the seeing, as well as on the limb darkening of the satellite and the personal equation of the observer. At best the visual techniques cannot be relied upon to yield radii of even the largest satellites with a precision greater than $\pm 10\%$.

A fourth classical technique is optical interferometry, employed by Michelson, Hamy, and Danjon to measure the diameters of the Galilean satellites but not of Titan (Dollfus, 1970). In the absence of limb darkening, the diameters measured in this way should be accurate to about $\pm 0.10''$. A more recent interferometric approach proposed by KenKnight (1972), could, in principle, yield diffraction-limited measurements of the sizes of small objects, but it has not yet been demonstrated in practice.

Table IV, adapted from Dollfus (1970), summarizes the radii of the five large satellites as determined by each of these methods. Systematic differences are apparent.

TABLE IV

Visually measured radii (in km) of the Galilean satellites and Titan (from Dollfus, 1970)

Method	Io	Europa	Ganymede	Callisto	Titan
Filar micrometer	1890	1660	2720	2520	2440
Interferometer	1780	1590	2380	2270	–
Diskmeter	1650	1420	2460	2290	2430
Double-image micrometer	1760	1550	2780	2500	2430
Accepted values	1820		2635		

Dollfus concludes that the most reliable of these radii are those obtained with the double-image micrometer, and he estimates that the uncertainties for the Galilean satellites are ± 75 km, or about 5%. For the two satellites with accurately measured radii (discussed in the following section), however, we note that the old filar micrometer measurements have proved slightly better than the values preferred by Dollfus.

3.3. Occultation radii of Io and Ganymede

A powerful method of measuring satellite diameters is to time the passage of the satellite in front of a bright star. Suitable events are rare (O'Leary, 1972), and only recently have satellite ephemerides been determined with sufficient precision to permit a stellar occultation to be predicted. For the Galilean satellites, the band from which a given occultation can be seen is only a few thousand kilometers wide, and in order to determine the radius the occultation must be observed photometrically from at least two stations. The effort is worthwhile, however, because occultations provide the only ground-based technique by which to measure radii accurate to within a few kilometers.

On 14 May 1971 Io occulted the 5th-magnitude star β Scorpii C. Photoelectric observations from four observing parties give a radius, on the assumption that Io is spherical, of 1830 ± 2 km (Taylor, 1972). If the satellite has the figure expected for a fluid in hydrostatic equilibrium, the mean radius is 1818 ± 5 km (O'Leary and van Flandern, 1972). For this review, we adopt a radius for this satellite of 1820 km. On 6 June 1972, Ganymede occulted the 8th-magnitude star SAO 186800; the analysis by Carlson *et al.* (1973) yields a radius of 2635 ($+15$, -100) km, which we adopt for this review.

The occultation radius of Io is 4% larger than the value preferred by Dollfus (1970), and that of Ganymede is 5% smaller. A comparison with the radii in Table IV suggests that there is no major systematic error in the classical determinations by filar micrometer or double image micrometer, but that the radii obtained with the interferometer and diskmeter are systematically low. It should be noted, however, that this confirmation of the visual radii for two Galilean satellites may not apply to Titan, which may suffer greater limb darkening with unknown effects on the derived radius. A number of authors have used radii near 2500 km for Titan in recent publications, and for this review we adopt this value as the best now available. The uncertainty in this radius is about $\pm 10\%$.

3.4. Radii of Phobos and Deimos

The satellites of Mars are far too small to be resolved from Earth, but as a result of close-range imagery by the Mariner spacecraft (Pollack *et al.*, 1972, 1973a) they are among the most thoroughly studied of the satellites. The best Mariner 9 pictures resolve features only 1% the linear size of the satellites. Because of their very irregular shapes (discussed further in Section 5), it is meaningful to speak of their radii only in the sense of the radius of a sphere whose projected area equals the average projected area of the satellite. Using this definition, Pollack *et al.* (1972) obtain radii of 5.7 ± 0.5 km for Deimos and 10.9 ± 1.5 km for Phobos. Combining these radii with the photometry of Kuiper (Harris, 1961), Pollack *et al.* arrive at geometric visual albedos of about 0.05 for these two satellites. Similar results were obtained for Phobos by Smith (1970), based on a Mariner 6 photo that shows the satellite in projection on the disk of Mars.

3.5. Radii based on estimates of albedo

The visual magnitude of a satellite is given in terms of $V_\odot$, the magnitude of the Sun, and p_V, the geometric visual albedo, by:

$$V = V_\odot - 2.5 \log p_V - 5 \log r + 5 \log(R \cdot \Delta), \tag{2}$$

where r is the satellite radius and R and Δ are the distances from the satellite to the Sun (in AU) and to Earth (in the same units as r), respectively, and $V_\odot = -26.8$ (Harris, 1961; Johnson, 1965). If V is measured and p_V can be estimated, it is possible to derive a photometric radius, r. This method has at various times been applied to all of the satellites with essentially arbitrary choice of albedo; its real usefulness, however, is felt in cases where p_V can be estimated with some reliability.

Perhaps the simplest way to estimate the albedo is from visual or photometric measurements of contrast as the satellite transits the planet. Of course, such estimates can be made only if the disk is nearly resolved. Transit observations of the Galilean satellites yield less precise radii than do other visual methods. Dollfus (1970) has used this technique, however, to estimate an albedo of 0.50 ± 0.05 for Tethys from the transit of 12 June 1966. The corresponding radius is 675 ± 30 km; however, Morrison (1974) has noted that this radius indicates an anamolously low density for Tethys (cf. Section 8) and suggests that the albedo may be substantially higher than the value reported by Dollfus.

It has been shown by Widorn, KenKnight, Veverka, Zellner and their coworkers that both the depth of the minimum and the slope of the rising branch of the curve of visual polarization as a function of phase angle depend on the albedo of the re-reflecting surface. Calibration of this dependence from laboratory measurements of pulverized terrestrial rock, of lunar soil, and of crushed meteorites (Veverka and Noland, 1973; Bowell and Zellner, 1973) shows that the slope of the rising branch is a function primarily of the albedo alone, while the depth of the minimum is a more ambiguous indicator of albedo. Since the maximum range of phase angle for the satellites of the outer planets is not sufficient to define the slope, the only recourse is to obtain a rough value for the albedo from the minimum polarization. These estimates are consistent with the albedos known for the Galilean satellites, and Zellner (1972a) and Bowell and Zellner (1973) have applied the method to Rhea and Iapetus, suggesting radii of about 800 km for each of these satellites.

A more useful method of estimating the albedos and radii of satellites is from combined visual and infrared photometry (Allen, 1971; Murphy *et al.* 1972; Morrison, 1973a, b, 1974). If both the directly reflected radiation and the energy that is absorbed at the surface and re-radiated in the thermal infrared are measured and appropriate modeling assumptions are made, the albedo can be determined from the ratio of the two fluxes. Morrison (1973a, b) has calibrated this method against the Galilean satellites and discussed its sources of error; for dark surfaces (i.e., $p_V < 0.3$) the albedo can be determined to $\pm 20\%$, and for lighter surfaces perhaps to $\pm 30\%$.

Radii of 3 of Saturn's satellites have been measured by this photometric/radiometric technique: Iapetus, with $r = 900 \pm 100$ km; Rhea, with $r = 800 \pm 125$ km; and Dione, with $r = 575 \pm 100$ km (Murphy *et al.* 1972; Morrison, 1973a; 1974).

In cases where no disk is measurable and where no polarimetric or radiometric data allow the albedo to be estimated, the only recourse is to assume a plausible range of geometric albedos and derive the corresponding range of radii from Equation (2). The visual magnitudes summarized by Harris (1961) are in many cases still the best estimates, although we will discuss more recent photometry of some of the satellites later in this paper. Choice of albedo for this purpose is not easy. The geometric albedos of the Galilean satellites range from 0.2 to 0.7. Typical albedos of asteroids are ~ 0.1, and that of Phobos and Deimos is ~ 0.05. The small irregular satellites probably have dark surfaces. At the other extreme, Saturn's inner satellites Rhea, Dione, and Tethys have albedos $\geqslant 0.5$, suggestive of ice-covered surfaces, and probably Enceladus, Mimas, and perhaps Janus have similar albedos. To estimate the possible range in size, we compute a lower limit based on a geometric albedo of 1.0. The upper limit corresponds to the smaller of: (1) a diameter of $\frac{1}{3}''$, which would be detectable visually; or (2) an albedo of 0.03, the lowest known in the solar system (Matson, 1971). While the resulting range in size is large, we cannot justify restricting it further in our present state of ignorance.

Table V summarizes all of the data on the radii of satellites. Two radii (Io and Ganymede) are derived from stellar occultations; two (Phobos and Deimos) from spacecraft imagery; three (Callisto, Europa, and Titan) from ground-based visual measurements; and three (Iapetus, Rhea, and Dione) from radiometric/photometric observations. In order to make best guesses of the radii of the irregular satellites of Jupiter and Saturn, we chose an albedo of 0.1, and for the inner satellites of Saturn (Janus, Mimas, Enceladus, and Tethys) we chose 0.8. In all other cases, only the extreme limits discussed in the previous paragraph can be computed.

3.6. Masses

Mass determinations for the satellites have been reviewed by Brouwer and Clemence (1961), Kovalevsky (1970), and Duncombe *et al.* (1973a, b). No estimates of mass are available for the smaller satellites and none are in prospect, even now that flyby vehicles will be sent through some of the satellite systems in the next decade. Our attention is thus confined to those satellites of mass greater than 10^{22} g whose gravitational perturbations, either upon each other or (in the case of Triton) upon their primary, are observable from Earth. Since the paper cited above thoroughly review satellite masses, we will simply summarize their conclusions.

The masses of the Galilean satellites have been determined with formal errors of less than 10%; however, the listing (in Duncombe *et al.*, 1973a, b) of the individual values suggests that the true uncertainty for Io and Callisto may be larger than these formal values, while in contrast different mass determinations for Europa and Ganymede are quite consistent. Ganymede, the largest Galilean satellite, is probably the most massive of the satellites, although the measurements are not accurate enough

TABLE V

Basic physical data for the satellites

Satellite	$V(1,0)$[a]	p_V	R(km)	R_{max}(km)	R_{min}(km)	M (10^{23} g)	ϱ(g cm^{-3})
Moon	+ 0.21	0.12	1738			735	3.34
1 Phobos	+11.9	0.06	10.9 ± 0.5				
2 Deimos	+13.0	0.07	5.7 ± 0.5				
1 Io	− 1.68	0.62	1820 ± 10			800 ± 60	3.17 ± 0.30
2 Europa	− 1.41	0.68	1550 ± 150			480 ± 10	3.08 ± 1.00
3 Ganymede	− 2.09	0.44	2635 ± 25			1540 ± 2	2.01 ± 0.06
4 Callisto	− 1.05:	0.19	2500 ± 150			910 ± 80	1.39 ± 0.35
5 Amalthea	+ 6.3			210	35		
6	+ 8.0		~80	150	22		
7	+ 9.3		~30	50	10		
8	+12.1:		~ 8	15	3		
9	+11.1:		~10	18	3		
10	+11.9:		~ 9	16	3		
11	+11.4:		~11	20	3		
12	+12.1:		~ 8	14	3		
1 Mimas	+ 2.6		~200	1000	200	0.37 ± 0.01	~1.1
2 Enceladus	+ 2.2		~250	1000	240	0.85 ± 0.03	~1.3
3 Tethys	+ 0.7		~500	1000	480	6.26 ± 0.11	~1.2
4 Dione	+ 0.88	0.60	575 ± 100			11.6 ± 0.3	1.45 ± 0.80
5 Rhea	+ 0.16	0.60	800 ± 125				
6 Titan	− 1.20	0.21	2500 ± 300			1401 ± 2	2.14 ± 0.80
7 Hyperion	+ 4.6			460	80		
8 Iapetus	+ 1.6	0.12	900 ± 100				
9 Phoebe	+ 6.9			160	30		
10 Janus	+ 4		~110	600	100		
1 Ariel	+ 1.7			1700	300		
2 Umbriel	+ 2.6			1100	200		
3 Titania	+ 1.3			2000	360		
4 Oberon	+ 1.5			1900	330		
5 Miranda	+ 3.8			650	110		
1 Triton	− 1.2			3500	1000	3400 ± 2000	
2 Nereid	+ 4.0:			600	100		

[a] $V(1,0)$ is the visual magnitude at zero phase reduced to 1 AU distance from both Earth and Sun. It is generally derived from observations at phase angles of 1°–5°, so it does not necessary include the opposition surge in brightness shown by a few satellites.

to establish clearly the first rank among Ganymede, Titan, and Triton. No other Jovian satellites have measurable masses.

The masses of several of the satellites of Saturn have been determined in spite of their small size, because of the orbital commensurabilities within this satellite system. The value for Titan (1.91 times the lunar mass) is known with an uncertainty of only about 1% from its influence on the motion of Hyperion. The masses of members of

the pairs Dione-Enceladus and Mimas-Tethys have formal uncertainties of about 5 and 20%, respectively. The masses of Rhea and Iapetus have been estimated, but since neither of these satellites possesses an orbital commensurability with another satellite, these masses are highly indeterminate and should not be taken too seriously; perhaps a better approach to estimating their masses would be to calculate them from the measured radii and plausible range in density. The only other satellite with a measured mass is Triton, found from its effect on the position of Neptune. The uncertainty in its mass is, however, quite large.

3.7. Mean densities

There are (excluding the Moon) 10 satellites with measured masses and 10 with measured radii, but for only 6 have both quantities been determined: the Galilean satellites, and, with substantial uncertainties, two satellites of Saturn. These values, together with the data on radii and masses, are all summarized in Table V.

All of these satellites have densities lower than those of the terrestrial planets, suggesting a basic difference in composition, consistent with the models discussed in the following section. Figure 1 (taken from Morrison, 1974) illustrates the densities and geometric albedos of these satellites and also the permitted range of these parameters for Tethys, Enceladus, and Mimas. A correlation of density with size is sug-

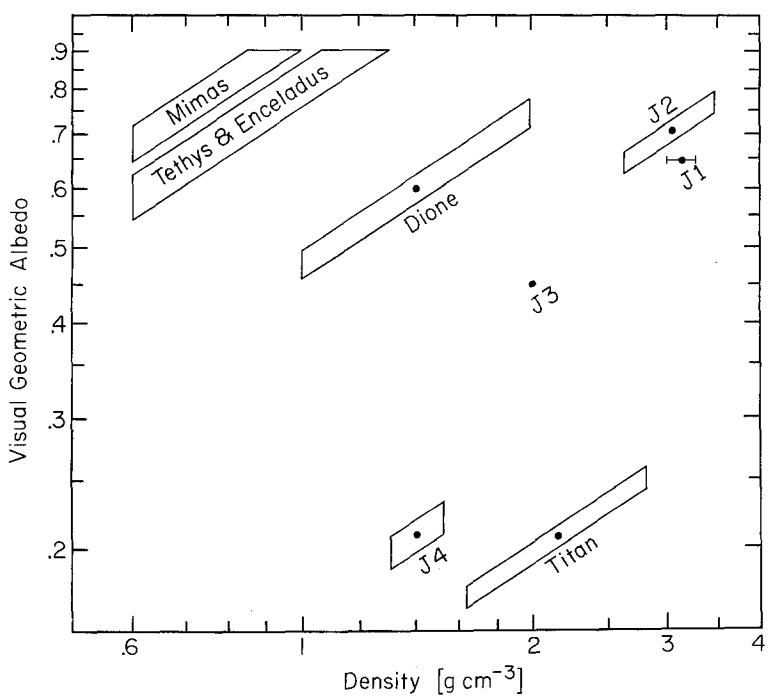

Fig. 1. Densities and visual geometric albedos of the Galilean satellites and of five satellites of Saturn, together with estimated 1ϱ uncertainties in these quantities. The maximum albedo and the minimum density have abritrarily been set at 0.9 and 0.6 g cm^{-3}, respectively. From Morrison (1974).

gested, but more striking are the large range in densities (decreasing with increasing distance from Jupiter) among the Galilean satellites and the difference between these objects and the satellites of Saturn. Because of its important cosmogonic implications, a more accurate determination of radii and masses (and hence the densities) of the satellites of Saturn would be extremely valuable.

One can only guess at the probable densities of the other satellites. If one assumes that the inner satellites of Saturn all have densities near unity, it is possible to derive a mass for Rhea that is consistent with the very uncertain dynamical value. Neither the mass nor the radius of Triton is known with sufficient accuracy to set any useful constraints on its density. In view of the apparent rocky nature of Phobos and Deimos and of the probable capture of the irregular Jovian satellites from the asteroid belt, it is reasonable to expect that these are silicate objects with densities between 2 and 3, but such a speculation cannot be verified at this time.

4. Bulk Composition and Structure

4.1. Introduction

Since the satellites were presumably formed over a wide range of distances from the Sun, the conditions in the solar nebula at the time of their formation must have varied substantially among them. There is an extensive literature on the history of small objects in the inner solar system, derived largely from analysis of meteorites (cf. Anders, 1971), but studies of the composition and internal structure of small bodies (except perhaps the comets) at distances beyond the asteroid belt, which is where most of the satellites are located, have been more limited. However, Kuiper, in the late 1940's and 1950's, discussed the likelihood that these low-density objects condensed at low temperatures from the volatiles in the solar nebula, and more recently chemical equilibrium calculations by Lewis (1971a, b, 1972, 1973) have brought these topics into prominence.

4.2. Composition

In recent discussions of the origin and evolution of the outer planets, various authors (e.g., Cameron, 1973) have suggested that these bodies consist of a relatively involatile material that is admixed with a solar-composition, volatile-rich component in proportions that vary with distance from the Sun. Such a composition can be understood in terms of a solar nebula in which the composition of the condensing material changes with heliocentric distance, being rocklike inside the orbit of Jupiter but becoming increasingly rich in ice-forming compounds at greater distances. A similar range in compositions of satellites is suggested by the tendency for density to decrease and albedo to increase as heliocentric distances increase, although the data on both of these basic quantities are sketchy at best in the outer solar system (see Section 3). In addition, it has been shown (Watson *et al.*, 1963) that unprotected frozen volatiles will not be stable against evaporation over the lifetime of the solar system inside the orbit of Jupiter, while they can persist on the surfaces of the satellites of the outer planets.

Lewis (1972, 1973) has provided semi-quantitative models for the chemistry of the condensation-accretion process as a function of temperature and pressure in the solar nebula. He limits his discussion to 15 abundant elements, including those most important for the formation of rock and ice. He also shows that, over the expected range in pressure (i.e., 10^{-1} to 10^{-9} bar), the chemistry of the condensate will be essentially independent of pressure but strongly dependent on temperature. Two extreme scenarios for the condensation process are suggested: (1) the equilibrium model, in which the condensates are assumed to remain in chemical equilibrium with the nebular gases as the material changes in temperature with a resulting homogeneous solid body; and (2) the disequilibrium model, in which the accretion of condensed material into large bodies is rapid compared to the cooling of the nebula, and the solid bodies develop a layered structure, with the first material to condense near the center and the more volatile species near the surface. In the first case, the accreted body stores gravitational potential energy, which can be released by heating and density-dependent differentiation. In the second, it stores chemical potential energy, which can also be released if the interior melts, allowing the materials to mix.

It is not possible on the basis of present knowledge to choose between these alternative models for the formation of the satellites, or to exclude an intermediate case, but Lewis expresses some preference for the equilibrium model based on experience in the inner solar system. In any case, the predictions of the two modes of formation of solid bodies are not very different for the properties that can best be related to the observations – mean density, and composition of the surface and (in some cases) atmosphere. Here we will briefly describe the equilibrium condensation model and refer the interested reader to Lewis (1972, 1973) for details of the alternative process.

Figure 2 illustrates a computation of the cumulative mass and density of a body condensing in equilibrium from the cooling solar nebula. Steps (1) and (2), which take place at temperatures above 1000 K, involve the condensation of 'rock' and lead to densities between 3 and 4. The next important event as the temperature drops (step 8) is the condensation of H_2O ice (near 150 K); a satellite formed at this temperature would have an uncompressed density of about 1.6. Below 100 K retention of hydrates of ammonia and methane is expected, but these additions have little effect on the total density. Only as the temperature approaches 20 K in these models does the retention of A and of the remaining CH_4 result in a mean density near unity. We emphasize that, in each case, the figure illustrates cumulative density and assumes that the rocky component, which condenses first, remains a part of the satellite (although representing a decreasing fraction of the total mass as the more volatile materials are added). The uncompressed density of pure methane ice is about 0.7, the lowest of any cosmically abundant volatile unless the temperature is low enough to condense hydrogen.

These models suggest that satellites with densities >3.0 will be composed of rock, that those with densities between 1.5 and 3.0 will be made of rock and water ice and possibly also ammonia and methane hydrates, and that if the density is much lower than 1.5, there must also be substantial quantities of pure methane. The satellites of

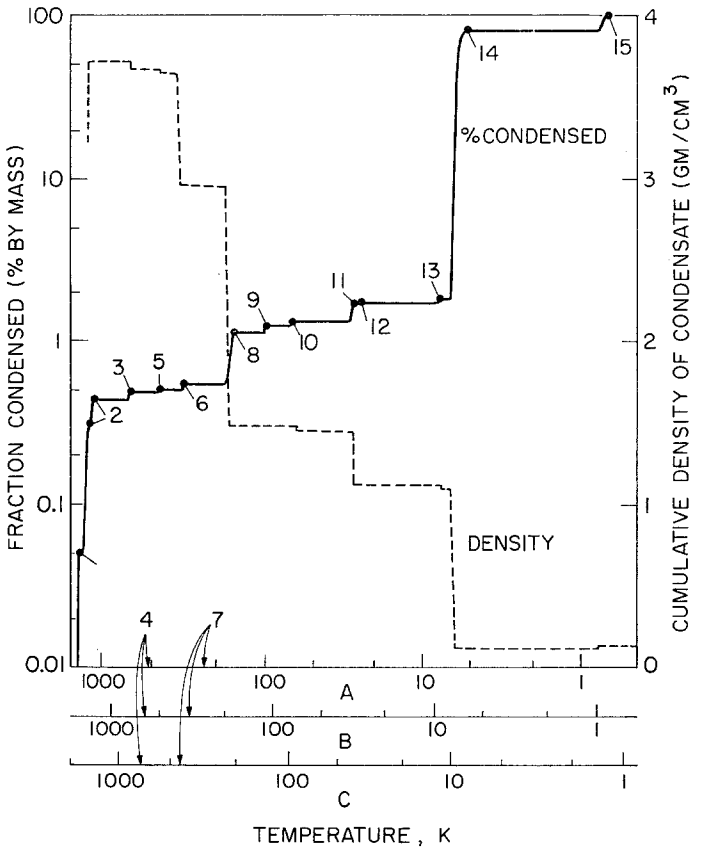

Fig. 2. Cumulative mass and density for equilibrium model condensation sequences from the solar nebula at 10^{-6}, 10^{-4}, and 10^{-2} bar total pressure. Temperature scales are given for (A) 10^{-6} bar, (B) 10^{-4} bar, and (C) 10^{-2} bar pressure. The 15 steps indicated are (1) condensation of Ca, Al, and Ti silicates, (2) $MgSiO_3$ and Fe condensation, (3) conversion of H_2S to FeS, (4) conversion of CO to CH_4, (5) conversion of Fe to FeO, (6) conversion of enstatite to talc plus brucite, (7) conversion of N_2 gas to NH_3, (8) condensation of water ice, (9) conversion of NH_3 to solid $NH_3 \cdot H_2O$, (10) conversion of ice to solid $CH_4 \cdot 8H_2O$, (11) condensation of solid CH_4, (12) condensation of solid Ar, (13) condensation of solid Ne, (14) condensation of solid H_2, (15) condensation of solid He. Steps 3 and 5 always occur at 670 and 510K, respectively, and should be read only on scale B. Steps 4 and 7 are not condensations, and are indicated on the temperature scales only. Figure and caption from Lewis (1972).

Jupiter may be in the rock-and-ice category; whether they also contain large amounts of ammonia and methane hydrates is a question that may be amenable to spectroscopic investigation. The densities of at least some of the satellites of Saturn appear to require the presence of methane ice.

4.3. Interior structure

All of the models discussed above include ices with melting temperatures not far above the present surface temperatures of the satellites, and all include rock, which is expected to contain radioactive sources of heat. Therefore, heating of these bodies

either in the late stages of accretion, or by dissipation of tidal energy, or by the release of radioactive energy, might have important effects on their structure.

Lewis (1971a, b) first discussed the evolution and structure of satellites that contain ices. He initially considered a homogeneous, cold satellite, such as would be predicted by the equilibrium condensation model, composed primarily of rock and H_2O. The melting point of primary interest is that of the H_2O-NH_3 eutectic at 173 K. On the assumption that the rocky component contains ^{40}K, U, and Th in chrondritic proportions, he found that the heat liberated over the age of the solar system is several times that necessary to raise the temperature of the whole satellite above 173 K. Such a mechanism will be effective, of course, only if the time scale for conduction of the heat to the surface of the satellite is long compared to the age of the satellite. Lewis computes that, for the expected thermal conductivity of ice, any satellite more than several hundred kilometers in radius will surely have been melted throughout much of its interior by radioactive heating within the first billion years of its formation. If other energy sources also contribute, such as tidal despinning or release of stored gravitational or chemical energy once melting begins, the melting and subsequent differentiation may take place fairly rapidly.

The arguments given above lead one to expect at least the larger satellites in the outer solar system to be differentiated, with most of the rocky materials in the core, surrounded by a mantle of liquid volatiles, with a crust of ice possibly mixed with silicates. The core, for the Galilean satellites, constitutes about 0.15 of the volume, and thus has a radius a little over half that of the satellite. The thermal structure of such a body can be estimated. Radioactive heat generation in the core is expected to amount to a few times 10^{-8} erg g^{-1} s^{-1} averaged over the mass of the satellite. This energy is transported by conduction through the muddy core and then by convection within the liquid mantle. The thickness of the solid crust will be such that a steady-state flow of heat will be maintained through it by conduction. It can easily be shown that the thickness of the crust (ΔR), if small compared to the radius of the satellite, is given by

$$\Delta R = \frac{3K\Delta T}{\varrho SR}, \tag{3}$$

where K is the thermal conductivity of the ice, ΔT is the difference between the mean surface temperature and the melting temperature of 173 K, ϱ is the density, S is the heat liberated (per unit mass) from the core, and R is the radius of the satellite. Lewis (1971) estimates that for a typical Galilean satellite $\varrho = 1.9$ g cm^{-3}, $K = 6 \times 10^5$ erg cm^{-1} s^{-1} K^{-1}, and $S = 1.7 \times 10^{-8}$ erg g^{-1} s^{-1}. To be specific, let us consider Ganymede, with $R = 2.64 \times 10^8$ cm and mean surface temperature 115 K. Then Equation (3) gives a thickness for the crust of 120 km. The temperature gradient in this crust is ~ 0.5 K km^{-1} and, for a given surface temperature, is proportional to the radius of the satellite. If the melting point of the H_2O-NH_3 eutectic is depressed at the base of the crust, as suggested by Lewis (1971a), the crust would be even thinner than calculated above.

The complex internal structure discussed here will apply only to the largest satellites. With the exception of Titan, Triton, and possibly Iapetus and Rhea, the satellites of Saturn, Uranus and Neptune probably are frozen throughout, while the small satellites of Jupiter and Mars are presumably solid rocky bodies.

4.4. Implications for surfaces

In the models of large icy satellites considered above, about 90% of the volume is liquid or slushy; any strong heating could melt the remaining 10% of the material, resulting in complete differentiation and a crust of pure ice. If complete melting did not occur, however, it is instructive to consider the fate of the relatively dense crust once the interior of the satellite melts. The crust would presumably be a primordial mixture of silicates and ices with density ~ 1.9 held by its own tensile strength above a mantle of density ~ 1. As pointed out by Lewis (1971a), any fracture of the crust would permit violent eruptive release of a magma of water and ammonia onto the surface, driven by hydrostatic pressures of the order of a kilobar. Extensive fracturing of the crust would permit foundering of large blocks of undifferentiated material, followed by catastrophic sinking of the entire crust – a dramatic event to contemplate indeed! The result would be the same as if the sateilite had completely melted early in its history.

Lewis concludes that the crusts of all the largest satellites are likely to be almost pure H_2O ice, as a result either of early heating or of foundering of the crust, while those of the smaller satellites are more likely to be representative of the undifferentiated materials from which they formed. Such an analysis is, of course, uncertain. It is not possible on the basis of present knowledge to estimate the importance of sources of heating that acted in the early history of the satellites, and calculations of the rate of tidal heating for satellites with liquid interiors, for instance, might be very instructive. If there was no initial melting, the problem becomes one of assessing the likelihood that a meteoric impact will fracture the crust. The thickness of the crusts of the Galilean satellites, discussed here, is about a factor of two greater than that given by Lewis, and is indeed substantially greater than that of the crust of the Earth. It thus appears to us an open question as to whether such a crust, if it survives initial melting, might be expected to persist for the lifetime of the satellite.

It should be stressed that the crust as discussed above is ~ 100 km thick, whereas the optically observed part of the crust is only at most a millimeter thick, and here one may expect a number of physical and mechanical processes to modify the material. Lewis (1971a) summarizes these as follows:

"First, evaporation of ices, even if extremely slow, will lead to formation of a 'skin' of unconsolidated dust or organic matter either of indigenous or exogenous origin. Second, degassing of volatiles such as CH_4 and the rare gases will provide a supply of condensable or (in the case of CH_4) photolytically labile material. Third, micrometeorite infall will provide a constant source of energy to evaporate ices, and a constant source of dust to obscure the surface. Fourth, solar ultraviolet light will constantly be producing reactive free radicals and ions by interaction with the surface

materials and atmospheric gases. Fifth, larger collisions will occasionally stir up icy material from greater depths and produce light-colored craters and rays."

The question of the lifetime of topographic features formed by meteoric impacts on icy satellites has recently been investigated by Johnson and McGetchin (1973). In spite of an uncertainty of almost 4 orders of magnitude in the viscosity of ice, they show that on a satellite with radius 1000 km or more, a topographic feature will be destroyed by creep in less than 10^6 yr at the distance of Jupiter, but may have a lifetime greater than the age of the solar system at the lower temperatures expected further from the Sun. In contrast, silicate bodies of this size can easily retain topography for the lifetime of the solar system. By similar arguments, major distortions from hydrostatic equilibrium even in satellites with a radius of about 200 km will not be maintained for more than a few million years if the satellite is made of ice at temperatures appropriate to Jupiter's distance, but can persist for billions of years if the body is at the distance of Saturn or is composed of non-volatiles. High-resolution imaging of the Galilean satellites may, according to these arguments, be able to distinguish silicate crusts from ice crusts, while similar observations of the smaller satellites of Saturn and Uranus may be able to establish whether the viscosity of their surface ice was ever lower than at present, indicating that there had been a high-temperature phase in the history of those satellites.

Finally, the interior composition and structure may be expected to influence the nature of any atmospheres on these satellites, since such atmospheres must be maintained by outgassing from the interior. Lewis (1971b) and Lewis and Prinn (1973) have discussed some of the implications of the condensation-accretion models for the atmospheres of Titan and the Galilean satellites. They make the important point that the vapor pressures of NH_3 and CH_4 must be calculated for their solid hydrates, not for their pure ices, in computing expected quantities of atmospheric gas. The atmospheres of these satellites will be discussed in detail in Sections 6 and 7, and here we will simply note that the absence of observable CH_4 and NH_3 in the spectra of the Galilean satellites argues against the presence of methane hydrate in the crusts of these satellites but does not exclude ammonia hydrate, while the presence of large quantities of methane in the atmosphere of Titan is evidence that this satellite condensed at a temperature low enough to retain methane hydrate.

5. Phobos and Deimos

5.1. Introduction

With this section, we begin detailed discussion of the observations of the surfaces of the better-studied individual satellites. Phobos and Deimos, which under the best conditions are of only 12th magnitude and are nearly lost in the glare of Mars, have only become objects of intensive interest as a result of studies made from the Mariner 9 spacecraft at ranges of the order of 10^4 km. Before turning to the Mariner 9 results, however, we review the few previous studies that are relevant to physical conditions on these objects.

Photoelectric photometry of Phobos and Deimos was first obtained by Kuiper in 1956 at the McDonald 2.08-m telescope (Harris, 1961). He found a visual magnitude, reduced to unit distance from Sun and Earth and to zero phase angle, $V(1, 0) = 12.2$ for Phobos and 13.3 for Deimos and $B-V=0.6$ for both objects, with uncertainties of perhaps ± 0.1 mag. These observations suggested diameters near 15 and 10 km, respectively, if their albedos were similar to that of the Moon. Smith (1970) first measured the size of Phobos directly from several Mariner 6 and 7 far-encounter pictures in which the satellite could be seen in projection against the lighter surface of the planet. They showed an elongated satellite, with apparent diameters of 18 and 22 km, implying an average albedo of 0.065. At the next opposition, Zellner (1972b) observed the linear polarization of Deimos as a function of phase angle (between 5° and 31°) and used the slope of the rising branch of the polarization curve to derive an albedo of 0.07. The corresponding mean diameter is 11 km. Polarization studies at phase angles up to 80° made of both satellites from Mariner 9 (Noland *et al.*, 1973) are consistent with these results. Thus, the pre-Mariner 9 studies showed that both satellites were exceedingly dark and comparable in $(B-V)$ color to many asteroids and that Phobos is non-spherical.

Two very recent photometric studies of Phobos and Deimos suggest that these satellites are a few tenths of a magnitude brighter than reported by Harris (1961), and thus that they have higher geometric albedos than 0.05. Pascu (1973), from a photographic study of plates obtained 26 April 1967, when both satellites were near western elongation and the solar phase angle was 9°, obtains a magnitude (reduced to unit distance but at 9° phase) of $V=12.06\pm0.1$ for Phobos and $V=13.11\pm0.05$ for Deimos. The corresponding values of $V(1, 0)$ are about 11.8 and 12.8, respectively, yielding geometric albedos for both satellites of between 0.06 and 0.07 when combined with the dimensions discussed in the following section. Zellner and Capen (1974), from photoelectric observations in 1973, obtain values of $V(1, 0)$ of 11.9 and 12.95 and geometric albedos of 0.06 and 0.07 for Phobos and Deimos, respectively.

5.2. The Mariner 9 pictures

Between its arrival at Mars in October 1971 and the end of the regular mission in March 1972, the Mariner 9 TV system obtained about 140 satellite pictures, most of which are of Phobos, at ranges down to about 5000 km. Two papers by members of the Mariner 9 imagery team (Pollack *et al.*, 1972, 1973a) have analyzed these data and provide most of the material for the following discussion.

Both satellites are irregular, heavily cratered objects whose present shapes are largely determined by cratering, associated impact fragmentation, and spallation. They are thus entirely different from the other, larger satellites discussed in this review, whose shapes and internal structure are controlled by gravitational forces. Figure 3 illustrates two of the highest resolution, contrast enhanced pictures: Phobos on the top and Deimos on the bottom. In both views the Sun illuminates the satellite obliquely from the left. Both objects are heavily cratered; the largest crater is on Phobos and has a diameter of 8 km, or a third of the diameter of the satellite! Some

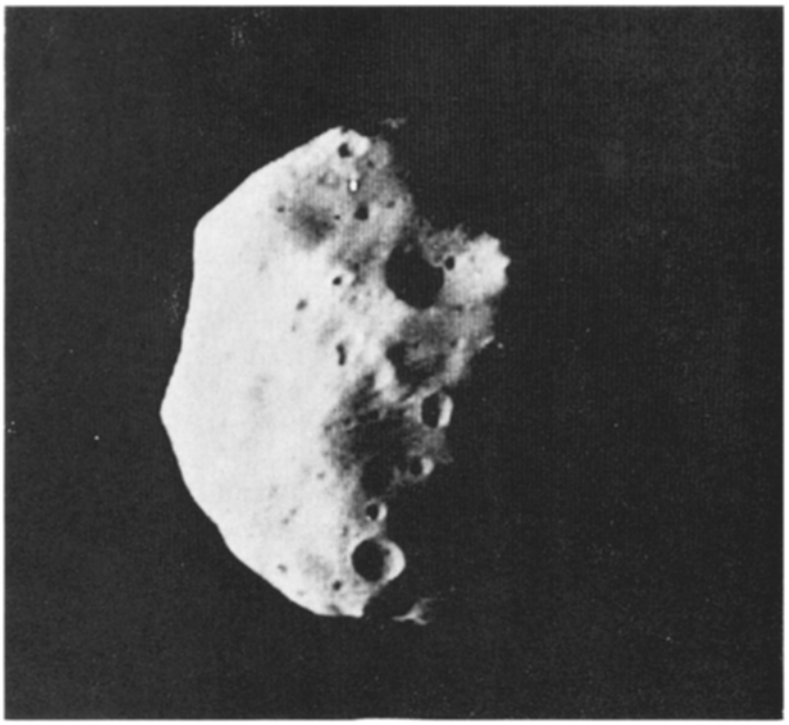

Fig. 3a.

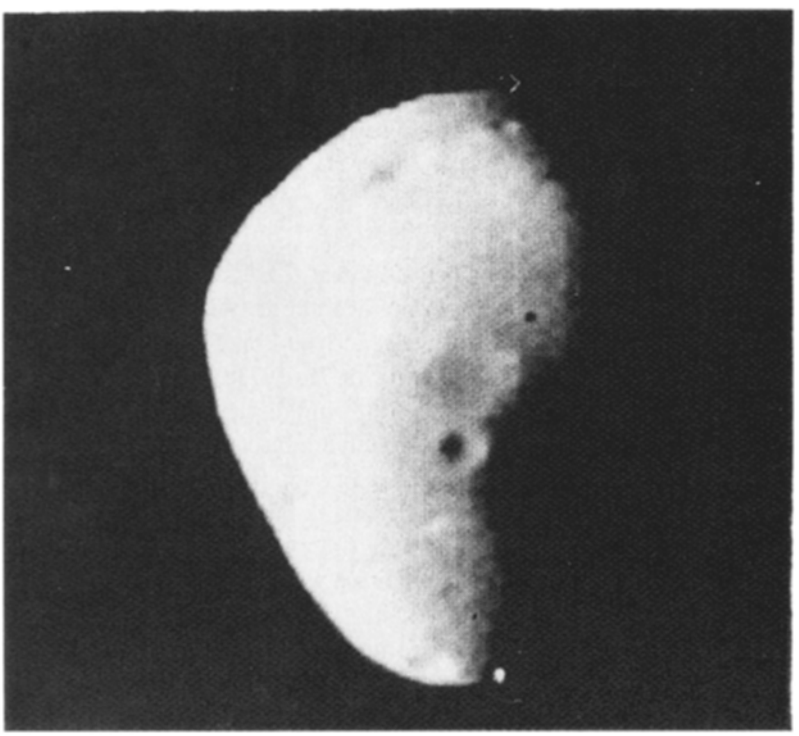

Fig. 3b.

of the larger craters have degraded, scalloped edges, while a few of the smaller ones are fresh with smooth rims. Many craters show raised rims, and in addition a step-like linear ridge runs the length of Phobos. The significance of some of these structures is further discussed below.

Both Phobos and Deimos are in synchronous rotation, with their longest axes radial to Mars, as expected in a stable configuration (Burns, 1972). Table VI lists the dimensions and volumes of the tri-axial ellipsoids found by Pollack *et al.* (1973a)

TABLE VI

Dimensions of Phobos and Deimos (from Pollack *et al.*, 1973)

Satellite	Largest radius (km)	Intermediate radius (km)	Smallest radius (km)	Volume (km^3)
Phobos	13.5 ± 1	10.7 ± 1	9.5 ± 1	5748
Deimos	$7.5(-1, +3)$	6.1 ± 1	5.5 ± 1	1054

to provide the best fit to the profiles. While the absolute photometric calibration of the spacecraft images is insufficient to provide a good independent measure of the albedo, the ratio of the surface brightness of Deimos to that of Phobos under the same viewing and lighting geometry is 1.05 ± 0.05. The mean geometric visual albedos, obtained by combining these dimensions with the ground-based photometry discussed in the previous section, are in the range 0.05 to 0.07 for both satellites. This albedo is similar to that of the lunar maria, and it suggests a surface composed of basalts or of carbonaceous chondritic materials. Seen under high Sun angle, Phobos shows no albedo differences on its surface, but Deimos has a number of areas of contrasting albedo, presumably due to differences either of composition or of structure of the surface. Pollack *et al.* (1973a) suggest that these features may have been produced by relatively recent large impacts, and are thus analogous to the lunar rays.

Although the large departures from sphericity make such an analysis difficult, Pollack *et al.* (1973a) have constructed a preliminary photometric function (surface brightness as a function of phase angle) for these satellites. The data indicate that Phobos and Deimos backscatter incident sunlight as strongly as does the Moon. Strong backscattering requires complex surface texture and a dark surface material, and together with the polarization data it suggests a texturally complex regolith.

5.3. Cratering and the Presence of a Regolith

Even a casual examination of the Mariner 9 pictures shows that the surfaces of

←

Figs. 3a–b. Television images of Phobos and Deimos from the Mariner 9 spacecraft. (a) Phobos; range 5758 km, phase angle 80°. The illuminated area is approx. 21.1 by 14.9 km. The crater to the upper right is 5 km in diameter. (b) Deimos; range 5465 km, phase angle 65°. The sharp crater below center has diameter ~1 km, and the diffuse crater above it ~2 km. From Pollack *et al.* (1972).

Phobos and Deimos have been molded in part by impacts that have excavated craters and apparently chipped away large pieces to produce the present irregular profiles. It is important to inquire into the fate of this excavated and spallated material for satellites of such low surface gravity, as well as to try to reconstruct the history of the impacts.

Figure 4 (taken from Pollack *et al.*, 1972) shows the frequency distribution of craters on Phobos and Deimos compared to mean distributions for the lunar uplands and for the Martian surface. The density if small craters on these satellites is an order of magnitude greater than on heavily cratered terrain on the planet, but it is similar to that on the lunar highlands, which represents a state of saturation in which old craters are eliminated as fast as new ones are formed. A lower limit to the age of the surfaces of Phobos and Deimos is the time needed to arrive at a saturated crater density. Although the rate of impacts in the past is not known, Pollack *et al.* conclude that this age is probably measured in eons.

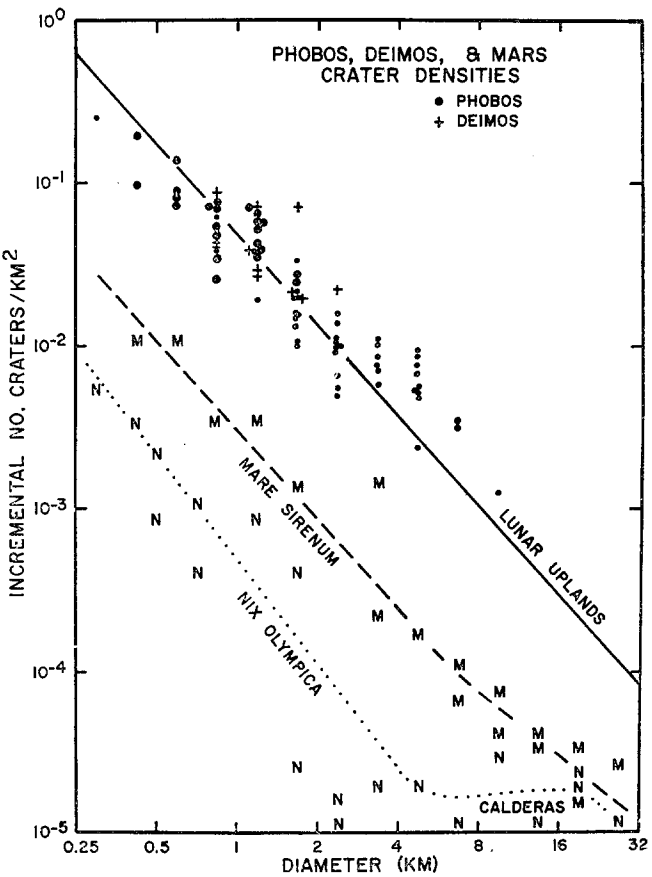

Fig. 4. Crater densities on Phobos and Deimos measured on Mariner 9 images. Also shown for comparison are densities for the lunar highlands and two regions on Mars. From Pollack *et al.* (1972).

From the size distribution of craters it is possible to estimate the present thickness of the regoliths on these satellites. The observations of Phobos show that 50% of the surface is covered by craters whose diameter exceeds 0.33 km (Pollack *et al.*, 1973a); if the average ratio of diameter to depth of a crater is 6, then the mean depth of excavation must be at least 50 m. An upper limit of several hundred meters is set by the size of the largest craters. The values for Deimos are about a factor of 2 smaller.

What is the fate of this large volume of excavated material? As a consequence of low surface gravity, virtually all of it escapes, and if these satellites were isolated we would expect their surfaces to be free of debris. However, Soter (1973) has traced the subsequent history of the ejecta; he finds most of it will form a dust belt around Mars and be recaptured by the satellites in very low velocity impacts, making it possible for Phobos and Deimos to acquire regoliths.

We have already noted that the photometric phase function (Pollack *et al.*, 1973a) and polarimetric observations (Zellner, 1972b; Noland *et al.*, 1973) imply a finely textured, dusty surface. Additional strong evidence for the presence of a porous dust layer is provided by measurements of the variation of thermal radiation observed by the Mariner 9 infrared radiometer during an eclipse of Phobos (G. Neugebauer, private communication, 1973). The very rapid change in surface temperature requires a low thermal conductivity similar to that deduced from eclipse radiometry of the Moon and the Galilean satellites and precludes the presence of significant amounts of exposed solid rock.

5.4. Structure

Two extreme models of the structure of these satellites have been considered. They may be aggregates of small grains, chiefly held together by gravity, or they may be well-consolidated rock with significant structural strength. Radically different evolutionary histories are implied by these two models. Pollack *et al.* (1973a) employ several lines of evidence to choose between them. First, they note that the presence of raised rims on many impact craters and of the long linear ridge on Phobos (well-illustrated in Figure 5) requires consolidated material. While the consolidation necessary for the crater rims could be produced by shock lithification of an unconsolidated material at the time of impact, the origin of the long ridge appears to require the dissipation of impact energy in a well-consolidated rock. In effect, this ridge represents a major fracture in the satellite produced by an impact that, had it been a little larger, would have disintegrated the satellite. Pollack *et al.* further argue that the fact that these satellites have survived at all strongly suggests a material with significant internal strength. Soter (1973) has calculated the frequency of collisions of these objects with meteoroids and finds that at least one impact large enough to release 10^{24} to 10^{26} erg (the range reflects the uncertainty in the calculation) should have taken place for Phobos. Pollack *et al.* show that the binding energy of an unconsolidated Phobos is $\sim 2 \times 10^{24}$ erg, while the binding energy of the consolidated, strength-dominated model is between 4×10^{25} and 4×10^{27} erg. Thus, it is likely that the largest impact suffered by Phobos would have released energy greater than the binding energy of an

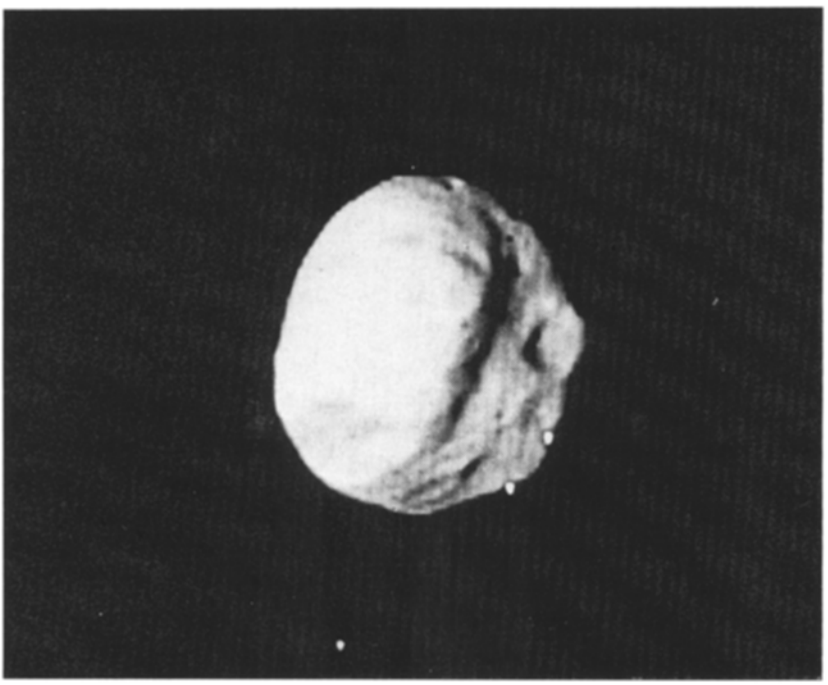

Fig. 5. Television image of Phobos from the Mariner 9 spacecraft. Range 12500 km, phase angle 18°. The illuminated area is approx 22.0 by 20.1 km. A linear ridge is well shown with a 5-km crater to the right. From Pollack *et al.* (1972).

unconsolidated satellite, in which case it would have fragmented. In contrast, it seems highly probable that a strength-dominated satellite would have survived until today.

The above arguments are used by Pollack *et al.* (1973a) to show that Phobos and Deimos are probably composed of well-consolidated material. It is difficult to see how such a degree of consolidation could have resulted from the accretion of small objects, and these authors therefore conclude that these satellites are fragments of one or two much larger objects.

Once we know that these satellites have significant internal strength it is possible to apply the theory of Goldreich and Soter (1966) to determine the time necessary for tidal forces to bring them into their presently observed state of synchronous rotation. Pollack *et al.* (1973a) carry out such a calculation and conclude that this despinning time is 10^6 to 10^8 yr for Deimos and 10^4 to 10^6 yr for Phobos. These values are lower limits to the time since the last collision that was large enough to impart significant angular momentum, and are entirely consistent with the expected frequency of such collisions.

5.5. Summary

Data from Mariner 9 indicate that Phobos and Deimos are well-consolidated frag-

ments of larger bodies and that their present size and morphology are the result of a long history of impact cratering and spallation. They possess regoliths, the uppermost layers of which must be fine-grained, porous dust similar to that on the Moon. Their low albedos suggest basaltic or carbonaceous chondritic composition.

Whether these properties may apply in whole or in part to any other group of satellites is not clear. The only others of similar size are the irregular Jovian satellites J8 through J12. These objects, and Phobos and Deimos as well, may have originated in and may be characteristic of the asteroid belt, although we have seen that the presence of a regolith on the Martian satellites is a consequence of their close proximity to the planet. In any case, most of the satellites that will be discussed in the following sections are very different from Phobos and Deimos.

6. The Galilean Satellites

6.1. Introduction

In this section we consider the observational and theoretical evidence on the nature of the surfaces, atmospheres, and interiors of the Galilean satellites. The observational evidence comes from photometry, spectroscopy, polarimetry, radiometry, and occultation studies. Since most of these techniques have been applied to all four of these satellites, we find it more conveneint or organize this discussion by technique rather than by object; in the conclusion, however, we draw upon all available evidence to try to characterize as well as we can the physical characteristics of each Galilean satellite.

6.2. Photometry and spectrophotometry

A prime goal of multi-color photometry and spectrophotometry of the Galilean satellites is to determine the wavelength dependence of the albedo with sufficient precision to permit identification of the composition of the surface materials. Minerals and ices that have been considered candidates for the surfaces of the Galilean satellites typically exhibit broad absorption bands in the near infrared. A second important goal of many photometric studies is to investigate the microstructure of the surface from variations of brightness or color with phase angle or to search for temporal variations that indicate large-scale inhomogeneities on the surfaces of these satellites.

Precision photometric studies of the Galilean satellites date from the work of Stebbins (1927) and Stebbins and Jacobsen (1928), who determined the solar phase functions of these four objects and established that their brightness varies with orbital position as well. Harris (1961) reduced the photometry of Stebbins to the *UBV* system and included it in Harris' own extensive multi-color photometric study of the Galilean and other satellites. The Harris paper has long remained the standard reference on photometry of satellites, although more recent observations of higher precision and often also with greater spectral resolution and extended coverage into the infrared have now superseded the broad-band photometry presented in his paper. We first discuss the evidence for photometric variations with orbital and solar phase angle and then return to the spectrophotometry.

The most extensive studies to date of the photometric variations of the Galilean satellites as a function of both orbital phase (θ) and solar phase angle (α) are by Johnson (1969, 1971) and Morrison *et al.* (1974). Johnson observed with 24 narrow-band filters; most of his data on variability, however, are given only for the 0.56-μm filter, which has an effective wavelength similar to that of the standard V magnitude. Morrison *et al.* observed with the intermediate-bandwidth filters of the *uvby* Strömgren photometric system ($u=0.35$ μm; $v=0.41$ μm; $b=0.47$ μm; $y=0.55$ μm$\simeq V$). Both sets of observations, the first made in 1969 and the second in 1973, cover a wide range of solar as well as orbital phase angles, and simultaneous solutions for the coefficients that express the dependence of magnitude and color on both angles are required. The orbital effects are easily separated from the variations in α for Io and Europa, which can both be observed for several orbits in a few nights, during which α changes very little. The orbital period of Callisto, in contrast, is more than two weeks; since this satellite also has a relatively large phase coefficient ($dV/d\alpha$), typically the magnitude changes due to variations in α will be comparable to those due to rotation over a single orbital period. The problem of separating these effects is further complicated by an apparent variation of the phase coefficient itself with rotation of Callisto (Stebbins, 1927; Stebbins and Jacobsen, 1928).

Figure 6 illustrates the orbital light curves of Io and Europa at 0.55 μm, based on all of the observations from Morrison *et al.* (filled symbols) and the high-weight nightly averages of Johnson (open symbols). All of these observations were reduced with a linear phase law; for Io, $dV/d\alpha=0.022$, and for Europa, $dV/d\alpha=0.012$ mag. deg^{-1}. The points at values of $\alpha<2°$ (from Johnson) lie slightly above the mean curves, as would be expected if there is an opposition effect, in which the magnitude changes at small α more rapidly than would be predicted by a linear phase law; however, this opposition effect must amount to no more than 0.1 mag. for either satellite. The older data were used to derive the two coefficients that specify a quadratic phase law (Harris, 1961); however, we see no evidence in the newer data to justify any more than a linear phase law for these two satellites. The variations in magnitude of both satellites with θ and hence with rotation are substantial; the peak-to-peak amplitude is 0.16 mag. for Io and 0.31 mag. for Europa. Within the accuracy of the data in Figure 6, both satellites are at maximum brightness at $\theta=90°$ (i.e., with the leading hemisphere exactly facing the observer) and at minimum at $270°<\theta<310°$. Neither curve is sinusoidal, however; in both cases, the minimum in brightness is narrower than the maximum, suggesting that the low-albedo features responsible for the minimum do not cover the entire trailing hemisphere.

The observations of variations of Ganymede and especially of Callisto are less satisfying. The peak-to-peak variation at 0.55 μm for Ganymede is, from the combined observations of Morrison *et al.* (1974) and Johnson (1971), 0.15 mag.; the minimum brightness is at $210°<\theta<300°$, and the maximum is at $40°<\theta<100°$. The phase coefficient is about 0.020 mag. deg^{-1}. In the case of Callisto, we can find no single phase coefficient that is consistent with the observations. Over most of its rotation, a satisfactory solution can be obtained with $dV/d\alpha=0.04$ mag. deg^{-1}, but

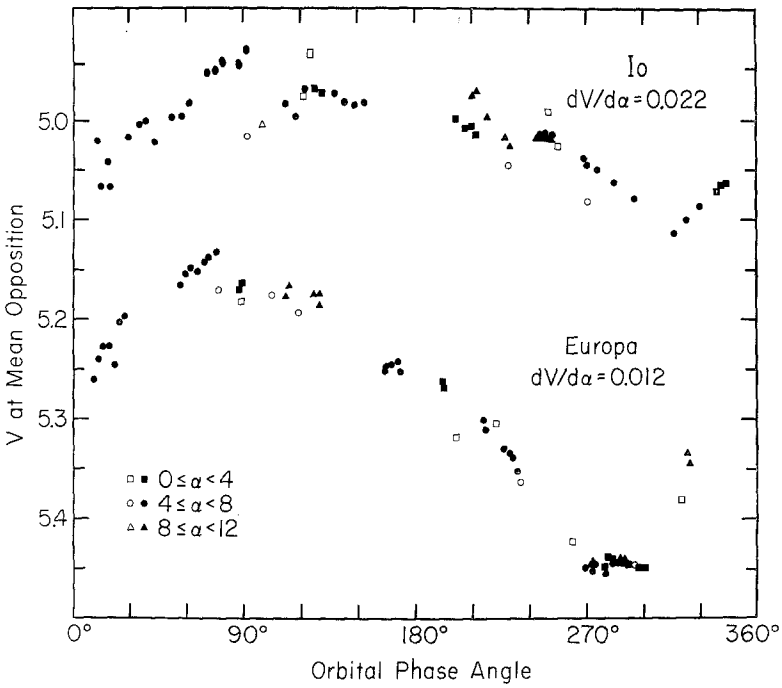

Fig. 6. Orbital photometric variations of Io and Europa. Filled symbols are the V magnitudes observed by Morrison *et al.* (1974); open symbols are nightly average magnitudes at 0.56μm from Johnson (1969; 1971). The observations from both authors have been reduced relative to o Vir ($V = 4.14$). The dependence on solar phase angle was removed using the phase coefficients indicated. Adapted from Morrison *et al.* (1974).

TABLE VII

Photometric data for the Galilean satellites (primarily from Morrison *et al.*, 1974)

	Io	Europa	Ganymede	Callisto
$V(1, 0)$	-1.68 ± 0.03	-1.41 ± 0.02	-2.09 ± 0.03	-1.05 ± 0.10[a]
ΔV (rotational)	0.16 ± 0.02	0.31 ± 0.02	0.15 ± 0.03	0.15 ± 0.06
$dV/d\alpha$	0.022 ± 0.003	0.012 ± 0.002	0.020 ± 0.004	0.040 ± 0.015
$b-y$	0.65 ± 0.02	0.54 ± 0.02	0.52 ± 0.01	0.55 ± 0.02
$v-y$	1.76 ± 0.04	1.18 ± 0.04	1.11 ± 0.02	1.16 ± 0.03
$u-y$	2.43 ± 0.05	1.25 ± 0.05	1.20 ± 0.05	1.26 ± 0.05
$(b-y)-(b-y)_\odot$	0.23 ± 0.03	0.12 ± 0.03	0.10 ± 0.02	0.13 ± 0.03
$(v-y)-(v-y)_\odot$	0.98 ± 0.06	0.40 ± 0.06	0.33 ± 0.04	0.38 ± 0.05
$(u-y)-(u-y)_\odot$	1.95 ± 0.12	0.77 ± 0.12	0.72 ± 0.12	0.78 ± 0.12
p_V	0.62	0.68	0.44	0.19
q_V	1.0	1.0	0.8	0.6
A_V	0.6	0.7	0.4	0.1

[a] The value of $V(1, 0)$ given for Callisto does not include the opposition surge, but is derived from magnitudes primarily at phase angles of 3 to 8°.

for $50° < \theta < 150°$, a much larger value is suggested by Johnson's data. Further, there is clear evidence of a substantial opposition effect at small α. In contrast with the inner three Galilean satellites, Callisto is brightest on its trailing hemisphere. Johnson (1971, and private communication, 1973) interprets his observations as showing a progressive shift through 180° in the position of maximum brightness as one moves outward from Io to Callisto; however, we conclude that the data are equally consistent with the hypothesis that the maximum is at $\theta = 90°$ for Io, Europa, and Ganymede, but at $\theta = 270°$ for Callisto. Table VII summarizes the photometric data, and is based primarily on the work of Morrison *et al.* (1974). Although we have discussed only linear phase coefficients, most observers (following Stebbins' example) have derived quadratic phase laws from their data, and in Figure 7 we illustrate these phase curves as obtained by Johnson (1971).

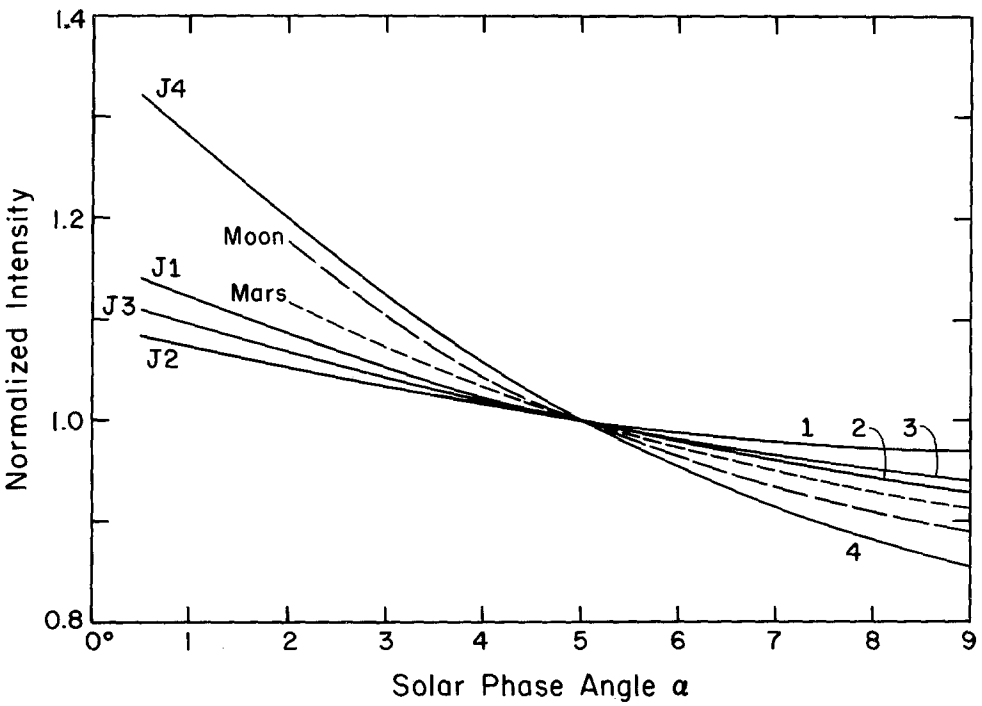

Fig. 7. Brightness versus solar phase angle, normalized to 1.0 at $\alpha = 5°$, of the Galilean satellites, the Moon, and Mars, showing the relative magnitudes of the opposition effects. From Johnson (1971).

Variations in *UBV* color of these satellites have been observed by Harris (1961) and Owen and Lazor (1973), but their observations do not cover a sufficient range in θ or α to define either the phase coefficients or the detailed shapes of the curves. Higher-quality data on the *uvby* system by Morrison *et al.* (1974) are not at this time fully reduced. However, a few color relationships are evident from the available broad-band and intermediate-band data. For all of the satellites, but especially for Io, the albedo declines rapidly for wavelengths shorter than 0.55 μm. Io is approx 2 mag.

fainter at u than at y, relative to the Sun. The $(b-y)$ and $(B-V)$ colors show no dependence on α; however, there appears to be a small dependence of $(v-y)$ and $(u-y)$ on α, consistent with an inverse relationship between albedo and phase coefficient that appears to apply to satellite surfaces (cf. Veverka, 1971a). The largest rotational color variations occur for Io and amount to about 0.8 mag. in $(u-y)$. The light curves in all filters have the same shape, except for a scale factor, indicating that the dark region on the trailing hemisphere (centered at $\theta=300°$ in the color curves) is much redder than the rest of the satellite. Europa similarly shows a larger amplitude in v and u than in y, with the trailing hemisphere the redder; however, the amplitude in b is smaller than in y. Neither Ganymede nor Callisto shows such large variations in color with rotation; however the data for these satellites also indicate that the darker hemisphere is redder, with the largest color effects in the ultraviolet. In his infrared photometry of the satellites, Lee (1972) found large variations in brightness, probably correlated with orbital phase, amounting to about 0.3 mag. at 2.2 μm, somewhat larger than in the visual region.

The difference in color between the lighter and darker sides of the Galilean satellites

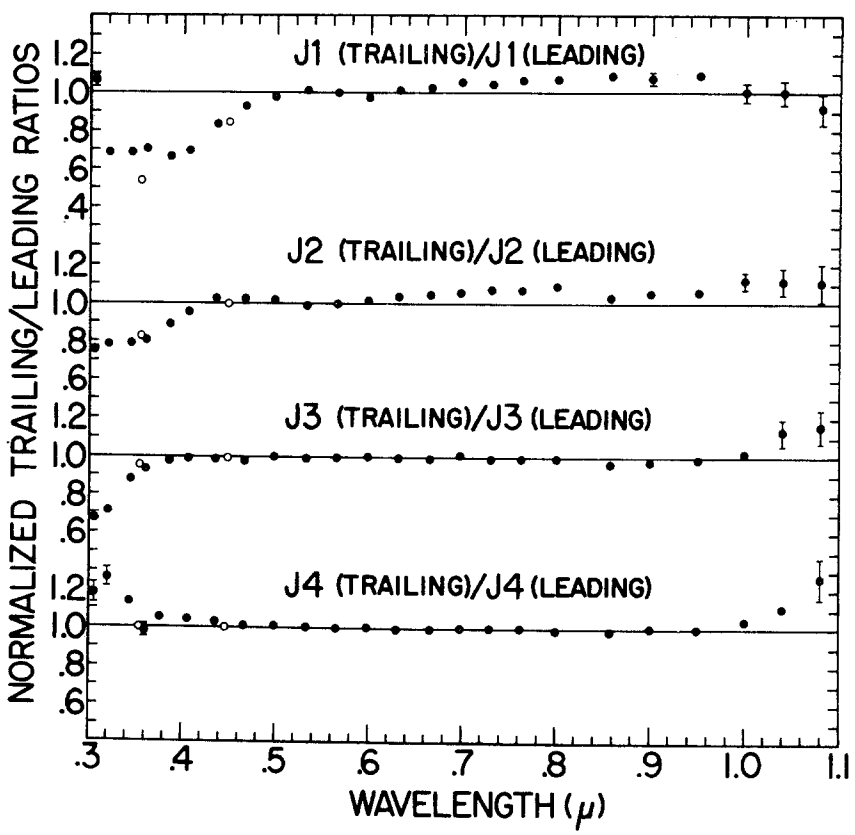

Fig. 8. Ratio of the spectral reflectivity of the trailing and leading sides of the Galilean satellites, normalized at 0.56 μm. From Johnson (1971).

can be seen clearly in Figure 8 from Johnson (1971). Plotted against wavelength is the ratio of the brightness of the satellites' trailing and leading hemispheres. As described above, the differences are greatest in the ultraviolet and are far greater for Io than for the other three satellites.

Geometric albedos of these satellites can be calculated from the observed magnitudes only when the sizes are known, and different authors have often adopted very different radii when reducing their photometry. Now that the radii of Io and Ganymede have been measured with high precision and it appears that the radii given in Table V for Europa and Callisto are likely to be within 10% of the correct values, it is possible to determine the geometric albedos with some confidence. We will confine our attention to a wavelength of 0.55 μm, which is near the reference wavelength used by Johnson (1969, 1971) and Johnson and McCord (1971) and is also near the effective wavelength of both the V and the y filters. Table VIII summarizes these albedos as derived from the independent measurements by Harris (1961) and Lee (1972) in the V band, by Johnson (1971) and Wamsteker (1972) in a narrow band at 0.56 μm, and by Morrison *et al.* (1974) as transformed to standard V mag. from their

TABLE VIII

Determinations of geometric visual albedos for the Galilean satellites

Author	Io	Europa	Ganymede	Callisto
Harris (1961)	0.76	0.76	0.47	0.21
Johnson (1971)	0.73	0.81	0.52	0.24
Lee (1972)	0.54	0.76	0.44	0.18
Wamstecker (1972)	0.74	0.71	0.49	0.21
Morrison *et al.* (1974)	0.62	0.68	0.44	0.19

y-band observations. The discrepancies among these values are surprisingly large. Since the observations by Lee and Wamsteker each extended over only a few days and neither author attempted to correct his data for rotational variations, we will not consider their albedos further. Johnson's observations span a wide range of both α and θ, and from them he derived mean values of the ratio of satellite brightness to o Vir reduced to $\alpha=0$. Morrison *et al.*, and presumably also Harris, calibrated their V mag. against a variety of UBV standard stars. Harris and Johnson assumed a V magnitude for the Sun of -26.81, but in calculating the albedos in Table VIII we used for all of the data a value of $V=-26.74$ (Johnson, 1965). The differences between Harris and Morrison *et al.* do not appear to arise in a simple shift of zero point in their magnitude systems and suggest either errors of up to 0.2 mag. by one or both observers or else real secular changes in the albedos of the satellites. The differences between Johnson and Morrison *et al.*, in contrast, are due primarily to a shift of 0.15 mag. in their calibrations, as documented by Morrison *et al.*, who derived a V mag. of 4.14 for o Vir, whereas Johnson found $V=3.99$ for this star. An additional difference in the case of Callisto arises because Morrison *et al.* employed a linear phase

law and therefore did not take into account the substantial opposition effect for this satellite. Since the albedos found by Morrison *et al.*, were obtained in a straightforward way from the standard system of stellar V mag., we will adopt their results rather than those of Johnson in this paper. The discrepancy with the older observations by Harris remains unexplained.

We now discuss the variations of albedo with wavelength as determined from spectrophotometry obtained with multifilter systems, with scanning spectrometers,

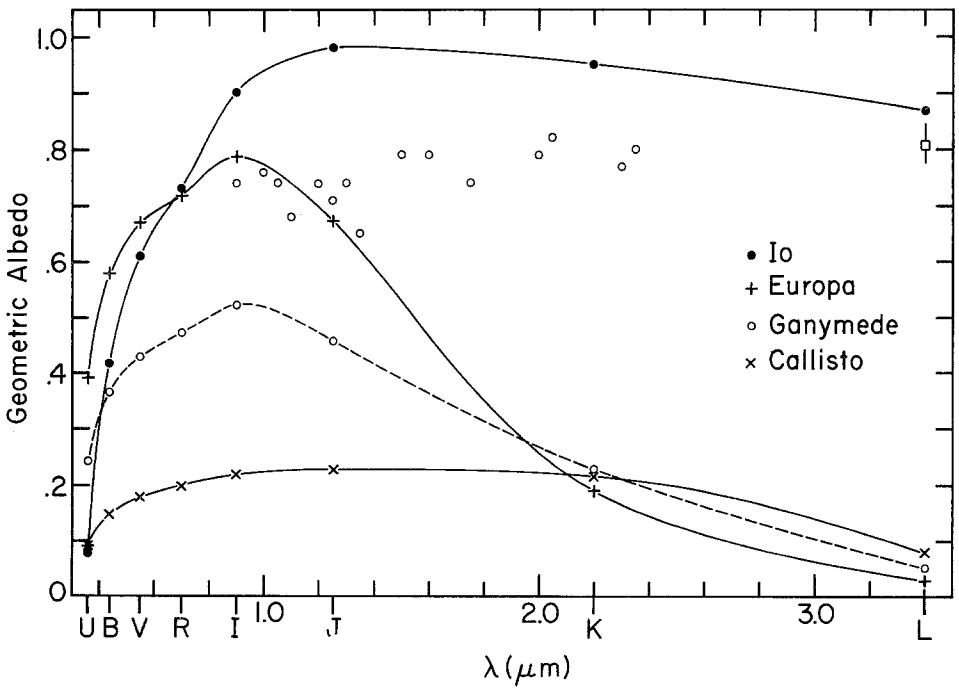

Fig. 9. Geometric albedos of the Galilean satellites from the broad-band data of Lee (1972). Lee's magnitudes were normalized to the geometric albedos at 0.55 μm given by Morrison *et al.* (1974); see Table VIII. Also included are data (unconnected circles) for Io from Johnson and McCord (1971) likewise normalized at 0.55 μm. Uncertainties in the Johnson and McCord data are approximately plus or minus 10%. The open square is a point for Io from Gillett *et al.* (1970).

and with interferometric spectrometers. We begin with the broad-band photometry from 0.3 to 3.4 μm by Lee (1972). From Lee's magnitudes, we have computed the geometric albedos, normalized to the geometric albedos at 0.55 μm given in Table VII; the results are shown in Figure 9. These and all albedos in this paper are corrected to correspond to the radii in Table V. The points plotted in Figure 9 are means of all of the measurements made of the individual satellites at the given wavelengths without correction for rotational variations. Because the observations were all made within a few days of opposition (in 1971), the computed albedos for Callisto, as a consequence of Callisto's larger opposition effect, may be systematically too high relative to those of the other satellites.

Also plotted on the same graph are some data points from the higher spectral resolution photometry of Io by Johnson and McCord (1971), normalized to agree with Lee at 0.55 μm. The disagreement between these data and those of Lee is substantial. The Lee data can also be compared with similar broad-band infrared observations by Gillett *et al.* (1970), who compiled data from several sources and added their own observations. We have included one point from Gillett *et al.* for Io at 3.4 μm in Figure 9 to demonstrate again the disagreement among different observers' results. Significantly, the shapes of the curves over this wavelength interval, as given by Lee and Gillett *et al.*, are in substantial agreement, but the absolute values of the albedos vary widely and not systematically. The Lee data have the virtue of having been obtained by one observer using a well-established photometric system, and probably have the highest internal accuracy of any similar data available, but we do not pretend to understand the discrepancies in the overall albedo differences.

Most information on the wavelength dependence of albedo of these satellites comes from multifilter spectrophotometry. Johnson (1971) and Johnson and McCord (1970) observed the Galilean satellites over the wavelength range 0.3 to 1.1 μm with a double-beam photometer and 24 filters with bandwidth varying between 0.02 and 0.05 μm. The same data with an improved calibration are also presented in a later publication (Johnson and McCord, 1971) together with the data at longer wavelengths, a part of which are plotted in Figure 9. Since the publication of this multifilter photometry, a similar investigation at higher spectral resolution has been carried out by Wamsteker (1972), who observed with 42 filters of bandwidth 0.02 μm. We list the data from both authors, normalized to the albedos at 0.55 μm adopted in this review, in Table VIII and plot them in Figure 10. These data clearly show the general variation of albedo with wavelength and reveal a shallow absorption feature at 0.55 μm in the reflectivities of Io and possibly of Europa and Ganymede as well. However, the data do not agree well in detail, particularly at the short- and long-wavelength extremes. A part of this difficulty, but not all of it, may result from the failure of Wamsteker to take into account the rotational variations of the satellites (cf. Figure 7); since different parts of his curves were obtained on different nights, substantial systematic errors could be present in his albedo curves. We conclude that definitive visible and near-infrared albedos for the Galilean satellites have not yet been measured.

The first spectrophotometric observations of the Galilean satellites in the infrared (1 to 4 μm) were made with scanning spectrometers by Kuiper (1957) and Moroz (1965). Kuiper never published his observations, and the low spectral resolution and lack of a sensitive detector limit the usefulness of Moroz's data; however, both of these investigators noted the high infrared albedo of Io and the decrease by a factor of more than 2 in the albedos of Europa and Ganymede beyond 1.5 μm. Kuiper suggested on the basis of the apparent absorption between 1.5 and 2.5 μm that the surfaces of Europa and Ganymede are covered with H_2O snow. Moroz's data extended to 3.4 μm and gave fairly strong evidence for discrete bands at 1.6 and 2.0 μm in the spectra of Europa and Ganymede; he too suggested their identification with H_2O ice. Gromova *et al.* (1970) observed Ganymede from 1.0 to 2.0 μm at a resolution 5 times greater

than that of Moroz in order to improve the definition of the 1.6-μm absorption band. Moroz's spectra of all the Galilean satellites at wavelengths from 1.0 to 2.5 μm were further confirmed by the multifilter observations by Johnson and McCord (1971).

All of these low-resolution infrared observations suggested that H_2O frost is present on Europa and Ganymede, but not on Io and Callisto. However, their resolution was

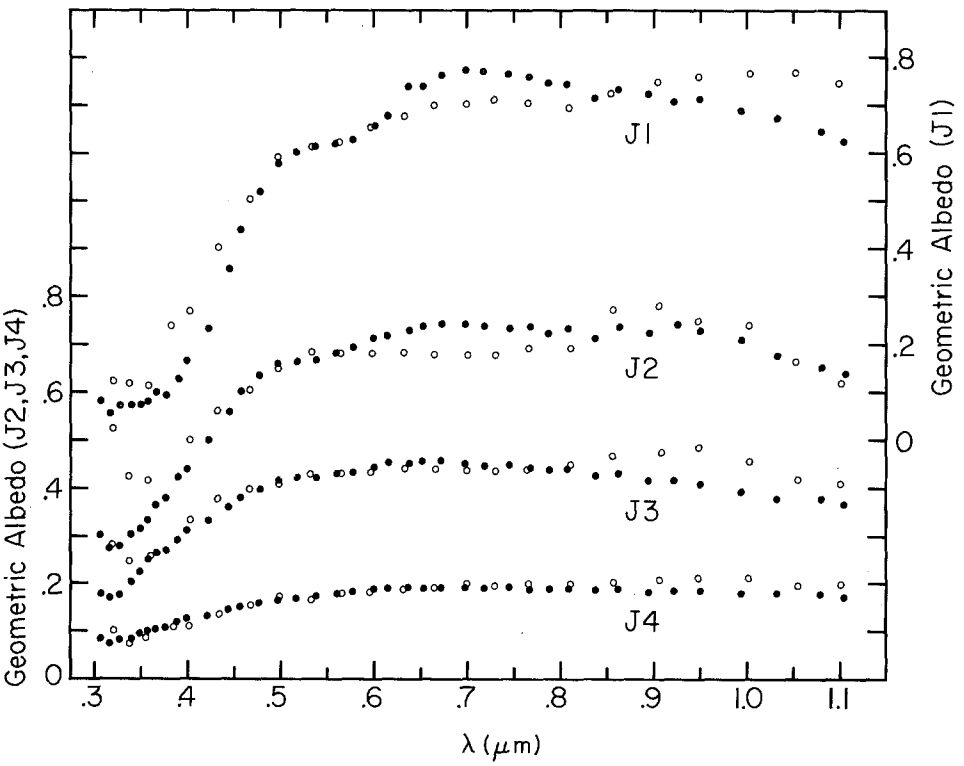

Fig. 10. Wavelength dependence of geometric albedo for the Galilean satellites from the data of Johnson (1971) and Johnson and McCord (1971) (open circles) and of Wamsteker (1972) (filled circles), normalized at 0.55 μm to the albedos given by Morrison *et al.* (1974); see Tables VIII and IX. The observations were made with narrow interference filters as described in the text, using S-20 (0.30–0.72 μm) and S-1 (0.72–1.1 μm) detectors.

insufficient to exclude the possibility that the absorbing material might be NH_3 frost, which has an infrared spectrum similar to that of low-temperature H_2O frost (cf. Kieffer, 1970; Kuiper *et al.*, 1970). Nor was it possible to attempt a quantitative analysis of these spectra in terms of the fraction of the surfaces of each satellite that might be frost covered.

A crucial improvement in spectral resolution and signal-to-noise ratio came with the application of interferometric spectrometers in 1972, when Pilcher *et al.* (1972) and Fink *et al.* (1973) simultaneously obtained spectra of the Galilean satellites between 1 and 4 μm with resolutions of about 30 cm^{-1}, ample to show broad features due to solid state absorptions. The data of Pilcher *et al.* are illustrated in Figure 11.

Both groups of authors conclude, from comparison of their observations with laboratory spectra, that H_2O ice is a dominant constituent of the surface of Ganymede and Europa, and Pilcher *et al.* also suggest that it is indicated weakly in the spectra of Callisto. Io, on the other hand, shows a high reflectivity throughout this spectral region with no deep absorption bands. Pilcher *et al.*, from an analysis of the depths of the ice bands, conclude that for Europa between 50% and 100% of the surface is exposed ice, for Ganymede between 20% and 65%, and for Callisto between 5% and 25%. These quantities of ice, if it is presumed that the rest of the surface consists of dark material, are consistent with the geometric albedos of these three satellites, and Pilcher *et al.* suggest that a variation in only one parameter – the fraction of the surface that is covered by ice – may explain the gross differences among them in both albedo and infrared spectrum.

The multi-color photometry and moderately high-resolution spectroscopy of the Galilean satellites have given a relatively clear description of the reflection properties of the surfaces of these bodies between 0.3 and 4.0 μm. In general, the satellites all show a very low ultraviolet albedo, although this effect is less pronounced for Callisto because its albedo at longer wavelengths is also low. The low ultraviolet albedo is atypical of pure frosts, leading to the suggestion that the probable surface frosts contain admixtures of other compounds. The change in shape of the albedo curves from Ganymede to Io might be related to the interaction of these satellites with the Jovian radiation belts. Such an interaction was suggested by Binder and Cruikshank (1964) as a possible source of temperature-sensitive free radicals on the surface of Io. Veverka (1971b) and Sagan (1971) also called attention to this possibility, suggesting specifically that water ice containing small amounts of CH_4 and NH_3 has been modified by the Jovian trapped radiation to form strongly ultraviolet absorbing radicals, polymers, and organic compounds. Among the suggested compounds are NH, CH, CH_3I, $(NH_2NH)_n$, CH_3, CS, polymers of HCN, C_2N_2 and $HCN \cdot NH_3$. Others have proposed NH_4SH (Kuiper, quoted in Lee, 1972), radiation damaged ammonium hydrosulfates (Lebofsky, 1972), and ultraviolet-irradiated ices (Lebofsky, 1973), but many of these compounds can now be eliminated on the basis of the near-infrared reflection spectra by Fink *et al.* (1973) and Pilcher *et al.* (1972) because of their strong absorption features in that spectral range.

Short-term brightness variations have been observed following eclipses of Io, beginning with the work of Binder and Cruikshank (1964). This topic will be discussed in the section on atmospheres of the Galilean satellites. Eclipse photometry can also be used to investigate limb darkening on these satellites. The rate of change of brightness as the satellite moves into or out of the shadow of Jupiter is a function of the angular size, the distribution of albedo features, and the east-west limb darkening. Reductions of eclipse photometry in which the satellites are assumed to be uniformly bright disks (Price and Hall, 1971) have yielded radii smaller than the correct values, suggesting the presence of limb darkening. In a preliminary report on the interpretation of a substantial body of observations, Green *et al.* (1973) use the recent occultation radius of Ganymede and show that this satellite definitely is limb darkened, al-

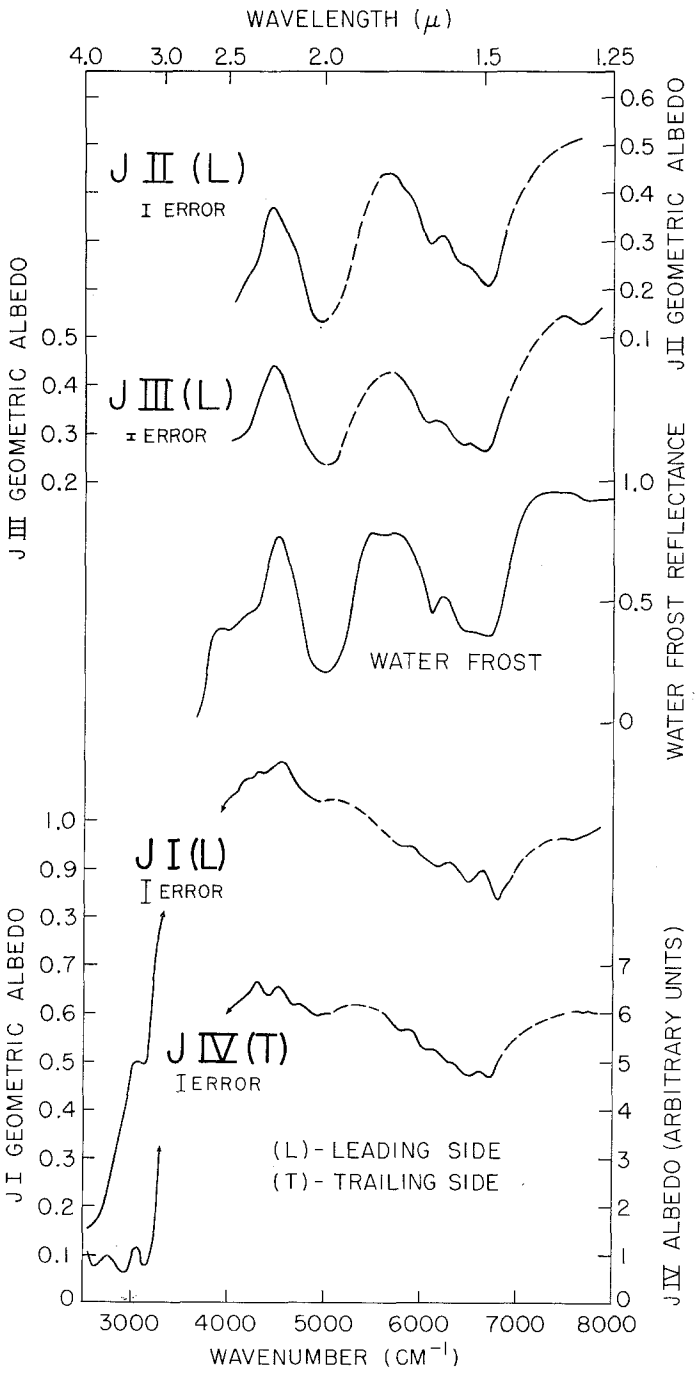

Fig. 11. Near-infrared reflection spectra of the Galilean satellites and water frost. The geometric albedo scales for J1, J2, and J3 were established by comparison of the curves given here with the multi-filter photometry of Johnson and McCord (1971) and are not necessarily consistent with the geometric albedos in Figures 9 and 10. Adapted from Pilcher *et al.* (1972).

though by less than a corresponding lambertian surface. Many new findings on both the limb darkening and the distribution of albedo features on the Galilean satellites can be expected to result from an extensive series of photometric observations of mutual eclipses and occultations as both Earth and Sun pass through the orbital plane of these satellites in the second half of 1973 (cf. Brinkman and Millis, 1973; Brinkman, 1973; Murphy and Aksnes, 1973).

In concluding this section on photometry and spectrophotometry of the Galilean satellites, we stress the surprising degree of inconsistency among observers and the frequent absence of high-quality data. In spite of the fact that these satellites are of visual magnitude 5 to 6, it is clear that there are substantial gaps in our understanding, as evidenced, for instance, by the spread of more than 0.2 mag. in the mean V-magnitudes of Io published within the past two decades. We conclude that even today the phase coefficients of Callisto are not known, and the variation in phase coefficient for this satellite with orbital phase reported 50 yr ago is not verified; for all of the Galilean satellites, the degree to which the bright and dark hemispheres are aligned with the orbital velocity is in dispute; the brightnesses near 1 μm are uncertain by at least 20%, and at longer wavelengths these uncertainties may be twice as large; and no investigation has been made of color variations with rotation at wavelengths longer than 1 μm. These are all straightforward problems that we hope will be settled in the near future.

6.3. Polarimetry

The variation with phase angle of the linear polarization of light reflected from the Galilean satellites, together with photometric data, give information on the structure of the microsurface. The phase angle of Jupiter varies over a sufficient range (12°) to permit the definition of a small but significant part of the polarization curves for the satellites. We have combined the published data of Veverka (1971b) and Dollfus (1971) in Figure 12. Veverka's broadband data include the spectral region between 0.3 and 0.8 μm and are reproducible to 0.1%, while the wavelength of Dollfus' data and the formal errors are not specified.

While the scatter in the data in Figure 12 is quite large, the maximum depth of the negative branch and the cross-over (inversion) angle, where $P=0$, can be estimated for each satellite. The depth of the negative branch of Io, Europa, and Ganymede is -0.4% or less and the inversion angles are in the range $7-12°$. This information, together with the photometrically established phase coefficients and high visual albedos, point to surfaces composed mostly of bright material in which incident sunlight is multiply scattered. Veverka (1971b) suggested on this basis that the surfaces of the inner three Galilean satellites are mostly covered with frost.

Callisto is different from the inner three satellites in that it shows a pronounced negative polarization and larger inversion angle. Taken with the photometric evidence for Callisto's relatively low albedo and the large opposition effect, the polarization data suggest a particulate surface of dark material in which multiple scattering is hindered. As Veverka (1971b) notes, a close analogy with the lunar surface cannot be drawn because the inversion angle is considerably less than the lunar value of 23°,

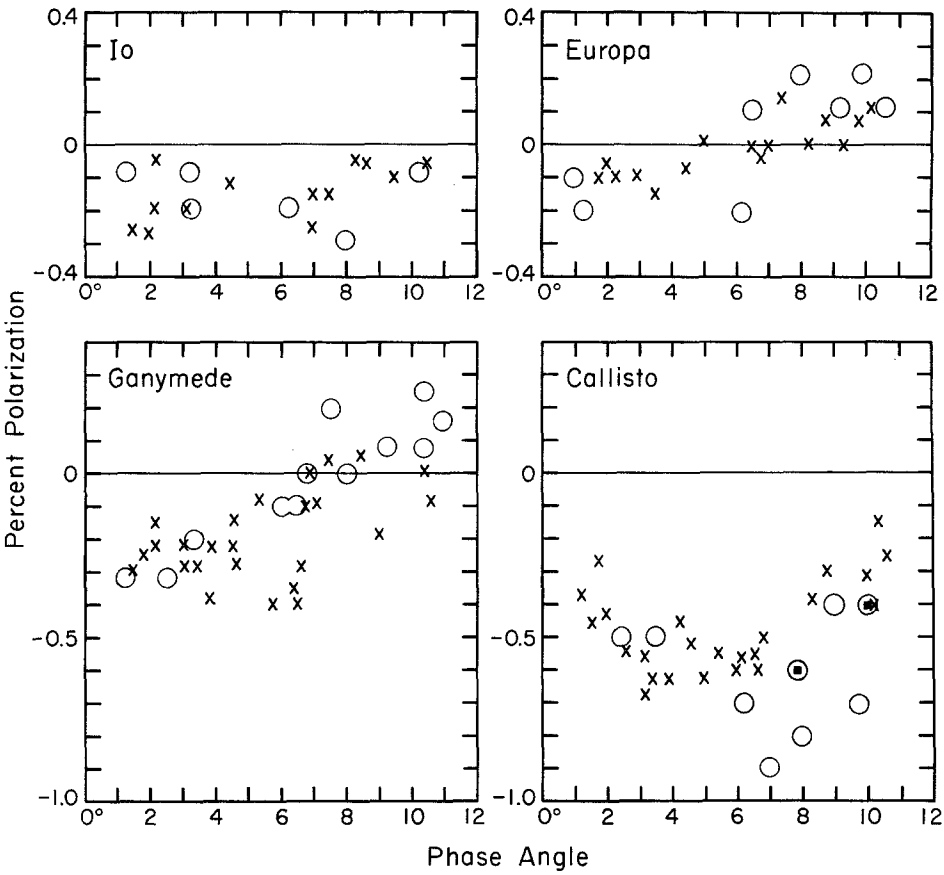

Fig. 12. Polarization observations of the Galilean satelites. Open circles are from Veverka (1971b); the circles with central squares on the Callisto graph are Veverka points for the trailing side of the satellite. Crosses are data from Dollfus (1971).

although the depth of the negative branch is to some degree comparable to that of the Moon (1.2%). Veverka (1917b) suggests that Callisto is covered either with patches of frost or with a uniform coating of frost with patches of dark absorbing material. We will return to this point after discussing the evidence for the microstructure of the surface of these satellites obtained from their thermal properties.

The most recent polarimetric observations of this satellite, by Gradie and Zellner (1973) and Dollfus and his collaborators (private communication, 1973), also clearly demonstrate substantial differences in the phase curves for the leading (darker) and trailing (brighter) sides. These differences are greater than would be expected for surfaces of similar microstructure that differ only in albedo, and their interpretation may yield important information on the influences of the nearspace environment of Callisto on its surface.

6.4. Temperatures and Thermophysical Properties

Thermal infrared radiation from the Galilean satellites was first measured in the 8- to

14-μm atmospheric window by Murray *et al.* (1964a) and Low (1965). Their results were expressed in terms of brightness temperature, which is the temperature of an isothermal black disk of the same angular size as the satellite that radiates an equivalent flux density; these temperatures varied from $\simeq 120$K for Europa to $\simeq 160$K for Callisto. The subsolar temperature of a blackbody at the distance from the Sun of the Galilean satellites would be 170K. The observed temperatures, while providing a convenient way to express the disk-averaged flux density within the passband, should not, of course, be interpreted as corresponding to the sub-solar or any other physical temperature on the satellite. The difference between the brightness temperature and 170K is a function primarily of Bond albedo and of the passband, but also probably of the emissivity and rotation rate of the satellite; in addition, any errors in the radii are carried over into the brightness temperatures, and often in the past observers have failed to give the radii that they used in their data reduction

Table X summarizes the more modern determinations of infrared brightness temperatures by Gillett *et al.* (1970), Hansen (1972), Morrison *et al.* (1972), and unpublished data by one of us (DM), all adjusted to the radii given in Table V. The agreement among observers, while generally consistent with grey-body emission when proper allowance is made for the expected passband dependence of the brightness temperature (cf. Morrison *et al.*, 1972), suggests a flux deficiency in the 20-μm band for Io and Europa. Hansen (1972) interprets this deficiency as indicating a lower emissivity in this band.

Sufficiently accurate broad-band radiometry can, in principle, be utilized together with the known radii and geometric albedos of these satellites to derive either the photometric phase integral q or the thermal emissivity in the forward direction. To understand this procedure, recall that the phase integral is defined at any wavelength as the ratio of the Bond albedo A to the geometric albedo p. We then define a 'bolometric' phase integral as follows:

$$q_{\mathrm{bol}} \equiv A_{\mathrm{bol}}/p_{\mathrm{bol}}. \tag{4}$$

Given the radius and the visible and near-infrared photometry, we can calculate p_{bol} for these satellites, while the radiometric flux density is proportional to $(1-A_{\mathrm{bol}})$ and to the emissivity. Thus, either q_{bol} or the emissivity can be found, but not both. Hansen (1972) has utilized this approach to derive values of the phase integral on the assumption that the Galilean satellites have emissivities that must, averaged over all angles, be near unity at 10 μm and that further show approximately the angular dependence observed for the Moon. Since the thermal conductivities of the satellites are very low (see following discussion), it is possible to ignore radiation from the unilluminated hemisphere. He finds that the observed brightness temperatures are a few degrees lower than would have been calculated with a lunar value for the phase integral; therefore, the value of A_{bol} must be larger than expected, and q_{bol} is larger than the lunar value. The method is most useful for objects of high albedo, such as Io and Europa. For these two satellites, Hansen finds values of q_{bol} between 0.8 and 1.1.

The observations by Hansen (1972), primarily at 10 μm, and by Morrison and Cruikshank (1973) at 20 μm, show variations in radiometric brightness with orbital phase of up to ± 0.5 mag. for the inner three satellites. No significant variations are expected for Callisto, due to its low albedo. The observed variations are generally consistent with the variations in the visual albedos as these satellites rotate, and as noted by Morrison (1973c), these variations can be used to derive a mean phase integral (q) for the satellites. Since the amplitude of variation in the visible is proportional to the variation in p_V, while the radiometric amplitude is proportional to the variation in $(1-A_{bol})$, it is possible, if the radius is known and the assumption is made that q does not vary greatly with wavelength or with position on the satellite, to solve

TABLE IXa

Geometric albedos derived from spectrophotometry by Johnson (1971) and Johnson and McCord (1971)

$\lambda(\mu m)$	Io	Europa	Ganymede	Callisto
0.319	0.13	0.53	0.28	0.11
0.338	0.12	0.43	0.25	0.08
0.358	0.11	0.42	0.25	0.09
0.383	0.24	–	0.42	0.11
0.402	0.27	0.51	0.33	0.12
0.433	0.40	0.56	0.38	0.15
0.467	0.50	0.61	0.40	0.17
0.498	0.59	0.65	0.41	0.17
0.532	0.61	0.69	0.43	0.18
0.564	0.62	0.68	0.43	0.19
0.598	0.66	0.68	0.44	0.19
0.633	0.68	0.69	0.44	0.20
0.665	0.70	0.68	0.44	0.20
0.699	0.70	0.68	0.44	0.21
0.730	0.71	0.68	0.44	0.21
0.765	0.71	0.70	0.45	0.21
0.809	0.70	0.69	0.45	0.21
0.855	0.73	0.77	.047	0.21
0.906	0.75	0.78	0.48	0.22
0.948	0.76	0.75	0.49	0.22
1.002	0.77	0.69	0.46	0.22
1.053	0.77	0.66	0.42	0.20
1.101	0.75	0.62	0.42	0.21

directly for q. Morrison (1973c) derived values of $q=1.0\pm 0.3$ for Io and $q=1.0\pm 0.1$ for Europa, and undoubtedly further refinements in the visible and infrared photometry will permit these values to be defined with still higher precision. The results for these two satellites are in agreement with those obtained by Hansen (1972). For satellites with lower albedos, such as Ganymede and Callisto, neither the method of Hansen nor that of Morrison is as sensitive; however, we would expect the phase integral for these two satellites to be intermediate between those of Io and Europa on the one hand and the Moon and Mercury on the other. For the calculation of the

TABLE IXb

Geometric albedos from spectrophotometry by Wamsteker (1972)

$\lambda(\mu m)$	Io	Europa	Ganymede	Callisto
0.308	0.08	0.30	0.18	0.09
0.318	0.06	0.28	0.17	0.07
0.328	0.07	0.28	0.18	0.08
0.340	0.07	0.31	0.21	0.09
0.350	0.08	0.31	0.23	0.10
0.358	0.08	0.33	0.25	0.11
0.368	0.10	0.37	0.27	0.12
0.378	0.10	0.38	0.27	0.12
0.390	0.13	0.42	0.29	0.13
0.399	0.17	0.44	0.31	0.13
0.423	0.26	0.50	0.33	0.14
0.444	0.36	0.56	0.36	0.16
0.457	0.44	0.60	0.38	0.16
0.478	0.52	0.64	0.40	0.17
0.498	0.58	0.66	0.42	0.18
0.518	0.60	0.67	0.42	0.18
0.538	0.61	0.67	0.42	0.19
0.560	0.62	0.68	0.43	0.19
0.578	0.63	0.70	0.43	0.20
0.599	0.66	0.72	0.45	0.20
0.615	0.68	0.72	0.46	0.20
0.637	0.74	0.73	0.46	0.20
0.652	0.74	0.74	0.46	0.20
0.672	0.76	0.74	0.46	0.20
0.698	0.78	0.74	0.45	0.20
0.717	0.77	0.74	0.45	0.20
0.746	0.77	0.73	0.45	0.20
0.767	0.76	0.74	0.44	0.20
0.787	0.75	0.73	0.44	0.20
0.808	0.75	0.73	0.44	0.20
0.838	0.72	0.72	0.43	0.20
0.862	0.74	0.74	0.44	0.20
0.894	0.73	0.73	0.42	0.20
0.923	0.71	0.74	0.42	0.20
0.950	0.71	0.73	0.41	0.20
0.996	0.69	0.71	0.40	0.19
1.032	0.67	0.68	0.38	0.19
1.080	0.65	0.65	0.38	0.19
1.195	0.62	0.64	0.37	0.18

equilibrium temperatures of the Galilean satelites in Table X we have adopted q values of 1.0, 1.0, 0.8, and 0.6 for Io through Callisto, respectively, each with an assumed uncertainty of ± 0.2.

In 1970 Gorgolevsky reported the possible detection of thermal radiation from Callisto at the much longer wavelength of 3.5 mm, with a brightness temperature of 250 ± 80 K. Although this temperature is higher than the infrared temperatures by less than twice the stated uncertainties, Kuzmin and Losovsky (1973) have accepted

this difference and attempted to explain it in terms of the structural models of Lewis. Laboratory studies of ice indicate that, if there is no significant admixture of silicates, then the 3.5-mm transparency could be sufficient for the effective depth of radio emission to be ~ 100 km, and the high temperature would be a natural consequence of the lapse rate in the crust. However, pure ice models are unlikely for the crust of Callisto. In the near future, improvements in radio equipment should permit much more accurate millimeter-wave measurements of the Galilean satellites.

Infrared radiometric observations of the thermal response of the surface to changing insolation can be used to study the thermophysical properties of the uppermost surface layers of the satellites. Earthbased observations cannot explore the diurnal temperature variations (maximum phase angle 12°), but they can be used to investigate the

TABLE X

Temperatures of the Galilean satellites[a]

	$\lambda(\mu m)$	Io	Europa	Ganymede	Callisto
A_{bol}	–	0.62 ± 0.13	0.68 ± 0.14	0.35 ± 0.08	0.11 ± 0.03
T_{max} (calculated)[b]	–	137 ± 10	132 ± 11	157 ± 5	170 ± 2
T_B (calculated)	10–20	126 ± 10	121 ± 10	144 ± 6	156 ± 4
Gillett *et al.* (1970)	11–12	139 ± 3	131 ± 3	142 ± 3	157 ± 3
Hansen (1972)	8–14	137 ± 3	130 ± 3	142 ± 3	152 ± 4
Morrison (unpublished)	8–14	138 ± 4	129 ± 4	145 ± 4	153 ± 5
Morrison *et al.* (1972)	17–28	128 ± 5	121 ± 5	138 ± 5	151 ± 7
Hansen (1972)	17–25	124 ± 4	120 ± 4	132 ± 5	142 ± 6
Morrison (unpublished)	17–28	130 ± 3	121 ± 3	143 ± 4	155 ± 5

[a] All values are reduced to the radii given in Table V, and the uncertainties are calculated without including any uncertainties in the radii.

[b] Calculated on the assumption that a black surface at the distance of Jupiter from the Sun would have a brightness temperature of 175°K when illuminated and viewed at normal incidence.

temperature changes resulting from eclipses, which take place once each orbit for the inner three Galilean satellites and less frequently for Callisto. The first measurements of thermal emission of a satellite during eclipse were made in 1963 by Murray *et al.* (1964b), who observed the intital cooling and final heating phases of an eclipse of Ganymede in the 8- to 14-μm band. Although they could not detect the satellite during mid-eclipse, they were able to conclude from the rapid temperature changes they observed that Ganymede must have a thermal conductivity at least as low as that of the Moon. The first radiometry throughout an eclipse was obtained in the 16- to 28-μm band by Morrison *et al.* (1971), who showed that the conductivity of Ganymede was substantially lower than that of the Moon. Subsequently, Hansen (1973) and Morrison and Cruikshank (1973) made extensive eclipse observations of all four satellites, and their results form the basis of the following discussion.

The easiest eclipses to observe and to interpet are those of the outer two satellites, Ganymede and Callisto. Both are very bright at 10 and 20 μm, and the eclipses take place sufficiently far from the planet that scattered thermal radiation does not con-

taminate the observations, which can be continued throughout the eclipse. Further, the interpretation does not require taking into account non-solar sources of energy, whether infrared radiation from Jupiter or particles in the magnetosphere of the planet. Figure 13, taken from Morrison and Cruikshank, shows observations at 10 and 20 μm of the eclipse of Callisto of 11 August 1972. Since the satellite passed near the edge of the planet's shadow, the rise and fall in insolation took place relatively slowly, each requiring about 25 min, as compared to 4 min for a typical eclipse of Io. In the upper part of the figure, we illustrate a homogeneous thermal model that has been used to generate eclipse curves in the two passbands, contrained to fit the observed minimum residual brightness at 20 μm of 0.09 ± 0.01 of the pre-eclipse value. Such a model is clearly inadequate. In the lower part of the figure, calculations are shown for a two-layer model, in which the thermal inertia (defined as $(K\varrho c)^{1/2}$, where K is thermal conductivity and ϱc is heat capacity per unit volume) of the upper layer

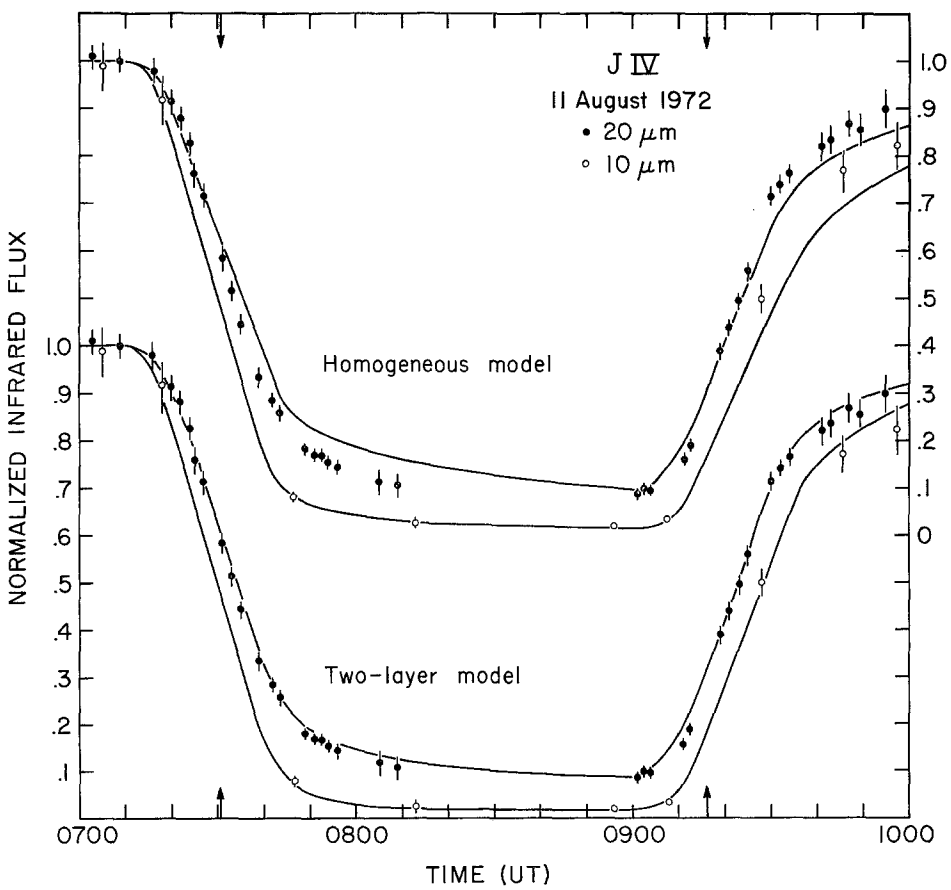

Fig. 13. Radiometric observations of an eclipse of Callisto at 10 and 20 μm with best-fit homogeneous and two-layer surface models. The arrows mark the photometric half-intensity times. The homogeneous model is characterized by a thermal inertia of 1.2×10^4 erg cm^{-2} s$^{-1/2}$K^{-1}; the parameters of the two-layer model are given in Table XI. From Morrison and Cruikshank (1973).

is much less than that of the lower one. This two-parameter model (thermal inertia and thickness of the upper layer) is able to fit to all of the observations satisfactorily. Since the cooling of a typical surface element during eclipse has a five-fold greater effect on the radiated flux at 10 μm than at 20, the agreement with the model at both wavelengths precludes the exposure on the surface of any significant amount of material of higher thermal conductivity and consequent smaller temperature drop during eclipse. A two-layer model with nearly identical numerical parameters has been found independently by Hansen (1973) and Morrison and Cruikshank (1973) to fit their combined observations of several eclipses of Ganymede.

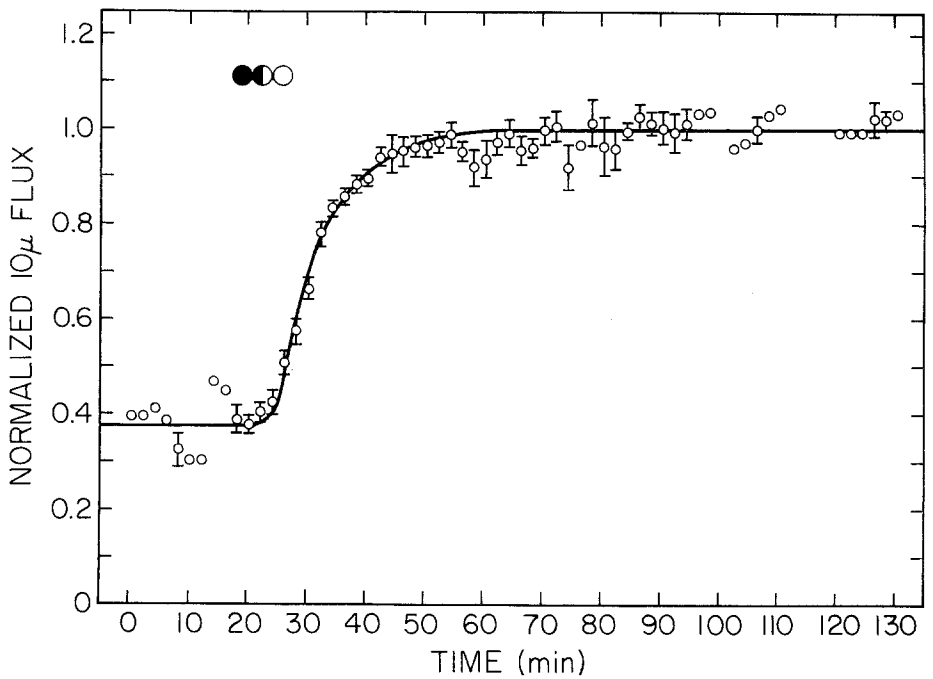

Fig. 14. Thermal observation of the heating phase of an eclipse of Io in the 10-μm band. Circumstances of the eclipse are shown by circles in the upper left. The continuous curve is the best fitting two-layer model, as given in Table XI. From Hansen (1973).

For the inner two satellites the eclipse radiometry is more difficult to obtain, in part because the cooling and heating curves must be observed at different eclipses and then combined with proper normalization, and the observations and interpretations are less satisfying. Figure 14 illustrates a composite 10-μm eclipse reappearance curve of Io obtained at the Hale 5-m telescope by Hansen (1973). While the same sort of two-layer model fits the data, note that the residual flux level just before third contact is nearly an order of magnitude higher than was the case for Callisto or Ganymede. In consequence, Hansen finds that the thermal inertia of the uppermost layer of Io is much larger than that of the outer two satellites. On the other hand, Morrison and Cruikshank, observing only at 20 μm, do not find the pre-third-contact

TABLE XI

Thermal models of the Galilean satellites from eclipse radiometry

Parameter	Io	Europa	Ganymede	Callisto	Reference
Thermal inertia $= (K\varrho c)^{1/2}$	1.3 ± 0.4	<4	1.4 ± 0.2	1.0 ± 0.1	1
(10^4 erg cm^{-2} s$^{1/2}$K^{-1})	3.8 ± 0.3	1.4 ± 0.4	1.2 ± 0.3	–	2
Thermal parameter $= (K\varrho c)^{-1/2}$	3200 ± 1000	>1000	3000 ± 400	4200 ± 400	1
(cal^{-1} cm^2 s$^{1/2}$K)	1100 ± 100	3000 ± 1000	3400 ± 700	–	2
Mass of upper layer	0.10 ± 0.04	–	0.15 ± 0.03	0.11 ± 0.02	1
(g cm^{-2})	0.11 ± 0.03	0.10 ± 0.05	0.19 ± 0.03	–	2

1: Morrison and Cruikshank (1972)
2: Hansen (1972)

brightness of this satellite to be anomalous, and they derive a thermal inertia for its surface similar to that for Callisto and Ganymede. No thermal model that involves only heat conduction in a solid surface material is compatible with both sets of observations, and the authors make only the comment, standard in such cases, that the observations should be repeated for verification. Sinton (1973), however, has advanced an explanation in terms of atmospheric thermal emission in the 10-μm band; this will be discussed further when we come to the problem of atmospheres of the Galilean satellites.

Leaving aside the anomalous behavior of Io, the eclipse radiometry provides some useful clues as to the nature of the surfaces, at least of Callisto and Ganymede. Table XI summarizes the results of fitting models to the observations. Even though the thermal models used by Hansen and by Morrison and Cruikshank are crude, they clearly show that the uppermost few millimeters of the surface must consist of a material of remarkably low thermal conductivity, nearly an order of magnitude lower than that on the Moon, and that below this layer there must be a fairly rapid transition to a material of much higher conductivity and, probably, of higher density. Further, there can be no significant exposure of this underlying material; Morrison and Cruikshank set the upper limit at 1% of the surface for Callisto and 5% for Ganymede. It is difficult to understand how such a structure could be maintained in an environment of repeated meteoroid bombardment, unless the surface material consolidates and refuses below the surface following impact. A model is therefore suggested in which volatiles play an important role: the low-conductivity layer is a low-density frost, and the high-conductivity layer is ice or an ice-dust-rock matrix. Such a model is consistent with the spectroscopic detection of water ice and with the presence of (possibly variable) atmospheres of very low density. It is not apparent, however, why the thermophysical properties of Callisto and Ganymede should be so similar when their albedos and infrared spectra are so different. We further note that there is no independent evidence for any substantial amount of frost on Callisto.

6.5. Atmospheres

Because of their low surface gravity, the Galilean satellites are not expected to have

substantial atmospheres, and those observations that suggest the presence of atmospheres have tended to be controversial. We will begin this discussion with the recently applied occultation technique before turning to the other observations. One of the most sensitive tests for the presence of an atmosphere occurs when a satellite occults a bright star. Refractive bending of the starlight by a tenuous atmosphere delays the extinction of the star's light for up to a few seconds, depending on the diameter of the satellite and its motion relative to the star and Earth. Accurate determination of the shape of the extinction curve of the star can thus be used to estimate the number density of molecules (of some assumed mean molecular weight) in the satellite's atmosphere. In 1971, Io occulted β Scopii C, as discussed in the section on satellite radii. Both the disappearance and reappearance of the star were essentially instantaneous. Smith and Smith (1972) use the occultation photometry to set upper limits of 0.9×10^{-7} and 1.3×10^{-7} for the surface partial pressure of CH_4 and N_2, respectively, and slightly larger values result from a similar analysis by Bartholdi and Owen (1972). More recently, Carlson *et al.* (1973) have reported photometric observations of an occultation of SAO 186800 by Ganymede on 7 June 1972. They indicate that the ingress and egress data show a gradual change in brightness over a period of several seconds, suggesting a pressure at the occultation level of at least 10^{-6} bar. However, the brightness change of star plus satellite was only about 5%, and the published photometric tracings are not strongly convincing. Combining their result with an upper limit indicated by eclipse radiometry (Morrison *et al.*, 1971; Morrison and Cruikshank, 1973; Hansen, 1973), they place the surface atmospheric pressure on Ganymede as greater than 10^{-6} bar but less than 10^{-3} bar. If the atmospheric surface pressure on Ganymede is greater than 10^{-6} bar, the gas is evidently not CH_4 or NH_3, because smaller upper limits have been placed on the number density of these gases from spectroscopic studies (see below). Nitrogen remains a strong possibility, but we urge caution in interpretation of these occultation observations.

Searches for atmospheres of NH_3, CH_4 and CO_2 by photographic spectroscopy of the Galilean satellites (Kuiper, 1952; Owen, 1965) yield upper limits of the order of 100 m-amagat; for CH_4, this abundance corresponds to a partial surface pressure on these satellites of $\sim 10^{-5}$ bar. A positive result reported by Kalinyak was shown by Binder and Cruikshank (1966b) to be in error. Low resolution spectra in the near infrared (0.9 to 2.5 μm) by Moroz (1965; 1967, p. 473) and Gromova *et al.* (1970) also failed to give evidence for atmospheres. The most restrictive upper limits have been set recently by Fink *et al.* (1973) from their higher-resolution (25 cm^{-1}) spectroscopy in the 1- to 4-μm region. For each Galilean satellite, they find an upper limit for CH_4 and NH_3 of 5 mm-amagat, corresponding to partial pressures of approx 6×10^{-8} bar.

The initial evidence for an atmosphere on one of these satellites came from eclipse photometry by Binder and Cruikshank (1964, 1966a). Immediately following the emergence of Io from the shadow of Jupiter they found an excess brightness of about 0.1 mag. in blue light, which persisted for about 15 min; similar observations of the

other satellites and of Io at eclipse ingress showed no comparable effect. Binder and Cruikshank therefore suggested that the post-eclipse anomaly might be due to an atmospheric constituent that precipitates during eclipse, leaving the surface slightly frosty and higher in albedo; in about 15 min after reappearance the frost sublimates, returning the surface to its normal appearance. The original eclipse curves published by Binder and Cruikshank are illustrated in Figure 15.

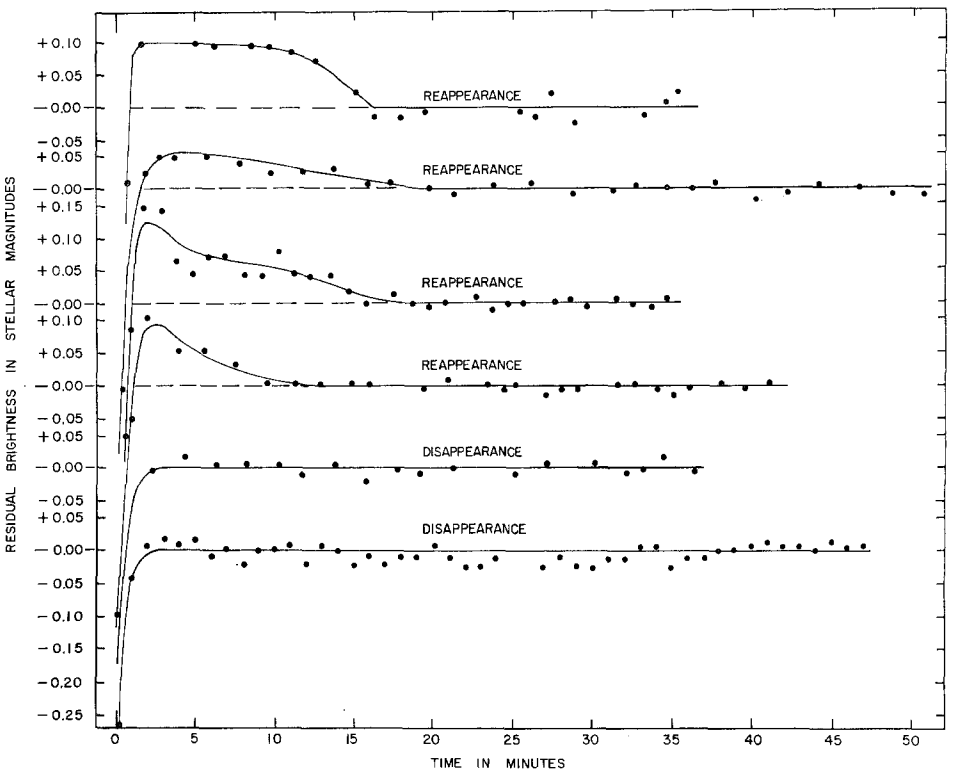

Fig. 15. Photometric (*B*-band) observations of four eclipse reappearances and two disappearances of Io in 1962 and 1963. The post-eclipse brightening varies between 0.05 and 0.12 mag. in the reappearance curves, persisting for about 15 min. From Binder and Cruikshank (1964).

A number of observers have subsequently searched for this post-eclipse anomaly, with both positive and negative results. Using an area-scanning technique, Franz *et al.* (1969) and Franz and Millis (1970) found no brightening greater than their uncertainty of 0.03 mag. in observations of several reappearances of Io. Johnson (1969, 1971) observed one reappearance with a double beam photometer and found a sharply peaked anomaly of 0.7 mag.(!); Veverka, observing the same eclipse with lower time resolution found an anomaly of about 0.1 to 0.2 mag. (O'Leary and Veverka, 1971). Two other eclipses observed by O'Leary and reported in the same paper yielded inconclusive results. Fallon and Murphy (1971) observed four events in 1970 and found no brightening at the 0.02 mag. level. O'Leary and Miner (1973) observed

one eclipse simultaneously with a marginal positive result. Most recently, Cruikshank and Murphy (1973) found, for 5 events, two positive results (brightening 0.1 mag.), one probable, one uncertain, and one clearly negative result.

Most of these observations were made in blue light, where the low albedo of Io increases the likelihood of detecting a brightening of the surface. Three photometric techniques have been used: conventional single-beam photometry with manual offset to the sky; double-beam photometry with automatic sky chopping; and area-scanning photometry. The virtues of each method are discussed by Cruikshank and Murphy (1973), who conclude that each can, with care, yield data of sufficient precision to detect the post-eclipse brightening. If this conclusion is correct and if the observers have correctly reported their observations, then the anomaly is both real and intermittent.

Several authors have attempted to explain this post-eclipse brightening, generally in terms of the atmospheric condensation model originally suggested by Binder and Cruikshank. Veverka (1970) and Lewis (1971a) both concluded that a frost condensate could produce the observed effect. In Lewis' model, the amount of condensate that can be evaporated within 15 min amounts to about 10^{-3} g cm^{-2} uniformly distributed over the surface. For either CH_4 or NH_3, this quantity corresponds to a surface partial pressure on the order of 2×10^{-7} bar, which is not very different from the upper limits established from the spectroscopy of Fink *et al.* (1973) and from the

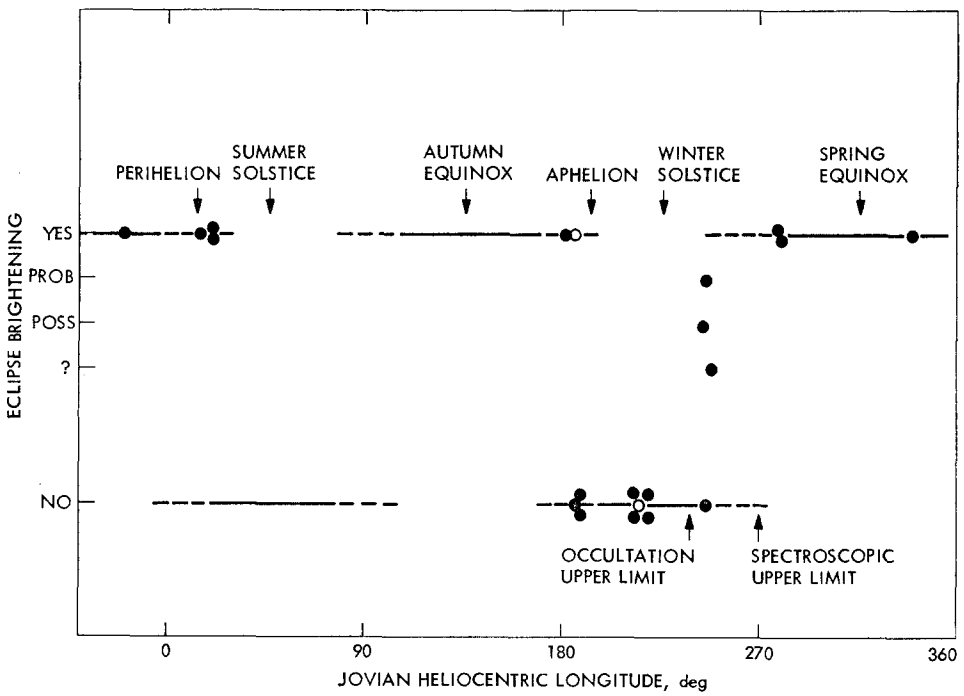

Fig. 16. Summary of post-eclipse brightening observations of Io plotted with respect to season. From Sinton (1973).

stellar occultation results of Smith and Smith (1972) and Bartholdi and Owen (1972).

We have considered the post-eclipse brightness anomaly in this section largely because the first interpretations of the effect stressed the possibility of its origin as an atmospheric phenomenon. The distinct possibility that its cause lies in a temperature or photosensitive surface phenomenon should be kept in mind, however. The original interpretation has in any case served as a stepping stone to the related observational and theoretical studies discussed below.

A particular difficulty in explaining the post-eclipse brightening of Io arises from the intermittency of the effect. Since the positive detections in 1962–63 and in 1971–72 all took place near perihelion, Cruikshank and Murphy (1973) suggest that the effect may occur preferentially near perihelion, when the higher mean temperature could result in a more substantial atmosphere. However, Sinton (1973) has noted that seasonal effects may be more important than distance from the Sun in determining the atmospheric pressure. Because the winter pole can act as a cold trap except near the equinoxes, he expects the maximum available atmosphere when the Sun is near the equatorial plane of Io. Figure 16 illustrates the relationship between times the eclipse anomaly was observed and season. In Sinton's model, Io has an atmosphere of 5 mm-amagat NH_3 (and possibly N_2 also) at a mean temperature of 245 K, where the high temperature is a consequence primarily of the flux at the satellite of 0.5-MeV protons from the Jovian belt of trapped particles. This model provides sufficient condensate to explain the post-eclipse anomaly without contradicting the upper limits set by spectroscopic and occultation techniques, and it also suggests an explanation of the difference between the 10- and 20-μm brightness temperatures and of the large 10-μm residual brightness during eclipse observed for this satellite by Hansen (1973). If the model is correct, this warm atmosphere of NH_3 should be readily detectable by low-resolution spectroscopy in the 8- to 14-μm window.

Sinton (private communication, 1973) has attempted observational tests of this theory, but with filters of rather broad transmission bandwidth, and the results are inconclusive. However, Hansen (1974) observed Io, Ganymede, Callisto, Ceres, and three other asteroids with narrow-passband filters in the 10-μm window and found an emission peak on the three satellites and Ceres, not at 10 μm, where Sinton predicted the NH_3 band, but at 12 μm. Since so many diverse objects show the same feature, it may be related to the surface mineralogy of these objects rather than to their atmospheres.

All of the evidence for an atmosphere on Io and the other Galilean satellites discussed above is to some degree inconclusive or controversial. However, apparently firm spectroscopic evidence for gaseous emission in the atmosphere of Io was discovered in 1972 by Brown (1974), who finds an emission component in the sodium D Fraunhofer lines seen in the reflected sunlight from Io. The other three satellites show only the normal reflected solar spectrum, while the Na emission lines on Io vary widely in intensity, sometimes completely filling the strong host absorption lines. They are clearly associated with the satellite, varying in position with changing line-of-sight velocity of Io. Brown confirmed his discovery with observations at the 1973

apparition of Jupiter and first presented them to the scientific community in September 1973. In Figure 17, we reproduce one of Brown's high-resolution interferometric spectra of Io, which shows the emission lines at a time when they were particularly intense.

As this paper goes to press, a number of observers are studying the Na emission from Io and its spatial and temporal variations. Observing with the coudé spectrograph at Mauna Kea Observatory in October 1973, Sinton found relatively weak Na–D emission lines in the spectrum of the satellite without having prior knowledge of Brown's work. Brown has continued his interferometric studies at Harvard and Mt. Hopkins; L. Trafton has used the coudé scanner at McDonald Observatory; and T. Parkinson has observed at Kitt Peak Observatory with a photoelectric spectro-

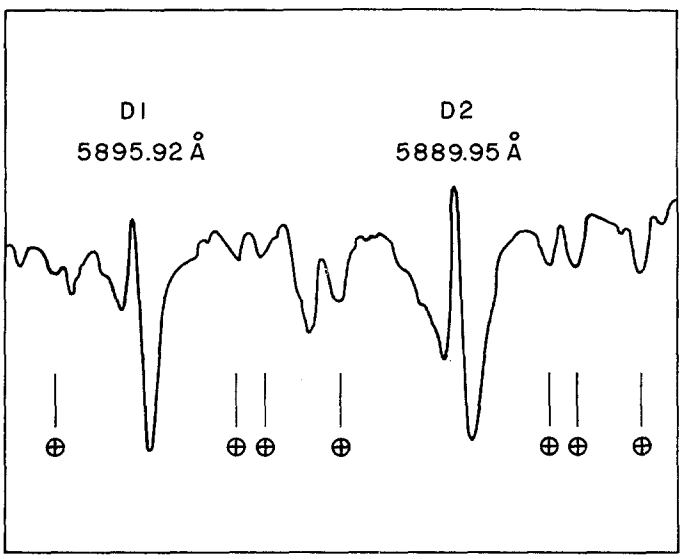

Fig. 17. Interferometric spectrum of Io showing the region of the sodium-D lines. The emission components are clearly visible against the broad absorption lines in the solar spectrum reflected from the satellite. Several telluric lines are indicated. From Brown (1974).

photometer. Although incomplete at this writing, these exciting studies have already demonstrated that the emission takes place within an extended region tens of thousands of kilometers in extent surrounding Io; that the strength of this emission, like the Jovian decametric bursts, is highly correlated with the orbital position of the satellite; and that the relative strengths of the Na–D lines are not consistent with emission from an optically thin gas.

Sodium and other emissions occur in the Earth's twilight airglow (cf. Hunten, 1967), and the sodium itself is apparently injected into the upper atmosphere by the influx of meteors, which vaporize at a height of about 100 km above the surface. At such a height the atmospheric pressure is $\sim 3 \times 10^{-7}$ bar, and most atmospheric constituents are ionized by solar ultraviolet and soft X-rays. Over much of its orbit

around Jupiter, the total space velocity of Io is comparable to that of the Earth, and therefore we expect meteors to enter the satellite's atmosphere with about the same kinetic energies as in the Earth's atmosphere and to vaporize at a level where the atmospheric pressure is on the order of 10^{-7} bar, irrespective of the height of this level above the surface. Whereas the excitation of neutral sodium atoms on Io might be affected directly by the particle flux from the radiation belts of Jupiter, some atmospheric constituent is required for the suspension of the sodium. In the terrestrial atmosphere, nitrogen provides the suspension and is also directly involved in the excitation of sodium; the atmosphere of Io could be N_2 or a noble gas.

A first theoretical discussion of this extended atmosphere of Io has been presented by McElroy *et al.* (1974). They note that an extensive corona of H_2 and N_2 could form around Io by photodissociation of a neutral atmosphere of NH_3, which in turn could evaporate from a surface frost of this material, as previously suggested by Cruikshank and Murphy (1973) and Sinton (1973). They estimate that the source strength of photodissociated N_2 could be of the order of 10^{11} molecules $cm^{-2}s^{-1}$. In order not to exceed the lower limit on the surface pressure deduced from the occultation observations, this gas must escape to form a toroid similar to that around Titan (see Section 7.7), and McElroy *et al.* propose that the auroral heating of the atmosphere by interaction with the Jovian magnetosphere provides the required high thermal velocities for the N_2. The sodium atoms are excited by collisions involving vibrationally excited N_2 and by resonance scattering of sunlight in the toroidal ring. In their model, this ring contains of the order of 10^{36} nitrogen molecules, 10^{37} hydrogen molecules, and 10^{31} sodium atoms, and the satellite itself should have an ionosphere readily detectable by spacecraft occultation techniques. At the time of this writing, several other authors are preparing papers on the extended atmosphere and ionosphere of Io, and undoubtedly this preliminary discussion will quickly be supplanted by an extensive literature on this subject.

Arguments for the presence of an ionosphere on Io have also been advanced to explain the well-known modulation by this satellite of the decametric radio bursts from Jupiter. To explain this phenomenon, Goldreich and Lynden-Bell (1969) suggest a very strong electrical current circulating along lines of the Jovian magnetic field through both Jupiter and the satellite. Dermott (1970, 1972) has shown that the electrical conductivities of rocks and ice at the temperature of Io are far too low to satisfy the requirements of the theory of Goldreich and Lynden-Bell. However, Webster *et al.* (1972) have shown that the electrical conductivity of a postulated ionosphere surrounding Io would be sufficient to provide the conduction path required by the theory of Goldreich and Lynden-Bell. An ionosphere of sufficient density will result from photoionization of a tenuous atmosphere of methane, for example, in which the surface molecular number density is as low as 3×10^{11} cm^{-3}, corresponding to a surface pressure of only 6×10^{-9} bar. The ionosphere could also be derived from an inert atmosphere of N_2.

Note Added in Proof. On 4 December 1973 the Pioneer 10 spacecraft passed within

130000 km of the cloud tops of Jupiter on a trajectory that carried it through the entire satellite system of the planet and included an occultation of the spacecraft by Io. Preliminary reports of this first *in situ* exploration of the outer planets and their satellites were published in *Science* for 25 January 1974. The most significant results for this review dealt with the atmosphere of Io. The occultation was observed at S-band (2200 MHz) and produced electron-density profiles of the ionosphere of the satellite (Kliore *et al.*, 1974). The entry data, which apply to the side of Io facing away from Jupiter and illuminated by the Sun, show an ionosphere extending for some 700 km above the surface, with a peak electron density of about 6×10^4 cm^{-3} at an altitude of between 60 and 140 km. The top-side scale height is about 220 km. Kliore *et al.* estimate that this electron density implies a number density of neutral molecules at the surface of between 10^{10} and 10^{12} cm^{-3}. The corresponding surface pressure is 10^{-8} to 10^{-10} bar, perhaps slightly higher if the molecular weight of the gas is very high. This range of pressures is consistent with the other evidence relating to the atmosphere of this satellite discussed above. The surprisingly great extent of this ionosphere is almost certainly related to the charged-particle bombardment of Io and the extended Na-D emission from its vicinity. Further direct evidence of the extended atmosphere of Io was obtained with the ultraviolet photometer on board Pioneer 10 (Judge and Carlson, 1974). In Lα, this photometer indicated a brightness of 10^4 rayleighs for this satellite, suggesting an extensive halo of hydrogen and an excitation mechanism in addition to resonant scattering of sunlight. Judge and Carlson also report the discovery of a toroidal cloud of neutral hydrogen occupying the orbit of Io. The intensity of this cloud in Lα is several hundred rayleighs. Finally, one other report from Pioneer 10 is highly significant for future studies of this satellite. From Doppler tracking of the spacecraft through the satellite system it should be possible to derive masses for the Galilean satellites that are accurate to at least 1%. The preliminary report by Anderson *et al.* (1974) indicates that Io and perhaps also Callisto are significantly more massive than had been concluded from ground-based dynamical studies. For Io, they find a mass of 9×10^{25} g, some 10% greater than that given in Table V. The density of this satellite is then 3.5 g cm^{-3}, comparable to that of the Moon and Mars.

6.6. Direct imaging

At the best observing sites, telescopes as small as 40 cm in aperture show faint dusky markings on the disks of the Galilean satellites. B. Lyot and his successors at the Pic-du-Midi Observatory have succeeded in producing rough maps of the distributions of the albedo features on these objects (Dollfus, 1961, plate 40). More recently, photographs made with the Stratoscope high-altitude balloon-borne telescope have been analyzed with computerized information processing techniques to produce a high-resolution composite image of Io (Danielson and Tomasko, 1971), which we reproduce in Figure 18. The markings are diffuse, with the suggestion of a dark polar cap, in agreement with the visual studies made by E. E. Barnard in the early 1900's and by Lyot (Dollfus, 1961).

Regions of different visual color on Io have recently been detected on ground-based color photographs of remarkably high resolution (0.2″) (Kuiper, 1973; Minton, 1973). The contrast of the colored regions on the satellite was enhanced by photographing it against a bluish-white zone on Jupiter as Io transited the planet's equatorial region. The polar regions of the satellite seen against the light background are clearly orange-brown while the equatorial region is yellow in tone. Although the spectral resolution of the color photographs is of course very low, Kuiper called attention to the apparent similarity in color of the polar regions of Io and the Great Red Spot

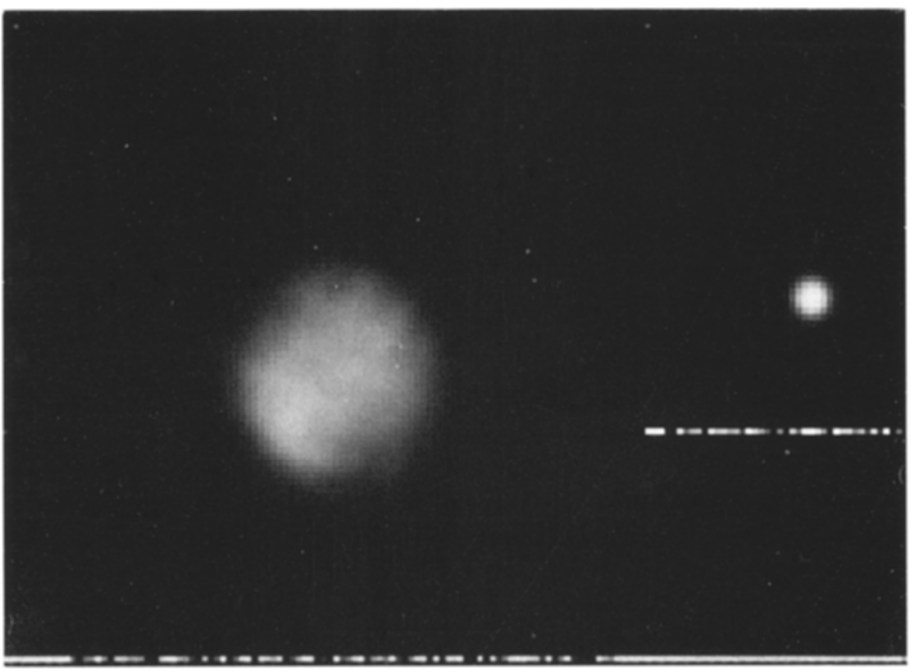

Fig. 18. Composite of 15 photographic images of Io obtained with the 90-cm telescope on Stratoscope II floating at altitude 24 km in 1970. The composite image was computed from digitized and electronically filtered individual images taken through an effective bandpass of 0.38–0.58 μm. The orbital phase angle of Io is approx 290°. The smaller image is that of a star filtered with the same point spread function used for the satellite image. From Danielson and Tomasko (1971).

of Jupiter, which he regards as probably due to ammonium polysulfides, colored polymers formed from the interaction of ultraviolet radiation with hydrogen sulfide and ammonia. There is no spectroscopic evidence to date for any of these compounds on Io, although they have strong absorption features in the spectral region studied by Pilcher *et al.* (1972) and Fink *et al.* (1973). However, lack of spectroscopic detec-detection does not rule out Kuiper's hypothesis, because the effects of abundance, temperature, and particle size on the strength of spectral features are largely unknown.

An alternative explanation for the color of this satellite has been suggested by McElroy *et al.* (1974), who propose that the absorptions may be due primarily to

alkali metals dissolved in NH_3. They attribute the broad spectral feature at 0.55 μm to dissolved sodium and the low ultraviolet albedo to dissolved calcium.

A semi-quantitative method of estimating the brightness of large surface features on the Galilean satellites from visual observations of their transits across the disk of Jupiter has been reported recently by Dollfus and Murray (1974). Observing at the Pic du Midi under excellent seeing conditions, they note the times during transit when the contrast between a given part of the satellite and the background Jovian disk goes to zero. From a knowledge of the distribution of albedo across Jupiter, they can then derive a low-resolution albedo map of each satellite at an orbital phase angle of 180°. These studies confirm the presence of dark polar caps on Io and of light caps on Europa and Ganymede. For Io, Europa, and Callisto, the maximum contrasts deduced are of the order of a factor of two, but for Ganymede these observers find that the polar caps are about a factor of four brighter than the equatorial regions. This result for Ganymede is consistent with the suggestion made by Pilcher *et al.* (1972) that about half the surface is frost covered while the rest is dark rock, and in addition it now indicates that most of this frost is concentrated in the polar regions of the satellite.

The question of what inferences about surface structure might be drawn from visual pictures of the Galilean satellites is unsettled. With greatly degraded resolution, even worse than that of the unaided eye, the Moon appears not unlike these satellites. It does not necessarily follow that the markings on the satellites correspond to areas with contrasting geologic histories, however, particularly when we consider the weak relationship between the traditional albedo features on Mars and the topographic and geologic structure of that planet. For the Galilean satellites, it is clear only that the photometric properties differ from one large region to another. In contrast, the thermophysical studies (Morrison and Cruikshank, 1973; Hansen, 1973) indicate thermally homogeneous surfaces. It has also been noted (Lewis, 1971a; Johnson and McGetchen, 1973) that isostatic adjustment of the surfaces of low-density ice-mantled bodies such as the Galilean satellites would be expected to obliterate all but the most recently formed topographic features. It is also possible that at least some of the features, particularly higher albedos in the polar regions, may be due to the preferential deposition of atmospheric volatiles on some parts of the surface. Clearly, it is premature to draw conclusions about the physical significance of the albedo markings, and attempts such as that of Katterfeld and Nesterovitch (1971) are entirely speculative.

6.7. Implications for Internal Structure and Surface Chemistry

In Section 4, we discussed models for the interiors of the satellites, based primarily on recent work by Lewis. The Galilean satellites, with their well-determined densities and radii, provide excellent examples for a discussion of these models. Lewis (1971a, b) suggests that each of these objects will be fully differentiated as a result of melting early in its evolution and will now have a crust consisting primarily of water ice, with an admixture of meteoric material. The densities of the Galilean satellites, the

spectroscopic discovery of water ice on the surfaces of at least two Galilean satellites, and the thermophysical and polarimetric evidence for some kind of frost on their surfaces are all consistent with this hypothesis. However, we note that each satellite has unique surface properties and their densities vary by a factor of two; therefore we should not too quickly accept one model, however promising, as necessarily representative of each of these four satellites.

Because of the expected process of continuous density differentiation of surface deposits of silicates and iron-bearing materials from ices in the crust, Lewis (1971b) concludes that the quantity of the heavier material in and on the upper layers of the surface should be exceedingly small. The variations in degree of darkening of the surfaces of the satellites might then be best explained in terms of surface deposits of low-density carbonaceous material from meteorites or from photochemical processes.

The tendency toward a progression of photometric properties of the satellites radially outward from Jupiter suggests some correlation with the field of trapped particles surrounding the planet. However, both the intensity of the field and the effects of impingement upon the surface (or atmosphere, or both) of a satellite are difficult to establish. The heating effects on the surfaces of J5 (Amalthea) and Io have been considered by Thomas (1972), who found that the surface flux on Amalthea is an order of magnitude greater than the solar flux. Heating of Io was found to be very small and that of the outer satellites negligible.

We have already noted the speculation on the occurrence of frozen free radicals and other compounds on the surface of Io and the other satellites, although none has yet been detected. Lewis (1971b) considered the presence of hydrate compounds of NH_3 and CH_4, showing that at the observed surface temperatures of the Galilean satellites the ammonia hydrate might exist, but not the methane hydrate.

It is clear that we cannot understand the peculiar aspects of the surfaces, atmospheres, and possible short-term variations of both until the nature of the interaction of these bodies with their near-Jupiter environment is clarified. *In situ* measurements of the Jovian radiation belt will naturally aid greatly in developing models of the interaction of charged particles with the satellites. It is also of great importance to establish whether or not these satellites are fully differentiated, and thus to what extent the differences among them can be attributed to initial differences in crustal composition.

6.8. Summary: Ganymede

In this and the following three sections we sumarize the state of knowledge of each of the Galilean satellites, based on the studies reviewed earlier in this section. We begin with Ganymede, which is the largest and perhaps the best understood of these satellites.

Ganymede probably condensed from a solar-composition aggregate of metallic oxides, silicates, and volatiles, resulting in a nearly spherical body of radius 2635 km, which contains a large volume percentage of ices of H_2O, $NH_3 \cdot H_2O$, and $CH_4 \cdot 8H_2O$. Since the mean density of this satellite is 2.0 g cm^{-3}, about 15% by mass is probably composed of silicate or other heavy materials. Within the first few hundred million

years of the formation of the satellite, internal radioactive heating and dissipation of tidal energy are likely to have raised the temperature above certain eutectic points, resulting in nearly total melting of the ice mantle and differentiation of materials in the interior. At present, Ganymede probably has a relatively dense core of metallic oxides and silicates surrounded by a thick mantle of liquid volatiles. The crust, about 100 km thick, may either consist primarily of solid H_2O ice with an admixture of darker and denser material deposited from space or may represent the primordial mixture of rocky and volatile condensates from the solar nebula.

The strength of the ice absorption bands in the near-infrared spectrum of Ganymede, together with the photometric, polarimetric, and thermophysical properties, indicates that about 50% of the exposed surface consists of water ice or frost, and the visual appearance indicates that this frost is concentrated in the polar regions. The homogeneity implied by the eclipse radiometry suggests that the dark material exists not as discrete patches of exposed rock alternating with expanses of frost, but rather as fine dust well mixed with the frost. Presumably much of this dark material is the product of relatively recent meteoroid impacts. However, the large-scale variations of albedo and of distribution of H_2O frost across the surface may be evidence that different parts of the surface have different histories. If the crust is undifferentiated, these large areas of differing photometric properties may date from the time of formation of the satellite. The rapid decrease in albedo toward the ultraviolet indicates that at short wavelengths there is substantial absorption in the surface material, due perhaps in part to radiation damage to the water frost or to an admixture of small amounts of organic or inorganic polymers.

Since the thermal inertia of the uppermost part of the surface is of the order of $(K\varrho c)^{1/2} = 10^4$ erg cm^{-2} s$^{-1/2}$ K^{-1}, the material (presumably H_2O frost) must have very low density. A few millimeters below the surface, the density and thermal conductivity increase substantially. The low-density, particulate nature of the surface is further indicated by the photometric and polarimetric behavior of this satellite. No large-scale topographic features are expected, since isostatic adjustment in the ice crust will quickly obliterate elevation differences.

Ganymede may have a rare atmosphere of 10^{-3} to 10^{-6} bar surface pressure; however, since no spectral features attributable to the atmosphere have been detected, the gas may be primarily N_2 or A, with perhaps a very little NH_3. Heat generated by meteoroid impacts vaporizes ice and frost locally, but this vapor quickly condenses as low-density dendritic frost. An occasional impacting comet may spread its vaporized ices and solid debris over the satellite's surface, creating a substantial temporary atmosphere, which will soon be frozen out.

6.9. Summary: Callisto

Callisto is much darker than the other Galilean satellites, and its infrared spectrum shows little if any evidence of features due to exposed H_2O frost. Eclipse radiometry indicates that the uppermost part of the surface is thermophysically similar to that of Ganymede, however, a conclusion not readily reconciled with the apparent absence

of frost. Photometrically, Callisto behaves as one would expect for an object with a surface composed of relatively high-albedo silicates or of darker minerals mixed with a small quantity of brighter material. It is the only Galilean satellite that is darker on its leading side than on its trailing, and it is the only one to exhibit a substantial opposition effect.

Callisto is approximately as large as Ganymede and possibly has a similar internal structure. However, its lower density (1.4 g cm^{-3}) indicates that it possesses a smaller proportion of heavy materials, and consequently that it probably has a smaller source of radioactive heat. Callisto, as the Galilean satellite with lowest density and greatest distance from Jupiter, is the least likely of the four to be fully differentiated, and it is tempting to argue that its photometric uniqueness derives from the presence of an undifferentiated crust of primordial material. However, if one postulates that Io and Europa are differentiated and Callisto is not, how does this scheme account for the intermediate properties of Ganymede?

Alternatively, if we assume that each of the Galilean satellites is fully differentiated and that each began with essentially identical ice crusts, then we must seek to explain the differences in color or albedo by the action of some external agent. The lower albedo of Callisto could be due to either a significantly higher flux of impacting meteoroids or an environment that inhibits the brightening of the surface. Two ways in which the environment differs on Callisto are (1) it has a lower flux of high-energy particles from the Jovian radiation belts, and (2) it has less frequent eclipses. Perhaps an explanation for its photometric uniqueness should be sought in one of these two areas.

6.10. Summary: Europa

The surface of Europa is almost entirely covered with water frost, and accordingly has a high albedo ($p_V = 0.7$). It is likely to be fully differentiated and to have a crust composed primarily of frozen H_2O. Either the quantity of dark material generated by meteoroid impacts is smaller than on Ganymede, or the material is bleached by the flux of high-energy particles or perhaps quickly covered by the lighter frost. Little is known about either the microstructure of the surface or the possible presence of an atmosphere. Both the radius and the density are less well known for this satellite than for the other three. The leading hemisphere is substantially brighter than the trailing one, and there may be bright polar caps. The large brightness and temperature variations that have been found from both visible and infrared photometry suggest an important interaction with its space environment.

6.11. Summary: Io

Io is an anomaly not only among the Galilean satellites, but among all the bodies in the solar system. Its surface has the thermal, photometric, and polarimetric properties, but not the spectral properties, of H_2O frost. It shows no recognizable near-infrared spectral features, and its albedo longward of about 0.5 μm is exceptionally high. Io exhibits photometric and thermal peculiarities in and out of eclipse that suggest

the presence of an atmosphere on the order of 10^{-7} bar surface pressure, composed of N_2 or NH_3 or both. Io evidently reacts strongly with the field of trapped particles surrounding Jupiter, as shown particularly by its modulation of the decametric emission of the planet, but the effect of the flux of particles on its surface is not understood. Io has the highest density of any of the Galilean satellites and is likely to be fully differentiated; however, there is no compelling reason to think that the implied difference in bulk composition or structure is the cause of the unusual nature of its surface. Since the trailing hemisphere is darker and much redder than the leading hemisphere, an interaction with its space environment is again suggested. High-resolution images obtained at an orbital phase angle of 180° show dark reddish polar caps and a bright central region.

Very recently, ground-based spectroscopy and spacecraft occultation measurements have clearly demonstrated the presence of an atmosphere with surface pressure of the order of 10^{-8} bar and of an ionosphere with a peak electron density of about 10^5 cm^{-3} at an altitude of about 100 km. The bulk of the atmosphere probably consists of NH_3 and its dissociation products N_2 and H_2, but it is most readily detected spectroscopically by emission in the Na lines. Charged particles from the Jovian belts impinging on the atmosphere may heat it substantially, contributing to the formation of an ionosphere and to the escape of gas into a toroid surrounding Jupiter. The new observations, especially those obtained from the Pioneer spacecraft at the time this review goes to press, assure that Io will be among the most intensively studied objects in the outer solar system during the next few years.

7. Titan

7.1. Introduction

Titan is unique among the satellites in having a substantial atmosphere. The largest satellite of Saturn, Titan is nominally 2500 km in radius; however, as discussed in Section 3.2, the size is not precisely determined, and Titan could be the largest satellite in the solar system. The mean density is $\simeq 2$ g cm^{-2} (see Table V) and the surface gravity is $\simeq 140$ cm s^{-2}; this relatively large acceleration, together with its great distance from the Sun, make Titan a plausible candidate for possession of an atmosphere. However, the great mass of this atmosphere has come to light unexpectedly and only within the past two years.

7.2. Photometry and spectrophotometry

Broad-band (*UBV*) photoelectric photometry of Titan has been obtained by Harris (1961) and Blanco and Catalano (1971), and recently an intermediate-band (*uvbyri*) study has been made by Noland *et al.* (1974). These authors find *V* magnitudes for this satellite at mean opposition of 8.39, 8.35, and 8.30, respectively. A magnitude of 8.35 ± 0.04, together with a radius of 2500 ± 300 km (Table V), implies a visual geometric albedo of 0.21 ± 0.04. Searches for variations in magnitude with orbital phase angle by these authors demonstrate that this satellite, unlike any other, does

not vary in brightness as it rotates; although Titan is usually assumed to be in synchronous rotation, there is no direct evidence about its period. Variations in magnitude with solar phase angle have been found however, by Noland *et al.* (1974), with phase coefficients ranging from 0.014 mag. deg^{-1} in u to 0.005 mag. deg^{-1} in y, with even smaller values in the near infrared. These values are similar to those of the major planets, and suggest that the phase integral (q) of Titan is between 1.0 and 1.5. Several authors have adopted $q=1.3$ as a reasonable value; with this q and the visual albedo of 0.21, the visual Bond albedo is ~ 0.3.

Titan is remarkably red, with a $U-V$ color index of $+2.04$ mag. Detailed studies of the variations of its albedo with wavelength have been made by McCord *et al.* (1971), Younkin (1974), and Barker and Trafton (1973). Figure 19 reproduces the spectrophotometry of McCord *et al.*, which covers the spectral region from 0.3 to 1.1 μm with a resolution that varies from 0.02 μm in the ultraviolet to 0.05 μm in the infrared. The variation of albedo in this figure is very similar to that of the equatorial belt of Saturn, and absorptions due to methane bands are evident. However, the more recent measurements by Younkin (1974) and Trafton (1974; and private communication, 1973) give higher geometric albedos in the infrared – up to $p=0.37$ between the absorption bands from $0.68 \leqslant \lambda \leqslant 0.83$ μm – suggesting a systematic error in the long-wave part of Figure 19. These higher infrared albedos also increase the estimate of bolometric Bond albedo over earlier values: Younkin (1974) computes $A=0.27$, which corresponds to an effective temperature of 84 K.

In the ultraviolet, the albedo of Titan is anomalously low, as demonstrated particularly in the recent work of Barker and Trafton (1973) and Caldwell *et al.* (1973). Since Titan has an atmosphere, it is to be expected that at sufficiently short wavelengths the effects of Rayleigh scattering should cause the albedo to rise above the low values observed near 0.4 μm, and indeed the spectrophotometry of McCord *et al.* (1971) suggested such an increase near 0.3 μm. However, the observations by Barker and Trafton obtained with a resolving power of 500 between 0.30 and 0.43 μm show a smooth, steady decline in albedo with decreasing wavelength, from 0.094 to 0.050. The variation of albedo with wavelength of Titan in this spectral region is, in fact, virtually identical to that of the rings of Saturn, which are solid particles. Caldwell *et al.* (1973) have extended the albedo data still further into the ultraviolet; they find from OAO-2 observations that at 0.26 μm the geometric albedo of Titan is 0.050 ± 0.025. These low albedos set severe upper limits on the amount of Rayleigh scattering from the atmosphere, as will be discussed more fully in Section 7.4.

7.3. Spectroscopy

The existence of an atmosphere on Titan was discovered by Kuiper (1944) during a systematic spectrographic survey of the brighter satellites. He found that the methane band at 6190 Å has an equivalent width only slightly smaller than that observed in the spectrum of Saturn. In a subsequent laboratory calibration, Kuiper (1952) reproduced the observed absorption with 200 m-atm of CH_4 at 986 mb pressure, which he interpreted as indicating a partial pressure of this gas of 2.0 mb on Titan.

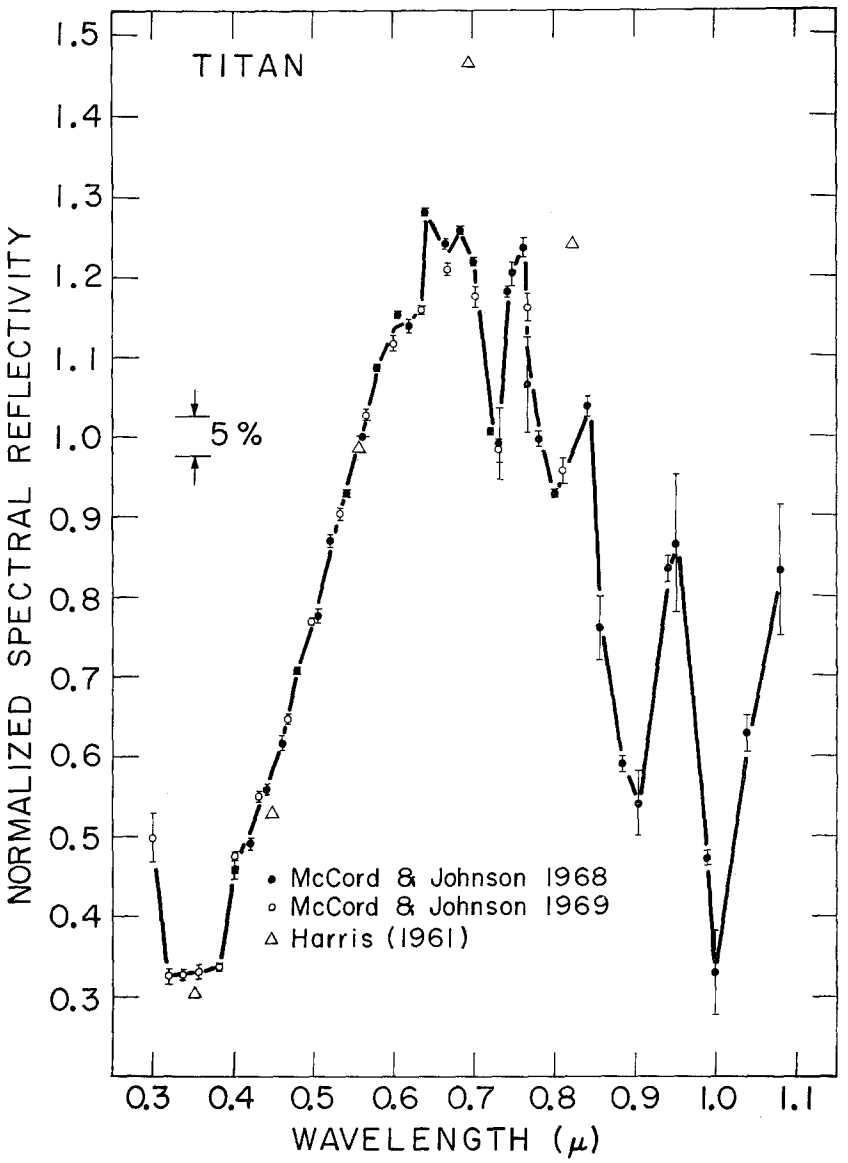

Fig. 19. Spectrophotometry of Titan from 0.3 to 1.1 μm. The spectral resolution varies from 0.02 μm in the ultraviolet to 0.05 μm in the infrared. Subsequent measures by other authors suggest that the albedo between the CH_4 bands in the long-wave part of the spectrum is higher than is indicated in this figure. From McCord *et al.* (1971).

No other atmospheric components had been detected until Trafton (1972a) reported the probable identification in photoelectric scans made with the McDonald 2.72-m telescope of the S(1) quadrupole line of H_2 at 8150 Å. Münch (1973) has confirmed these observations of H_2 in spectra obtained with the Hale 5-m telescope and has searched unsuccessfully for bands due to NH_3.

In addition to his discovery of H_2 on Titan, Trafton (1972b) presented an important reanalysis, later amplified by Hunten (1972) and Pollack (1973), of Kuiper's observations of CH_4. Since the observed band lies on the squareroot portion of the curve of growth, Kuiper's result can be written,

$$W \cdot P \simeq 0.2 \text{ km atm}^2, \tag{5}$$

where W is the abundance of methane and P is the mean broadening pressure. For a pure CH_4 atmosphere, Trafton finds an abundance and surface pressure of 1.6 km atm and 16 mb, respectively. A similar analysis of the new H_2 spectra (Trafton, 1972a) gives an abundance of 5 km atm and pressure of 6 mb, if hydrogen is the major constituent. A combined analysis (Pollack, 1973) indicates a minimum pressure of $\simeq 0.1$ atm, with methane and hydrogen about equally abundant.

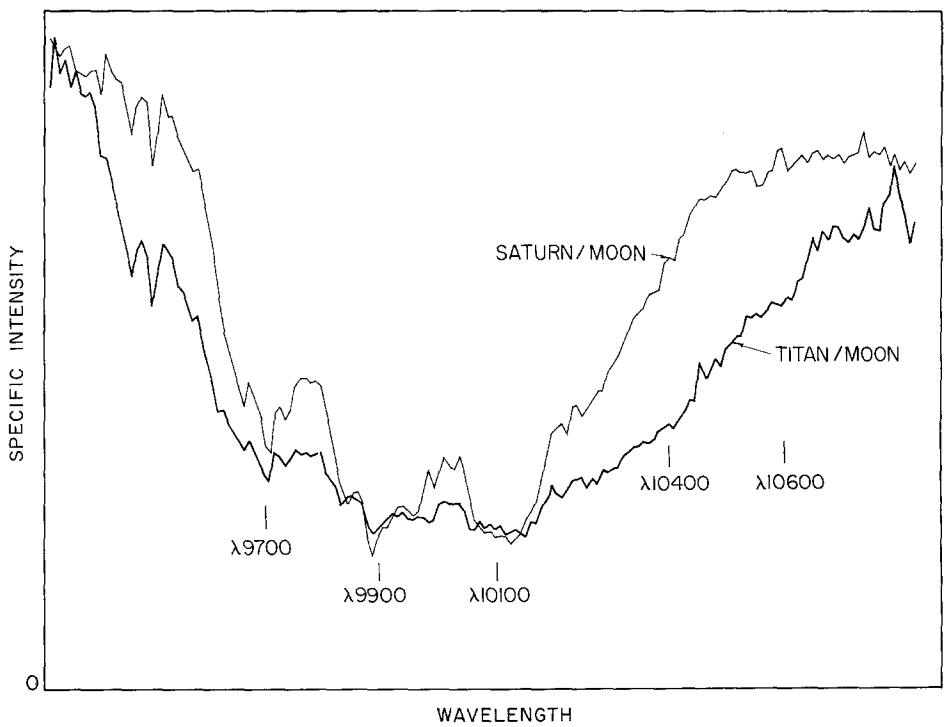

Fig. 20. Ratio spectra of Titan and Saturn to the Moon for the 1-μm band complex of CH_4. Note the enhanced absorption from 1.05 to 1.07 μm. The spectrum of Titan appears to be 'washed out' relative to that of Saturn. From Trafton (1974).

The main features of the spectrum of Titan – the strong bands due to CH_4 and the drop in albedo toward the ultraviolet – are remarkably similar to those in the spectrum of Saturn, and in the low-resolution spectrophotometry (e.g., Figure 19) the spectra of the two bodies are virtually identical. Recently, however, higher resolution spectra of Titan and Saturn have revealed equally remarkable differences between them,

particularly in the infrared (0.8 to 1.2 μm). These differences have been noted by Münch (1973) and Younkin (1974), but primarily their discovery is due to Trafton (1974), who has observed both objects, together with Uranus and the rings, with resolving power of about 10^3 with the photoelectric spectrum scanner of the 2.72-m telescope. Generally, the CH_4 bands on Titan are less deep, but wider in the wings, than those of Saturn, and this difference is more pronounced toward longer wavelengths. Figure 20 (from Trafton's paper) illustrates one of the more extreme examples of this effect. An additional feature of the spectra of Titan, evident especially at the highest resolution, is the presence of many unidentified lines, particularly in the long-wave wings of the CH_4 bands. Similar lines appear in Trafton's spectra of Uranus, but not in those of Saturn. Although the interpretation of these observations is

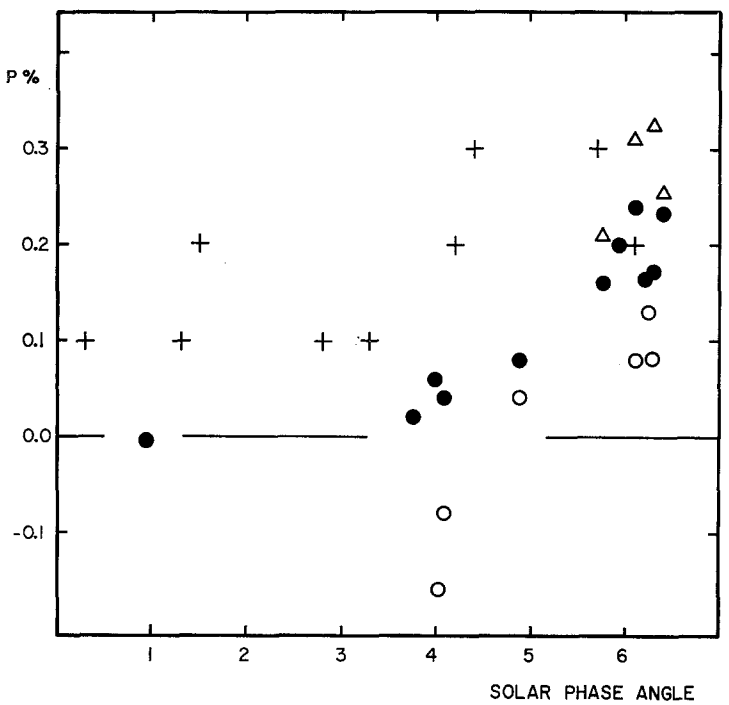

Fig. 21. Observations of the linear polarization of Titan as a function of solar phase angle. The open circles are in the ultraviolet (0.36 μm), filled circles in the green (0.52 μm), and the triangles in the near infrared (0.83 μm), all by Zellner (1973). The crosses are observations in white light by Veverka (1973), who calculates uncertainties for his points of ± 0.1 to $\pm 0.2\%$. From Zellner (1973).

unclear, Trafton notes that the unidentified lines indicate the presence of some complex and spectroscopically active molecule in Titan's atmosphere in addition to CH_4 (possibilities include an isotope of CH_4 or hydrocarbons), while the washing out of the bands in the spectrum could be explained by a haze of absorbing aerosols in the upper atmosphere of Titan. Particularly intriguing are the unexplained spectral similarities between Titan and Uranus.

7.4. Clouds

In addition to the above evidence, several other arguments suggest the presence of clouds on Titan. Perhaps the simplest derives from the anomalous combination of low albedo and small phase coefficient. Further, the CH_4 in the atmosphere is expected to condense to form thick clouds if the temperature drops below 80 K. But the two strongest lines of evidence come from linear polarization observations and from the apparent absence of Rayleigh scattering in the ultraviolet.

Even several years ago it was apparent from the low albedo of Titan in the ultraviolet that the satellite could not possess an optically thick clear atmosphere: the albedo of 0.07 in the *U* band, for instance, limits the optical depth at that wavelength to values of less than 0.1. Veverka suggested in 1970 that observations of the phase dependence of the linear polarization could distinguish between the remaining possibilities: reflection of sunlight from the surface of Titan or from an optically thick cloud layer. Recently, studies of the polarization have been made by Veverka (1973) in white light and by Zellner (1973) in bands at 0.36 μm, 0.52 μm, and 0.83 μm. Veverka finds a small but definite positive polarization, which increases with increasing phase angle. Zellner's data agree but in addition show a strong wavelength dependence, with maximum polarization near phase 6° in the infrared and with an indication of a slight negative polarization in the ultraviolet near 4°. The observations by both authors are illustrated in Figure 21. All other satellites show negative polarization in this range of phase angles. The conclusion is that there is no evidence for scattering from a dark particulate surface; the only possibility is that Titan has a substantial cloud deck with an optically thin atmosphere above it.

The extreme thinness of the atmosphere above the clouds is demonstrated by the measurements of the albedo of Titan in the ultraviolet. Caldwell *et al.* (1973) conclude that the observed albedo at 0.26 μm would be produced by scattering in only 0.15 km-amagat of CH_4, which is more than an order of magnitude less than the abundance of this gas measured spectroscopically. The absence of structure in the ultraviolet spectrum of Titan eliminates the possibility that the ultraviolet opacity is due to a gas, and an inhomogeneously mixed haze of particles that are very black in the ultraviolet seems to be required (Barker and Trafton, 1973). In the infrared, however, the spectroscopic evidence (Trafton 1972b, 1974) indicates that photons penetrate to substantial depths within this haze layer. Clearly, a simple reflecting layer model for the atmosphere and clouds of Titan is not adequate.

At least a part, and perhaps all, of the characteristic red color of Titan must be due to the absorption of blue and ultraviolet light in this haze layer, although at longer wavelengths there may also be significant reflection of light from a deeper cloud layer or from the surface. The close similarity in color between Titan and the central belt of Saturn suggests a similar composition for the high clouds on both objects. In fact, all of the major planets show a qualitatively similar drop in albedo at short wavelengths, and the existence of a similar high haze layer has been suggested previously for Jupiter (Axel, 1972). The differences between Titan and the major planets –

the lower albedo and the absence of evidence for Rayleigh scattering at very short wavelengths – could be understood if the haze layer were higher in the atmosphere of the satellite. Since pure CH_4 clouds do not absorb strongly in the ultraviolet, the haze is likely to consist, not of this compound, but rather of hydrocarbon products of photolysis reactions in the atmosphere, as discussed by Sagan (1971, 1973) and Danielson *et al.* (1973). A dark reddish-brown polymer with properties qualitatively similar to those postulated for this haze has been produced in the laboratory by Khare and Sagan (1973). As noted by Caldwell *et al.* (1973) and Barker and Trafton (1973), absorption of sunlight by this haze provides a substantial energy source for the upper atmosphere, probably leading to a temperature inversion in the haze layer.

7.5. Temperatures

Studies at visible frequencies are limited to the atmosphere and the clouds, but at microwave and infrared frequencies it may be possible to explore the lower atmosphere and surface. No detection of this satellite has been made in the radio, although with improved interferometric techniques such observations may be possible. However, infrared photometry in the 10- and 20-μm windows shows that the temperature in the atmosphere is much higher than the equilibrium temperature for Titan, and thus provides important clues to the structure of the atmosphere.

The anomalous infrared brightness temperature of Titan was first noticed by Allen and Murdock (1971), who obtained a temperature of 125 ± 2 K in a band from 10 to 14 μm (nominally 12.4 μm). This brightness temperature and all those quoted below assume a radius for Titan of 2500 km, and the uncertainties do not take into account the uncertainty in the radius. For comparison, the equilibrium infrared disk temperature of a non-rotating airless satellite at Saturn's distance is given by

$$118\left(\frac{1-A_{\mathrm{bol}}}{E_{\mathrm{bol}}}\right)^{1/4}\mathrm{K}, \tag{6}$$

where A_{bol} is the bolometric Bond albedo and E_{bol} is the bolometric emissivity. For Titan, $0.20\leqslant A_{\mathrm{bol}}\leqslant 0.35$, depending on the value of the phase integral and the radius, and $E_{\mathrm{bol}}\simeq 1.0$; therefore, the maximum temperature without an atmosphere would be 111 K. Allen and Murdock concluded that there was likely to be a greenhouse effect on Titan that increased the observed 12.4-μm flux by a factor of about 2 over the equilibrium level. An earlier brightness temperature of 132 ± 5 K in the 8- to 14-μm band published without comment by Low (1965) is consistent with this suggestion.

The actual magnitude of the change in brightness temperature with wavelength, and hence of the postulated greenhouse effect, became apparent with the publication of additional observations in the infrared. Morrison *et al.* (1972), observing in a broad band from 16 to 28 μm (nominally 20 μm) found a temperature of 93 ± 2 K. Morrison *et al.* further documented the range of observed temperatures by quoting unpublished observations by Gillett and Forrest at U.C. San Diego that yield brightness temperatures of 134 ± 2 K at 11 μm and 144 ± 3 K at 8.4 μm. Assuming that the

temperature in the atmosphere increased with depth, they concluded that the only abundant gas that could provide the indicated great opacity in the 20-μm band together with an opacity decreasing from 12 to 8 μm is hydrogen at sufficient pressure to induce translational – rotational transitions. Further, since the bulk of the radiation from such a cool body is at wavelengths between about 15 and 40 μm, they noted that this large opacity in the 20-μm band would result naturally in a greenhouse effect. They therefore argued for a massive hydrogen atmosphere with a surface pressure of hundreds of millibars and a surface temperature $\geqslant 150$K (see also Cruikshank and Morrison, 1972). At the same time, calculations by Sagan and Mullen (Sagan, 1973) indicated that a pure hydrogen greenhouse on Titan is capable of generating surface temperatures higher than 200K. An upper limit to the surface temperature may be inferred from a more recent attempt by Joyce *et al.* (1973) to detect the satellite at 4.9 μm, where the opacities of the proposed atmospheric constituents – H_2, CH_4, N_2, and NH_3 – are all very small. They set an upper limit of 190K, indicating that, unless there is some additional source of 4.9-μm opacity (in the clouds, for instance), the surface temperature is less than ~ 200K.

All of the infrared temperatures discussed above are broad-band values. A great improvement in spectral resolution within the 8- to 14-μm band has recently been achieved by Gillett *et al.* (1973), who have observed Titan at 8 wavelengths with a

TABLE XII

Brightness temperatures of Titan

Narrow-band

(Gillett *et al.*, 1973)

$\lambda(\mu m)$	T_b(K)
8.0	158 ± 4
9.0	130 ± 6
10.0	124 ± 3
11.0	123 ± 3
12.0	139 ± 1
12.5	129 ± 2
13.0	128 ± 2

Broad-band

$\lambda(\mu m)$	$\Delta\lambda(\mu m)$	T_b(K)	Reference
4.9	0.8	<190	Joyce *et al.* (1973)
8.4	0.8	146 ± 5	Gillett *et al.* (1973)
10.0	5.0	132 ± 5	Low (1965)
11.0	2.0	134 ± 2	Gillett *et al.* (1973)
12.0	2.0	132 ± 1	Gillett *et al.* (1973)
12.4	4.0	125 ± 2	Allen and Murdock (1971)
20.0	7.0	93 ± 2	Morrison *et al.* (1972)

cooled filter-wheel spectrometer having a resolving power of nearly 100. All of the radiometric observations, both broad- and narrow-band, are listed in Table XII. The new narrow-band data reveal substantial structure in the thermal spectrum, possibly due to line emission, which is readily understood if there is a large temperature inversion in the upper atmosphere of Titan. Danielson *et al.* (1973) have proposed that all of the data in Table XII are consistent with a model in which such an inversion exists, and therefore that the temperatures of Titan by no means require the existence of a greenhouse effect. Thus, basically the same observations have been used to support two very different models of the atmosphere of this satellite. These models are the subject of the following section of this review.

7.6. Atmospheric models

Two classes of models for the atmosphere of Titan have been suggested: greenhouse models, in which the temperature increases with depth and the surface temperature and pressure are high, and temperature-inversion models, in which the surface is cool but absorption of sunlight in a high cloud layer heats the upper atmosphere. The greenhouse models have been advocated by Allen and Murdock (1971), Morrison *et al.* (1972), Hunten (1972), Sagan (1973), Pollack (1973), and Cess and Owen (1973), and we will discuss them first, following primarily the detailed work of Pollack. In both cases, the main constituents of the atmosphere are taken to be CH_4 and H_2, both observed spectroscopically. Additional possibilities that have been suggested are He, N_2 (Hunten, 1972), NH_3 (Lewis, 1972), Ne and A (Cess and Owen, 1973), and trace amounts of hydrocarbons (Danielson *et al.*, 1973).

Pollack takes as basic constraints the requirement that the effective temperature of Titan be 87 ± 1 K and that the infrared spectrum be consistent with the avilable broad-band observations. He assumes that the atmosphere contains both methane and hydrogen above the clouds in amounts that are consistent with the observed spectra, and he considers the possibility that both He and NH_3 may also be present but undetected spectroscopically (in the case of ammonia, because it is frozen out below the visible clouds). Pollack does not include N_2 on the grounds that N_2 is unlikely (except in the form of NH_3) in a highly reducing atmosphere. He then computes non-grey, radiative-convective models, in which all solar energy is deposited at the surface, calculating for various assumed abundances the atmospheric structure, surface boundary conditions, and emergent infrared spectrum. Since the absorption of sunlight by the clouds is not considered, his models do not predict any temperature inversion in the atmosphere.

There are three molecular absorptions in Pollack's models: pressure induced transitions in hydrogen (primarily important for $10 < \lambda < 40$ μm) and in methane (primarily important for $\lambda > 25$ μm); and rotational transitions in ammonia (which may be important near 10 μm). Helium enters the calculations only through collisions with these three. Figure 22 compares the emergent spectrum for models containing only hydrogen and methane with the earlier broad-band infrared observations; for this model the best fit is for equal quantities of the two gases. For the model with equal

methane and ammonia, the surface temperature is 150K, the surface pressure is 0.5 atm, and methane clouds form above the 80K temperature level. The addition of helium and ammonia in other calculations by Pollack does not greatly alter this simple description of the atmosphere of Titan.

Pollack's major conclusions can be summarized as follows. The greenhouse on Titan is due to both hydrogen and methane, with methane the dominant broadening

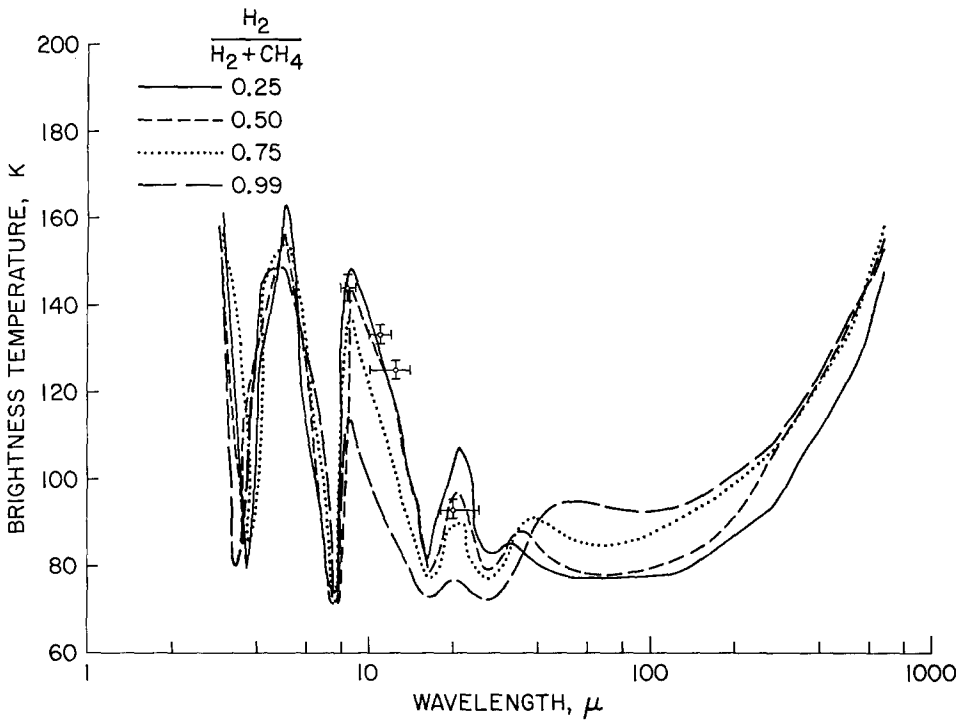

Fig. 22. Comparison of observed broad-band infrared brightness temperatures of Titan with the predictions of greenhouse models. The radiative-convective atmosphere models by Pollack are characterized by varying porportions of methane and hydrogen but contain no helium or ammonia. From Pollack (1973).

agent. The ratio of methane to hydrogen is 1.0 $(+2.0, -0.67)$; large amounts of helium may also be present, but an upper limit on the helium to hydrogen ratio is ~ 15. Except possibly near the surface, the amount of ammonia in the atmosphere is far below the saturation vapor-pressure curve. The minimum surface pressure is 0.4 atm and the minimum surface temperature is 155K. Finally, methane clouds are present in the upper troposphere, where they contribute significant optical depth in the visible but not in the thermal infrared, suggesting that the particle sizes are on the order of a tenth of a micron to a micron. Similar conclusions follow from the models by Sagan (1973).

In the alternative approach by Danielson *et al.* (1973), a substantial fraction of the incident solar radiation is absorbed in a layer of cloud or dust particles produced by

photolysis high in the atmosphere. The dust particles are postulated to be small compared with wavelengths characteristic of the thermal radiation from Titan, resulting in low thermal emissivities and elevated temperatures. Since the gases in the upper atmosphere of Titan are also very inefficient radiators of long-wave infrared radiation, both the dust and gas are hot, and there develops a large and stable temperature inversion in the atmosphere.

In the 20-μm band, the radiation from Titan arises primarily in the hot, optically thin dust layer. Danielson *et al.* show that if the temperature is 160 K and the emissivity of the dust varies as λ^{-1}, then the predicted temperature at 9- to 10-μm and in the

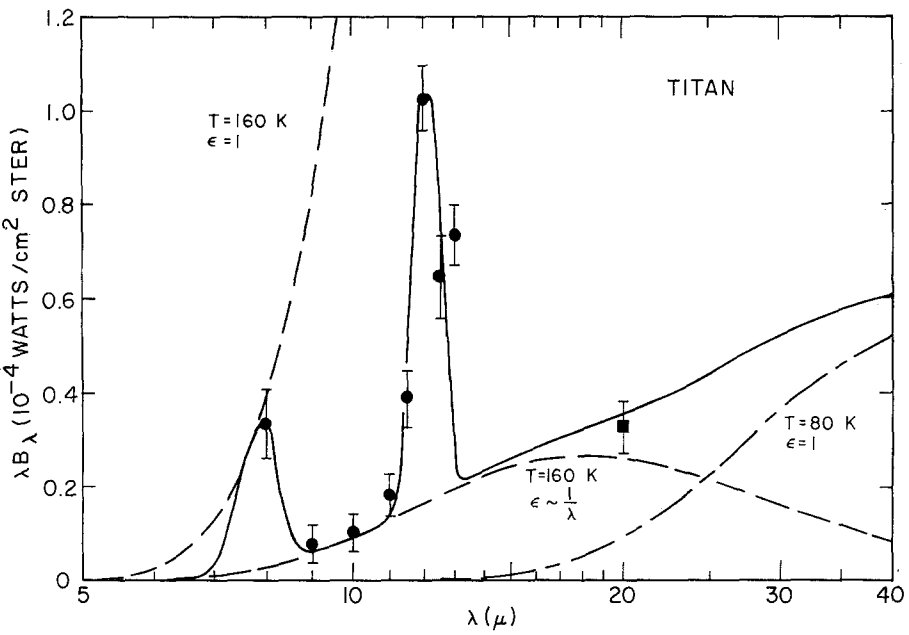

Fig. 23. Comparison of observed infrared emergent fluxes from Titan with the predictions of a temperature-inversion model. The model was calculated on the assumptions of a surface temperature of 80 K, a haze layer at 160 K in which the dust particles radiate with an emissivity inversely proportional to wavelength, and band emission from a 160 K atmosphere by CH_4 (at 7.7 μm) and C_2H_6 (at 12.2 μm). From Danielson *et al.* (1973).

broad 20-μm band agree with the observations. Their model also correctly predicts much of the structure in the 10-μm thermal emission (Gillett *et al.*, 1973) by invoking line emission from the hot gas. The very strong CH_4 band at 7.7 μm should be optically thick, with a brightness temperature equal to the physical temperature of 160 K in the inversion layer. They propose that the other major emission peak is due to the 12.2-μm band of C_2H_6. Figure 23 compares the observations with the spectra predicted by their model.

This model with its high cloud layer and large temperature inversion suggests that most of the infrared radiation of Titan between 8 and 28 μm arises high in the atmosphere. The variations in infrared brightness temperature are all due to variations in

the optical thickness of the emitting regions of the atmosphere. Danielson *et al.* suggest that such a model should apply to the upper atmosphere whether or not conditions suitable for a greenhouse effect obtain in the lower atmosphere of the satellite. However, having explained the high infrared temperatures without being required to postulate high surface temperatures, they discuss the conditions that might apply at the surface if there is no significant greenhouse effect. The temperature everywhere on the surface is close to the equilibrium value of ~ 85 K, which is also near the condensation temperature of CH_4. They suggest that much of the surface of the satellite is covered with frozen CH_4 and that the sublimation and condensation of this material further moderates any tendency for diurnal or seasonal temperature variations.

The two models discussed here – the greenhouse model and the temperature-inversion model – predict different long-wave thermal spectra, and measurements with spectral resolving powers of ~ 10 in the 20-μm window or of ~ 100 in the 10-μm window could distinguish between them. Even more definitive would be a measurement of the brightness temperature of Titan at microwave frequencies, where the radiation must arise near the surface. The greenhouse model predicts $T_B > 150$ K, and the temperature-inversion model predicts $T_B < 100$ K. An observational choice between these two alternatives should be possible in the very near future.

A first look at large-scale dynamical processes in the atmosphere of Titan has been published by Leovy and Pollack (1973), based on the massive atmosphere predicted by the greenhouse models, but with application to the temperature-inversion model as well. The time scale for radiative heat loss, proportional to the mass per unit area of atmosphere, is $\sim 10^9$ s if the surface pressure is ~ 0.5 bar, and is therefore substantially greater than one rotation period (assumed equal to the orbital period) even if the atmosphere is an order of magnitude less massive. These considerations allow little variation in temperature in the lower atmosphere of Titan for either the greenhouse or the temperature-inversion models. Leovy and Pollack further conclude that, at least for the case of the greenhouse models, Titan may be unique in the solar system in having a weak axially symmetric circulation strongly influenced by rotation.

7.7. Escape and Replenishment of the Atmosphere

Among the interesting questions raised by the discovery of the massive atmosphere on Titan are: (1) why does the atmosphere, especially the H_2, not escape rapidly from so small a gravitational field; and (2) given that there must be a substantial flux of escaping gas, what is the source of replenishment for the atmosphere? McGovern (1971) calculated the escape rates of hydrogen and helium from Titan and on the basis of his models concluded that neither gas could have an equilibrium mixing ratio, relative to CH_4, greater than 10^{-3}. Trafton (1972a) calculated somewhat lower escape rates but still concluded that the observed presence of at least 5 km-atm of H_2 is unexpected, a result that finds support in subsequent discussions by Hunten (1972, 1973), Sagan (1973), Pollack (1973), and Gross (1973). Below we follow primarily the analysis of these problems by Hunten (1973).

Loss of a light constituent, present in the atmosphere in large proportions, can occur in two ways. In the first, the scale height is sufficiently large relative to the radius of the satellite that the variation of gravity with height is important; at some altitude the thermal energy of the molecules exceeds their gravitational energy, and if this level is below the critical level for escape, the gas simply blows away (cf. Öpik, 1963; Trafton, 1972a; Sagan, 1973). For a pure H_2 atmosphere at a temperature of 100 K, Hunten (1973) shows that the time scale for loss of the atmosphere by this blow-off mechanism is only 4 h! The obvious inapplicability of this picture to Titan leads us to consider the second and more plausible process for loss. If the scale height is sufficiently reduced by the presence of heavier gases, the flux of escaping H_2 is controlled by its diffusion through the lower atmosphere, and blowoff does not occur. In Hunten's models the escape fluxes of H_2 are between 10^{11} and 10^{12} cm^{-2} s^{-1} for cases where the heavier gas is either N_2 or CH_4. Above the region of mixing, the escaping H_2 will form a corona extending to several Titan radii. In these calculations, the H_2 density is $\sim 10^6$ cm^{-3} at the critical level for escape, which is at an altitude of $\sim 10^4$ km.

The fate of the escaping H_2, totalling a few hundred kilograms per second, has been the subject of papers by McDonough and Brice (1973a, b). The escaping atoms will generally lack the velocity necessary to escape from Saturn, and consequently they will be distributed into a toroidal volume around the orbit of Titan. Although much of the gas may be recaptured by Titan, this mechanism will not affect the rate of loss, which is controlled by diffusion in the homosphere. Estimates of the density of gas in this hydrogen torus suggest that it might be observable in Lα radiation from an observatory above the atmosphere.

If Titan has been losing hydrogen at the present rate throughout the history of the solar system, the total loss amounts to a few hundredths of a percent of the mass of the satellite. Hunten (1973), following in part earlier discussions by Lewis (1971a) and Sagan (1973), suggests two possible origins for this material: (1) liberation from the hot ammonia solution in the interior and subsequent fumarolic outgassing; or (2) photolysis of the gases already in the atmosphere. An important problem with the photolysis mechanism is that the average flux of escaping H_2 is comparable to the incoming flux of solar ultraviolet photons, so that a highly efficient process is required. Further, the most likely source of the hydrogen is NH_3, which is frozen out of the upper atmosphere of Titan, where most of the ultraviolet radiation is probably absorbed. If NH_3 is the source of the H_2, however, Hunten notes that the postulated escape of $\sim 10^{22}$ g of H_2 would leave more than 10^6 g cm^{-2} of nitrogen on Titan.

7.8. Surface conditions

Lewis and Prinn (1973), Hunten (1972), and Sagan (1973) have all speculated about the chemistry of the lower atmosphere and surface of Titan. The presence of CH_4 in the atmosphere indicates that both methane hydrate and ammonia hydrate were originally present, and Lewis and Prinn suggest that NH_3 and CH_4 make up about 10% and 4%, respectively, of the object by weight. Photolysis of CH_4 in the atmo-

sphere will tend to produce saturated hydrocarbons, and as suggested by Hunten the heavier of these materials (e.g., tars and asphalt) will tend to precipitate out of the atmosphere and accumulate on the surface. A layer of such material (perhaps floating on a liquid methane and ammonia solution if the surface temperature is sufficiently high) would insulate the atmosphere from the volatiles underneath, inhibiting any tendency of the vapor pressure in the atmosphere to be in equilibrium with the solid or liquid forms at the surface temperature. The actual temperature of the surface is in any case entirely unknown. The temperature-inversion model suggests a value as low as 80 K; the greenhouse models suggest $150 < T < 200$ K; and in extreme models where postulated materials in the lower atmosphere have high infrared and microwave opacities, it is not really possible to exclude temperatures as high as 300 K.

The interior structure of Titan is likely to be similar to that of Ganymede (cf. Sections 4.3 and 6.8), with the exception that both ammonia and methane hydrates appear to have been present in the condensed material that formed the satellite. In the models discussed by Lewis and Prinn and Lewis, Titan is differentiated as a result of heating during the first few hundred million years of its existence. In this case, the rocky and muddy core would be surrounded by a convective mantle of aqueous ammonia solution, and the crust would be composed primarily of solid methane hydrate. If the surface is heated, as suggested in the greenhouse models, then the methane in the crust is released to form an atmosphere. In an extreme case, the ice crust might melt completely so that the convective mantle would interface directly with a dense methane atmosphere. For all temperatures above 150 K, ammonia gas should also be present in the atmosphere. As noted by Lewis (private communication, 1973), on theoretical grounds one could imagine a surface for this satellite composed of any of the following: solid CH_4, liquid CH_4, solid CH_4 hydrate, H_2O ice, aqueous NH_3 solution, or precipitated photolysis products. The crucial datum needed to eliminate most of these possibilities is the surface temperature.

Finally, we note that Titan has been discussed, principally by Sagan (1973), as a possible abode for life. This satellite has the highest ratio of methane to hydrogen of all known reducing atmospheres, and it is believed that many organic materials are being produced by photolytic reactions in the atmosphere and subsequently accumulating on the surface. The surface temperature may be high enough to maintain an ocean of liquid methane and ammonia solutions. Interest in the biological consequences of these conditions is great, and Titan will almost certainly be the first satellite (other than the Moon) to be explored directly by spacecraft: first by entry probes (now being considered for the early 1980's) and perhaps later by softlanders.

7.9. Summary

Titan is one of the largest satellites, similar to Mercury in radius but substantially smaller in both mass and density. It may also be the most interesting satellite in consequence of its substantial atmosphere, which is not only unique among the satellites, but which also appears to be the most accessible to direct investigation by entry

probes and landing vehicles of the reducing atmospheres characteristic of the major planets.

The one well-documented constituent of the atmosphere is methane. Although its total abundance cannot be determined without knowledge of the other constituents and of the depth of the atmosphere below the clouds, this gas alone provides a minimum surface pressure three times greater than that on Mars. The additional spectroscopic detection of some 5 km-amagat of H_2 by Trafton is particularly exciting, since the loss of this gas from Titan by escape must be large, and a correspondingly large source must then be sought. As has been shown by Hunten, an atmosphere dominated by H_2 is unbound and would blow off in a few hours. Presumably, a heavier gas, such as N_2, is present to retard this loss, and an atmosphere composed of CH_4, H_2, and N_2 would have a minimum surface pressure of about 0.1 bar. The time constant for loss of H_2 is increased by the presence of this additional gas to $\sim 10^6$ y, but a source of hydrogen is still required that can generate $\sim 10^{11}$ mol cm^{-2} s^{-1}, and no really credible one has been suggested. A verification of the presence of H_2 in the atmosphere of Titan is a crucial observational problem.

The total bulk and structure of the atmosphere cannot be deduced directly from spectroscopic studies because of the presence of optically thick clouds, as established from studies of linearly polarized light and from the anomalously low albedo of Titan in the ultraviolet. A sharp drop in albedo at wavelengths short of 0.5 μm is characteristic of most high-albedo satellites and of the major planets, but Titan possesses this property to a remarkable degree. There must be a haze of material that absorbs most of the incident solar ultraviolet radiation before it can be scattered in the bulk of the atmosphere. A photochemical haze (or smog) is the most likely material for this aerosol. In addition, there may be a deeper cloud layer of solid CH_4, and indeed it is not impossible that the aerosol that produces the low ultraviolet albedo is radiation-darkened CH_4.

Much of the current wave of interest in Titan is due to the striking variations with wavelength observed in the infrared brightness temperatures of the satellite, variations that suggest important thermal structure in the atmosphere. However, these observations have led to two entirely different classes of atmospheric models. Initially there was unanimity in interpreting the temperatures in terms of a greenhouse effect, and we have discussed the greenhouse models of Pollack in some detail in this section. This consensus was shattered by the suggestion by Danielson and Caldwell that the data could be matched as well or better by a model in which the stratosphere is heated by absorption in the smog layer, while the surface remains relatively cool. The most recent infrared observations, by Gillett *et al.*, strongly favor a warm stratosphere on Titan, but a significant greenhouse effect could still exist at greater depths. Improved radiometric data between 8 and 30 μm, and, perhaps even more important, a measurement of the brightness temperature at microwave frequencies, may be able to discriminate between these two classes of models.

The photochemistry of the atmosphere of Titan must be complex, with irradiation of CH_4 (and possibly NH_3) almost sure to result in the production of numerous

organic compounds. Most of these compounds will precipitate to the surface, which may be covered with a thick layer of tars. If the surface pressure and temperature are high enough, an ocean of liquid methane is also possible. The surface of Titan may be the best place in the solar system for the investigation of prebiotic organic chemistry.

While we have discussed in this Section a great many recent papers on Titan that are being published in the scientific journals, there is an additional important source that we have not cited explicitly. In July 1973 a NASA-sponsored Titan Workshop, under the chairmanship of D. M. Hunten, was held at which 12 papers on this satellite were presented. These papers, together with additional useful material on Titan, will be published as a NASA Special Report contemporaneously with the appearance of the present review. (NASA SP-340, Ames Research Center, 1974.)

8. Other Satellites of Saturn

8.1. Introduction

The family of 10 satellites accompanying Saturn ranges widely in size, including a number of objects with diameter of 1000–2000 km that have no equivalent in the Jovian system. The brightest of these satellites (excluding Titan) has a V mag. of only 9.8 and an apparent diameter of less than $\frac{1}{2}''$, and in general all of these satellites are difficult to observe except with large telescopes. The information we have on their physical characteristics comes from photometry and spectrophotometry, and to a lesser extent from polarimetry and infrared radiometry. In the following subsections we will consider each satellite in order of decreasing distance from Saturn, with particular emphasis on the two largest, Rhea and Iapetus. The main photometric data for all of these satellites are summarized in Tables V and XIII.

8.2. Phoebe (S9)

For this outermost of the known satellites of Saturn, Kuiper (1961) determined a photographic blue magnitude of 17.3. Photoelectric photometry by Andersson (1972, and private communication, 1973) yields $V=16.5$, $B-V=0.66$, and $U-B=0.29$; these colors are similar to those of the bluest asteroids, such as 2 Pallas. Andersson also derives the very large value for the phase coefficient of 0.08 mag. deg^{-1} in V, suggestive of a dark surface with a substantial opposition effect. The photometric data show some evidence for rotational variations, but no period has yet been determined. All of these observations suggest that Phoebe may be a dark, rocky object like Phobos and Deimos and perhaps the outer satellites of Jupiter. If its albedo is 0.04 and its V mag. is 16.5, Phoebe is more than 100 km in radius.

8.3. Iapetus (S8)

Iapetus rivals Io and Titan for the title of most peculiar object reviewed in this paper. Ever since its discovery in 1671, Iapetus has been known to vary in brightness by about a factor of 6 between eastern and western elongations. While it is common for satellites to vary as they rotate, no other object has an amplitude greater than a factor of 2,

TABLE XIII

Photometric data for the satellites of Saturn

	Tethys	Dione	Rhea	Titan	Iapetus (leading)	Iapetus (trailing)	Ref.
$V(1, 0)$	0.72 ± 0.06	0.88 ± 0.04	0.16 ± 0.03	-1.20 ± 0.03	2.30 ± 0.10	0.70 ± 0.05	1, 2, 3, 4
ΔV (rotational)	0.16 ± 0.06	0.20 ± 0.04	0.19 ± 0.03	0.00 ± 0.01	–	–	4
$dV/d\alpha$	0.019 ± 0.010	0.009 ± 0.009	0.025 ± 0.004	0.005 ± 0.002	0.065 ± 0.005	0.023 ± 0.005	3, 4
$B-V$	0.73	0.71	0.76	1.29	0.75	0.69	1, 2, 3
$U-V$	1.07	1.01	1.11	2.04	1.07	0.97	1, 2, 3
$(B-V)-(B-V)_\odot$	0.10	0.08	0.13	0.66	0.12	0.06	1, 2, 3
$(U-V)-(U-V)_\odot$	0.30	0.24	0.34	1.27	0.30	0.20	1, 2, 3

1. Harris (1961)
2. Blanco and Catalano (1971)
3. Millis (1973)
4. Noland *et al.* (1974)

and in addition most other synchronously rotating satellites are brightest on the leading side, whereas Iapetus is brightest on the trailing side.

Widorn (1952) deduced from photoelectric photometry in 1949 that the variations in brightness are nearly sinusoidal, with maximum exactly at western elongation, and subsequent photometry over limited parts of the cycle by Harris (1961) and McCord *et al.* (1971) generally confirmed this conclusion. More recently, extensive photometric investigations have been carried out by Millis (1973) at Lowell Observatory and by Noland *et al.* (1974) at Mauna Kea Observatory to define an improved light curve and to search for color variations. Millis (whose observations are illustrated in Figure 24) found that the two minima he observed in 1971–1972 differed by 0.3 mag., and he interprets the difference in terms of different mean phase coefficients for the leading and trailing hemispheres, deriving values for $dV/d\alpha$ of 0.065 and ~ 0.02 mag. deg^{-1} at $\theta = 90°$ and 270°, respectively. The larger phase coefficient is similar to that of dark objects, such as the Moon and a number of asteroids, when observed over the same range in α. The 1972–1973 observations by Noland *et al.* confirm this effect and also provide a more accurate determination of $dV/d\alpha$ at

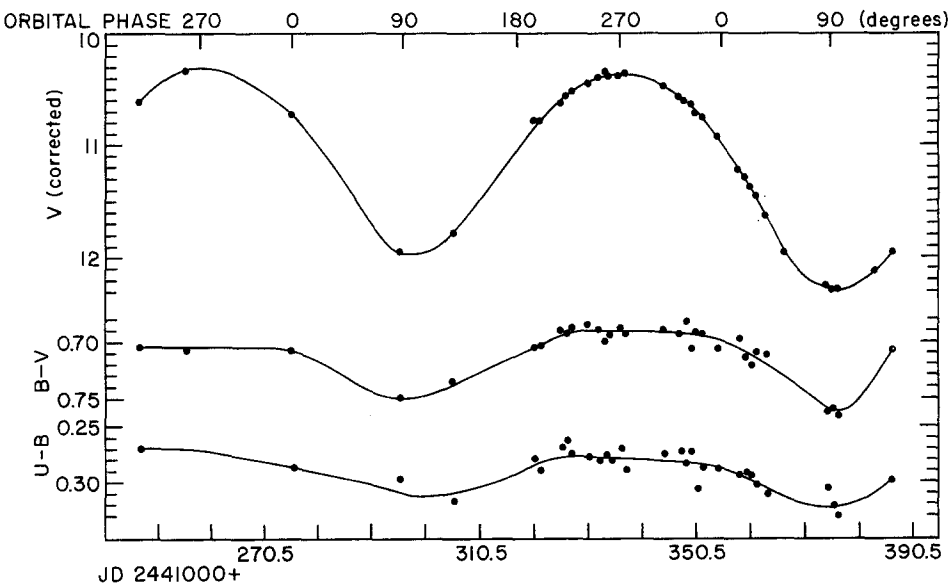

Fig. 24. Photometric measurements of the brightness and color (*UBV* system) of Iapetus in 1971–1972. The formal error in most of the points is ± 0.01 mag. From Millis (1973).

$\theta = 270°$ of 0.023 mag. deg^{-1}, a value similar to that of Io, Europa, and Ganymede (cf. Morrison *et al.*, 1974, and discussion in Section 6). When the photometry by Millis *et al.* is corrected for dependence on α, the total range in V is from 10.2 to 11.9 (at mean opposition). This amplitude is smaller than that traditionally given (e.g., Harris, 1961).

Millis (1973) also presented the first detailed observations of color variation with

orbital phase. The range of variation is 0.07 mag. in $(B-V)$ and 0.045 mag. in $(U-B)$, with the minimum values of both $(B-V)$ and $(U-B)$ at maximum light. McCord *et al.* (1971) observed the relative colors of the leading and trailing sides of Iapetus; their data between 0.4–1.05 μm for the trailing side and 0.4–0.8 μm for the darker leading side are illustrated in Figure 25 together with similar spectrophotometry of Rhea, Dione, and Tethys. The reflectivity curves for both leading and trailing hemispheres of Iapetus are the most nearly neutral of the satellites of Saturn, although the leading side is slightly redder than the trailing side.

Although it has been suggested that the photometric variations of Iapetus might be a result of an elongated shape for the satellite (e.g., Dollfus, 1970), it has generally been assumed that the satellite is nearly spherical but has a mean albedo on the leading side that is about a factor of 6 smaller than on the trailing side. This assumption was demonstrated to be correct by Murphy *et al.* (1972) on the basis of the thermal flux from this satellite measured at a wavelength of 20 μm. They found that the infrared and visual brightness were negatively correlated, with a 20-μm flux density from the dark side about 3 times greater than from the light side. In addition, Murphy *et al.* (and subsequently Morrison, 1973a) used the combined radiometry and photometry to show that the radius of this satellite is about 900 km (cf. discussion in Section 3) and that the albedo of the leading hemisphere is 0.04 ± 0.01, making this one of the darkest surfaces in the solar system. The corresponding albedo for the light hemisphere is about 0.3. Measurments by Zellner (1972a) of the degree of negative linear polarization of each hemisphere near maximum phase angle yield albedos that generally agree with the albedos derived from the radiometric measurements (cf. Bowell and Zellner, 1973).

Since the maximum phase angle of Saturn as seen from Earth is only 6°, it is not possible to derive the phase integral q for any of its satellites. However, the similarity between the dark side of Iapetus and the Moon in albedo, phase coefficient, and polarization all suggest a lunar value of q for this part of the satellite. The smaller phase coefficient for the lighter side suggests, however, that it has a larger phase integral, and the radiometric/photometric method of deriving the radius also yields more consistent results if a larger value of q is assumed for the trailing side of the satellite (Morrison, 1973a).

The large difference in mean albedo between the two hemispheres, together with the fact that the maximum and minimum brightness occur very near to elongation, suggests that some interaction with the environment has modified the surface material. Cook and Franklin (1970) have proposed that if the satellite initially had a relatively thin coating of high-albedo ice on a darker surface, the greater influx of meteors striking the leading hemisphere might have preferentially eroded the ice from that part of the satellite to produce the observed conditions. However, since the calculated meteor fluxes for the two hemisphere differ by less than a factor of two, it appears that this mechanism will produce the observed albedo differences for only a very limited range of thicknesses for the ice layer. Another difficulty with the model of Cook and Franklin is that it does not address the more general problem of explaining

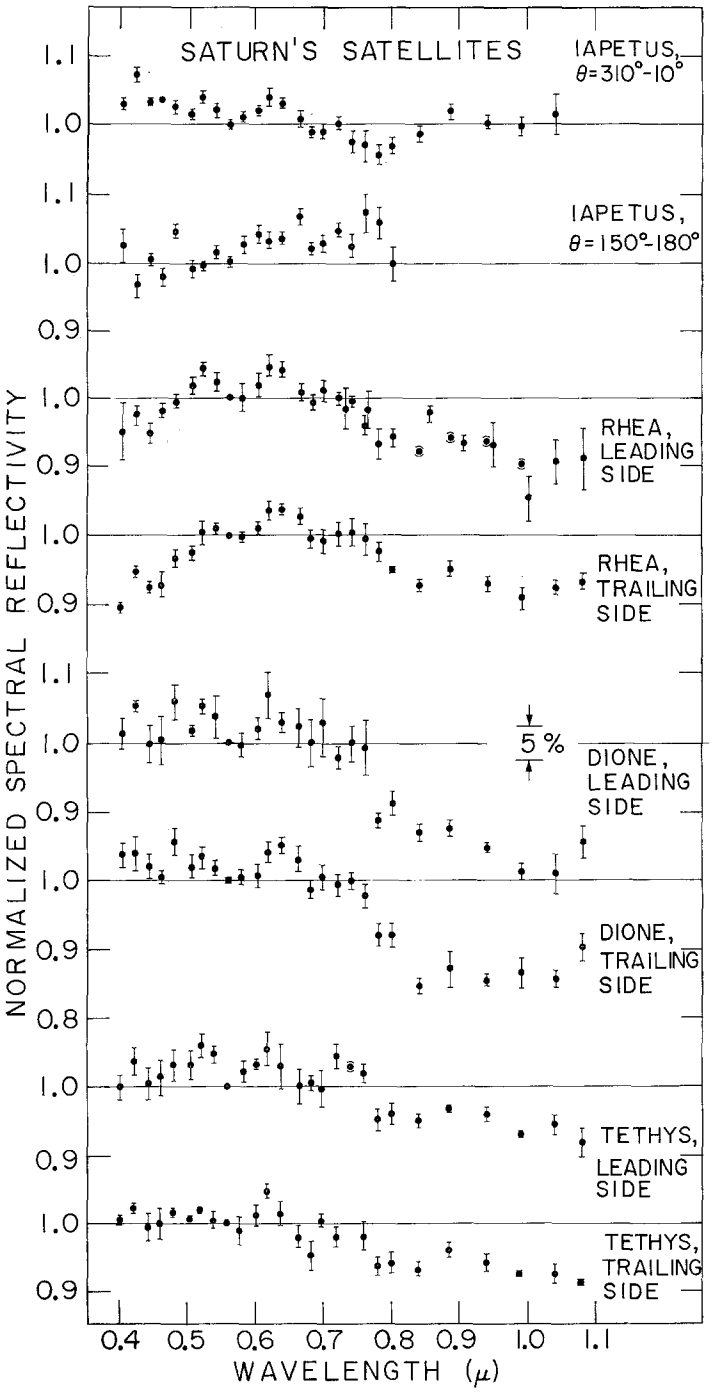

Fig. 25. The colors of Iapetus, Rhea, Dione, and Thethys, from narrow-band photometry, with leading and trailing side data included. From McCord *et al.* (1971).

the fact that most of the satellites of Jupiter and Saturn are brighter on their *leading* hemispheres.

Since the mass of Iapetus is very poorly known, its bulk composition cannot be inferred. As discussed in Section 4, Lewis (1972, 1973) anticipated that all of the satellites of Saturn, if they formed together, will be composed in large part of ices. It is difficult to reconcile this idea with the very low albedo of at least part of the surface of Iapetus.

In summary, the cause of the unique photometric behavior of this satellite is not known, nor is it understood how substantial parts of the surface of a satellite presumably composed of ices can have an albedo of 0.04 or less. Further observational and theoretical studies are required to clarify the compositions of the two types of surface material and their distribution and to investigate the ways in which the surface can be influenced by the environment of the satellite.

8.4. Hyperion (S7)

The only observation of this satellite that is relevant to its physical nature is the photometry from Harris (1961) given in Table V. It would be worthwhile to obtain additional photometry to determine its phase coefficients and rotational period. If it has a low albedo, its radius could be as large as 200 km, in which case it might also be detectable radiometrically.

The next innermost satellite is Titan, which was discussed in Section 7. We therefore move on to the inner group of regular satellites of Saturn.

8.5. Rhea (S5)

Rhea is the second brightest satellite of Saturn (after Titan) and is the best studied of the inner satellites. Multicolor photoelectric photometry has been published by Harris (1961), Blanco and Catalano (1971), McCord *et al.* (1971), and Noland *et al.* (1974). The most complete coverage of orbital and solar phase angle is the *uvbyri* data of Noland *et al.*, who find in all of their filters a variation of magnitude with orbital phase with peak-to-peak amplitude of 0.20 ± 0.02 mag. and maximum brightness at eastern elongation (to within $\pm 10°$). These observations are illustrated in Figure 26. These authors find that the phase coefficient is 0.025 mag. deg^{-1} at wavelengths of 0.45 μm and longer, and increases to 0.030 mag. deg^{-1} at 0.41 μm and 0.037 mag. deg^{-1} at 0.35 μm, with uncertainties in these coefficients of ± 0.005. Together with the observed linear polarization of Rhea of -0.47% at a phase angle of 6° (Zellner, 1972a), these phase coefficients suggest a surface of relatively high albedo.

The spectrophotometry by McCord *et al.* (1971) from 0.3 to 1.1 μm is illustrated in Figure 25. The albedo varies by less than 15% over this wavelength region, with a maximum near 0.6 μm. The generally flat reflectivity and the gradual drop toward the infrared are both consistent with the spectra of H_2O and NH_3 frosts (Keiffer, 1970). The decrease in albedo toward the ultraviolet, which is a common phenomenon on all of the presumably ice covered satellites, as well as Titan and the rings of Saturn, may be due to radiation damage to the frosts, as discussed in Section 6.

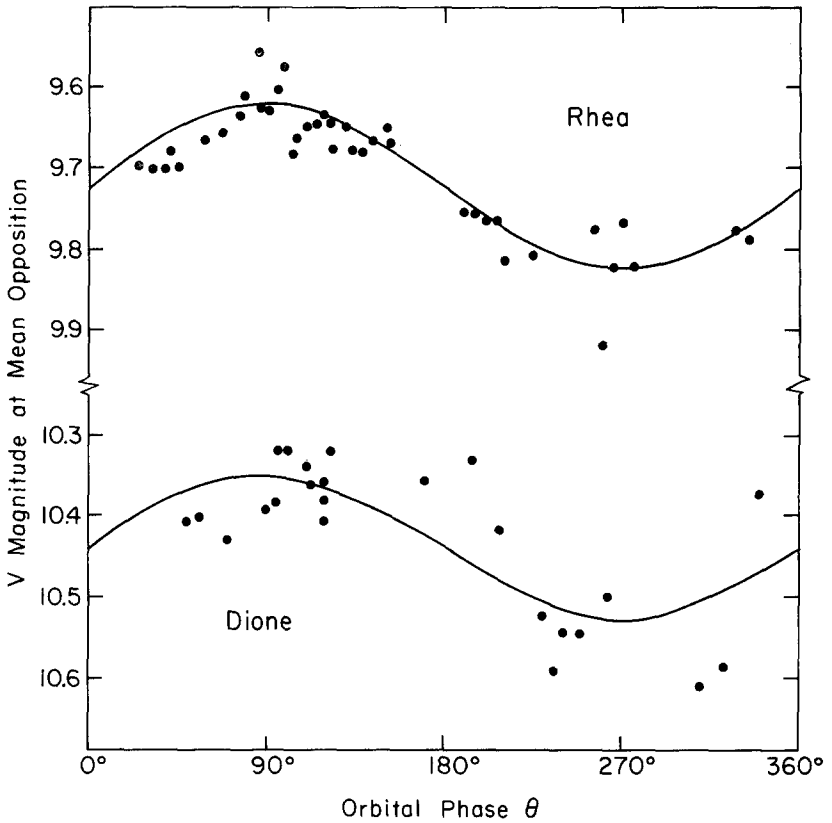

Fig. 26. Orbital photometric variations of Rhea and Dione in the y band (0.55 μm). The solid curve for Rhea is given by $y = 9.72 - 0.10 \sin \theta$, and for Dione is given by $y = 10.44 - 0.09 \sin \theta$. The dependence of the magnitude on phase angle was removed using phase coefficients of 0.025 and 0.009 mag. deg^{-1}, respectively. Adapted from the observations by Noland *et al.* (1974).

Thermal radiation from Rhea in the 20-μm band has been detected at the Mauna Kea 2.24-m telescope, as discussed by Murphy *et al.* (1972) and Morrison (1973a, 1974). The flux densities show a substantial scatter, but nevertheless they clearly establish that the geometric visual albedo is in the range 0.5 to 0.8, values that suggest a surface that is largely frost-covered. As discussed in Section 3, the radius is then 800 ± 125 km, making Rhea the third largest satellite of Saturn. Unfortunately, since its mass has not been measured, its bulk density remains unknown. However, by analogy with the other inner satellites, its density is probably less than 2.0 g cm^{-3}, suggesting a composition rich in ices of H_2O, NH_3, and CH_4 and their compounds. Infrared spectrophotometry to establish the composition of the surface material might be the simplest means to obtain further information on the bulk composition.

8.6. Dione (S4)

Photoelectric photometry of this satellite has been published by Harris (1961), McCord *et al.* (1971), Franz and Millis (1973), and Noland *et al.* (1974), but only the last

mentioned authors determined the depedence of brightness on both orbital and solar phase angle. Their observations in y are shown in Figure 26. The peak-to-peak amplitude is about 0.2 mag., and as with Rhea the leading side is brighter. The phase coefficients are not well determined, but it is clear that they are small, probably between 0.00 and 0.03 mag. deg^{-1} in each filter used by Noland *et al.* The spectrophotometry (Figure 25) by McCord *et al.* shows that the color of Dione is similar to that of Rhea, except that the drop in albedo toward the infrared is somewhat more pronounced, suggestive of a broad absorption band centered near 0.9–1.0 μm.

A detection of 20-μm thermal radiation from this satellite by Morrison (1974) permits an estimate to be made of the albedo and radius as discussed in Section 3. Morrison concludes that the radius is 575 ± 100 km, and the visual geometric albedo is about 0.6; together with the mass (well determined from the resonant interaction of this satellite with Enceladus), this radius yields a mean density of 1.45 ± 0.8 g cm^{-3}. Dione thus joins Callisto in having a measured density less than 1.5 g cm^{-3}, the value predicted by the models discussed in Section 4 that correspond to condensation from the solar nebula at temperatures of less than 20 K, the point at which CH_4 is retained. However, the uncertainty in this radius is certainly great enough to allow models with other compositions.

Dione is apparently very like Rhea, except for its smaller size. Both satellites have similar photometric behavior and similar colors, and the similarity may extend to bulk density and composition as well.

8.7. Tethys (S3)

With the discussion of Tethys we enter a part of the Saturn system that has not been explored in detail. The increasing glare from the bright disk and rings of the planet together with the decreasing brightness of the satellites as we move inward renders all types of photometric, spectrophotometric, and radiometric observations very difficult and leads to a real danger that systematic errors will result from incomplete correction for scattered light. We therefore emphasize that the results discussed for Tethys, and even more for the innermost three satellites, must be considered with caution, and that in general confirming data, preferably obtained with large-aperture instruments, are needed for any detailed study of these objects.

Photometry of Tethys has been obtained by Harris (1961), McCord *et al.* (1971), Franz and Millis (1973), and Noland *et al.* (1974). Like the other inner satellites, Tethys is probably brightest on its leading side, and Noland *et al.*, analyzing their data on the assumption that the light curve is symmetric with respect to $\theta = 0°$, derive an amplitude for the variations of 0.2 mag. Franz and Millis, however, find that their photometric data are better fitted by the nonsynchronous rotation period of 1.886 days and an amplitude of 0.4 mag. If this period is correct, then Tethys is the only satellite known to be in non-synchronous rotation. Noland *et al.* derive a phase coefficient in the visible of 0.02 ± 0.01 mag. deg^{-1}, similar to those found for Dione and Rhea. According to the spectrophotometry illustrated in Figure 25 from McCord *et al.*, Tethys is similar to these two satellites in color as well.

Morrison (1974) has noted one important respect, however, in which this satellite differs from those we have already considered. When the mass and photometric brightness of a satellite are well known but its radius is unknown, it is still possible to determine the quantity $\varrho' \equiv \varrho p_V^{-1.5}$, which contains information on both surface and bulk composition of the satellite. Morrison calls ϱ' the 'photometric density'; physically it is the density corresponding to unit geometric albedo. For the Galilean satellites $\varrho' > 4$, for Dione it is 3.3, but for both Tethys and Enceladus it is only about 1.5 g cm^{-3}. This low value for ϱ' requires that these two satellites have simultaneously a high albedo and a low density, as we discussed in Section 3 and illustrated in Figure 1.

From visual observations of the satellite in transit of the disk of Saturn, Dollfus (1970) estimates that the geometric albedo of Tethys is 0.50 ± 0.05. If the mass is correctly known, this albedo indicates a density of only 0.5 g cm^{-3}, an unreasonably low value. We must therefore conclude that either Dollfus' albedo or the mass is in error. In order to obtain a density as high as 1 g cm^{-3}, the albedo must be 0.8 and the radius similar to that of Dione ($\sim$600 km). Because of the important cosmogenic implications of these values, a verification of the mass of this satellite and an independent measurement of the albedo are desirable. Further photometry to resolve the problem of the rotation period is also needed.

8.8. Enceladus (S2)

Only Harris (1961) and Franz and Millis (1973) have published photometry (both on the *UBV* system) of this satellite. According to Franz and Millis, Enceladus is in synchronous rotation and is 0.4 mag. brighter at western elongation than at eastern elongation; this satellite then joins Callisto and Iapetus in being darker on its leading, rather than its trailing, side. This important photometric conclusion is based on only two measurements of the magnitude of the trailing side, however, and more observations are needed for verification. The $B-V$ color is similar to those of the other inner satellites, and the albedo and density are constrained by the measurements of the mass to be similar to those of Tethys, as discussed by Morrison (1974). The radius is than probably $\sim$300 km.

8.9. Mimas (S1)

The magnitude of Mimas has been determined from photographs only (Harris, 1961), although with area scanning techniques photoelectric measurements should be possible with large telescopes. Morrison (1974) has noted that the published magnitude and mass lead to a value of the 'photometric density', ϱ', of only 1.1 g cm^{-3}, substantially smaller than for any other solid body in the solar system. If this value is correct, then a value of p_V greater than 0.9 is required if the mean density is greater than 1.0 g cm^{-3}. These results are sufficiently peculiar to justify a fair degree of skepticism until more data are available. If $p_V \simeq 1.0$, the radius of Mimas is 150–200 km.

8.10. Janus (S10)

The magnitude of Janus can be estimated only from photographs taken near the time

of discovery in 1966. When the rings are even slightly inclined relative to the Saturn-Earth plane, their brightness completely masks the presence of the very nearby small satellite. If the magnitude is 13.5–14 (Dollfus, 1967; Texereau, 1967) and the albedo is comparable to that of the other inner satellites and of the ring particles (cf. Section 9), the radius of Janus is on the order of 100 km, making it a substantial member of the satellite family, but still probably the smallest of the Saturn system. There is no further information about Janus, and additional studies from Earth or Earth orbit will necessarily wait for the next passage of the Earth through the ring plane. One of the discovery photographs of Janus is illustrated in Figure 27.

8.11. Summary

The inner, regular satellites of Saturn all appear to be 'snowballs', or to quote F. Whipple, 'giant comets', composed primarily of ices of H_2O, CH_4, and NH_3. Their surfaces, insofar as they have been studied, appear to be covered with a material of high albedo and nearly neutral color, which is presumable H_2O frost. Their densities are anomalously low, sufficiently so to cause us to question the measured masses, particularly for Mimas. They may be similar in composition to the particles in the rings of Saturn, but we note that they lack the strong ultraviolet absorption seen in the spectrum of the rings.

Among the outer satellites Iapetus in by far the most interesting. Its rotational variation by a factor of 6 in brightness is now known to be due to a variation of albedo, but the cause of the variation, particularly in view of the low average albedo on the leading hemisphere, is not understood.

Undoubtedly interest in the satellites of Saturn will increase in the next few years.

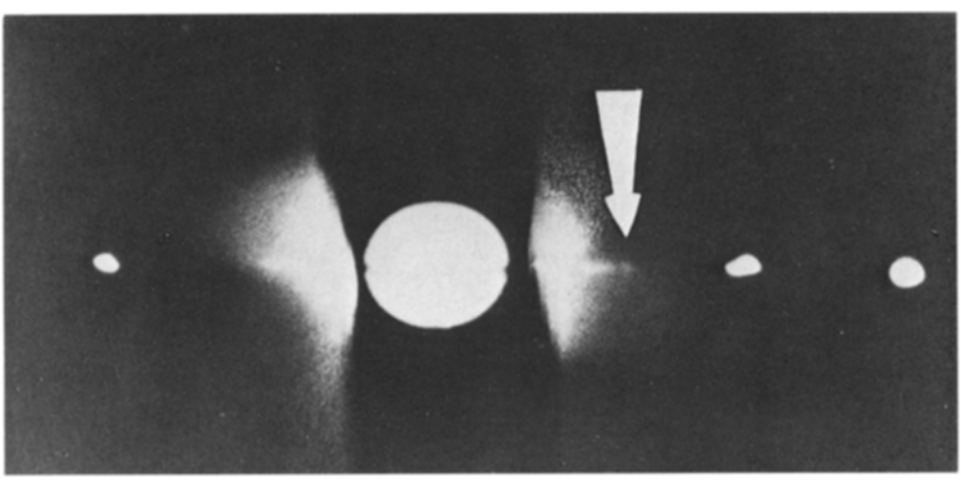

Fig. 27. Photograph of the inner satellites of Saturn showing Janus (white arrow). The image of Saturn was occulted with a neutral filter. From left to right, the brighter satellites are Dione, Enceladus and Tethys (combined image), and Titan. Photographed 15 December 1966, 1820 UT. From Dollfus (1967).

Titan, Iapetus, and the middle and inner satellites have no analogs in the inner solar system, and with the application of larger telescopes to their study and the projected space probes to the vicinity of Saturn, we expect a substantial expansion of the literature on these satellites.

9. Rings of Saturn

9.1. Introduction

In a review of the natural satellites, it is appropriate to discuss briefly the rings of Saturn, which are in fact a collection of very small satellites. As a consequence of their uniqueness, beauty, and ready observability, the rings have a long history of investigation, and even today one frequently refers to visual or photographic studies 50 or 100 yr old. However, the recent publication of excellent reviews by Bobrov (1970) and Cook *et al.* (1973) makes it unnecessary for us to discuss the older material here. These reviews deal almost exclusively with the visual and photometric observations and their interpretation, and with the dynamics of the ring system. Our main reason for including a discussion of the rings in this review is that neither of these review papers discusses a number of important recent spectrophotometric, radiometric, and radar studies of the rings. Our emphasis will be upon these new data and their interpretation, as well as on a comparison of the rings with the other satellites discussed in this review.

9.2. Visual and photometric studies: the 'classical' model

In this section we will summarize very briefly the models for the rings derived from visual and photometric studies. In general, we will follow the discussion by Bobrov (1970), which was written in 1968, with some updating based on the more recent review by Cook *et al.* (1973).

The dimensions and surface brightness of the rings, taken from the critical review by Cook *et al.* (1973), are listed in Tables XIV and XV. Rings A and B contribute more than 99% of the light from the ring system, and nearly all studies of the physical properties of the rings refer to these two main components. For the purposes of our review we consider only rings A and B, although any complete dynamical study of the system and its origin must also consider ring C, the newly discovered interior ring D

TABLE XIV

Dimensions of ring elements at 9.5388 AU
(from Cook *et al.*, 1973)

Feature	Radius (arcsec)	Extreme value (arcsec)
Outer A	19.82	20.30
Inner A	17.57	17.38
Outer B	16.87	17.09
Inner B	13.21	12.81
Inner C	10.5	10.2

TABLE XV

B and *V* photometry of rings at opposition of 1959 (from Cook *et al.*, 1973)

Feature	*V* (mag. arcsec^{-2})	*B* (mag. arcsec^{-2})
A_1	7.23	8.04
A_2	6.69	7.58
B_1	6.36	7.24
B_2	6.48	7.38
B_3	6.90	7.65

(Guerin, 1970), and the broad exterior ring extending nearly to the orbit of Dione (Kuiper, 1972). In this paper we do not consider the intensity variations within the A and B rings; recent discussions of the photometric profile of the rings can be found in papers by Guerin (1973) and Coupinot (1973).

The rings consist of many small particles in orbit around Saturn. The basic objectives traditionally associated with their study are: (1) to find the distribution of particles, both radially and normal to the ring plane; (2) to determine the mean size and size distribution of the particles; and (3) to derive the photometric properties of the particles. The first problem is essentially one of dynamics and lies outside the scope of this review. Both (2) and (3), however, can be attacked on the basis of visual and photometric observations, which have led to a class of models in which the particles are large compared to the wavelength of light but small compared to the thickness of the rings and are individually of high albedo, with the total optical depth of the B ring of the order of unity. We call these 'classical' models of the rings.

We first consider the photometric properties of the rings as a whole. The surface brightnesses quoted in Table XV indicate that the rings are very bright; a perfectly reflecting Lambertian disk ($p_V = 1.0$) would be only 0.3 mag. brighter than is the brightest part of the B ring (Cook *et al.*, 1973). This consideration alone requires that neither the optical depth nor the albedos of the individual particles can be very low.

Attempts to measure the optical depth of the rings (always reduced to normal incidence) have been made by visually noting the visibility of a bright star as it is occulted. Stars have been seen faintly through most of the A ring but not through the B ring, leading to estimates of optical depth $\tau_A \simeq 0.5$ and $\tau_B \geqslant 1.0$; a similar optical depth for the A ring is also derived from observations of the visibility of the polar regions of Saturn through it (Bobrov, 1970). Kemp and Murphy (1973) have measured the transmission of polarized light from the disk through the B ring and directly find $\tau_B \simeq 0.7$. A photometric determination of τ_B by Ferrin (1974) also yields a value of τ_B of a little less than unity. Although none of these observations individually has high precision, their interagreement is gratifying, and most discussions take $\tau_B \simeq 0.7$–1.0, and $\tau_A \simeq 0.4$–0.5.

Rings with these optical depths could be formed either of a monolayer of particles nearly in contact with each other or of a cloud of more widely scattered bodies distributed in depth. In the classical model, the second alternative is chosen, based on an

analysis of the variation of surface brightness with phase angle originally suggested by Seeliger in the 1880's. The rings show possibly the largest 'opposition surge' in brightness of any object in the solar system, amounting to ~ 0.4 mag. as illustrated in Figure 28. What makes this surge remarkable is that both theory and laboratory studies find that such large effects are to be expected only for very dark, particulate surfaces in which multiple scattering is not important, whereas the albedo of the ring particles is > 0.6. But if an explanation is not to be found in the photometric properties of the individual particles, it can be sought in the mutual shadowing of a cloud of particles. Not only does such an analysis satisfy the observations in Figure 28, it leads to the determination of an important parameter, the volume density D, which is the fraction of the total volume occupied by the particles. Since the length of the umbral shadows cast by the particles is about $\sim 10^3$ times the diameter, the size of the opposition surge that is predicted by the shadowing theory is sensitive to the particle spacing. Most of the recent studies have been done by Brobov, who concludes that D is a few times 10^{-3}; i.e., that typical interparticle distances are about 10 times the particle diameters.

Two difficulties with the Seeliger shadowing theory are emphasized by Cook *et al.* (1973). First, it predicts no dependence on color of the size of the opposition surge, whereas recent observations by Irvine and Lane (1973) show a substantial variation, with the greatest changes in brightness (~ 0.4 mag.) in the ultraviolet and near their long-wave limit of 1.06 μm, and with a minimum opposition surge (~ 0.2 mag.) in the visual. Second, it requires a mechanism, as yet unspecified, to keep the cloud from collapsing into a monolayer due to dissipation of energy in collisions. Cook *et al.*

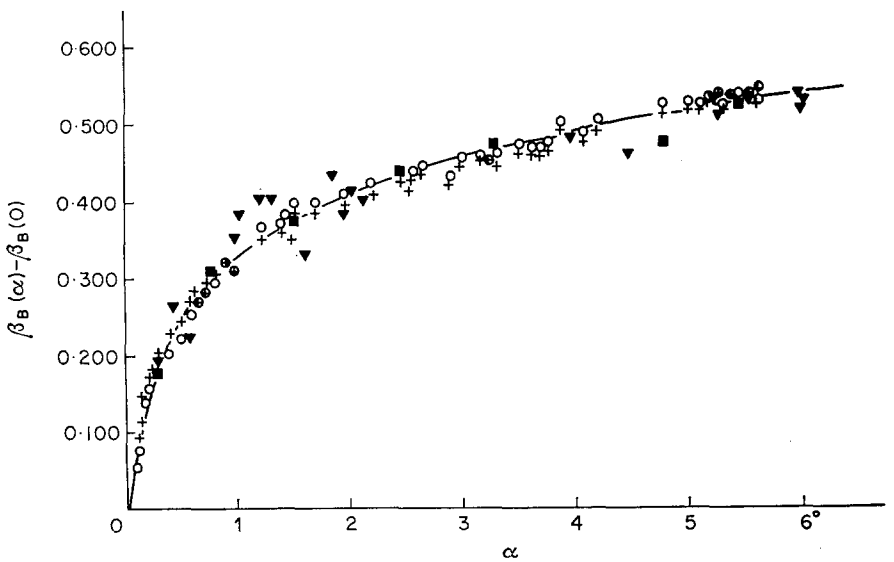

Fig. 28. Observed phase curves of the B ring of Saturn, reduced to the same zero point. The original photometry is from Schoenberg (filled squares), Lebedinets (filled triangles), and Franklin and Cook (open circles and crosses). The large opposition effect, amounting to about 0.4 mag., is apparent. From Bobrov (1970).

propose that the rings may be composed of a monolayer of particles with diameters of 1–2 km, and that the opposition surge is a result of scattering on the surface of each particle; this latter feature does seem to be required (to some degree at least) by the observations by Irvine and Lane. If only a part of the opposition surge in the classical models is due to shadowing, the spacing of the particles will be larger than that calculated by Bobrov. It remains particularly puzzling, however, how scattering on the surfaces can contribute substantially to the opposition surge near 1 μm, where the albedo of the rings is very high.

A lower limit to the sizes of the ring particles can be established from consideration of their lifetime against orbital decay by the Poynting-Robertson effect, as discussed by numerous authors. Brobov (1970, 1972), reviewing earlier work by Radzievsky, finds that for a particle to have a lifetime of 4×10^9 yr, the minimum radius is about 3 cm, a conclusion also reached by Pollack *et al.* (1973b). Other authors have in even the recent past suggested that the particles might be as small as a few microns, but the very short lifetimes implied by such sizes would require that a surprisingly recent origin for the rings be considered (cf. Clarke, 1968, pp. 178–184).

Once it is established that the particles are macroscopic and widely spaced and that the optical depths of the rings are approximately known, it is possible to model the albedos and phase function of the particles in order to fit the observations of surface brightness and its variation with ring tilt (specifically, with the Saturnicentric declination of Sun, B', and of the Earth, B). There is a wealth of observational data, as reviewed by Bobrov (1970), although many of the older visual and photographic studies may be subject to substantial errors. Particularly useful are observations of sunlight transmitted through the rings, made principally in 1966, when B and B' had opposite signs. As far as we know, no full theoretical treatment of this problem, in which the optical depth and volume density as well as the albedo and scattering function are allowed to vary and the dependence of the observed parameters on wavelength is taken into account, has been given. Less complete discussions of the B ring, which nevertheless do allow for multiple scattering in the rings, have been published by several authors. For $\tau = 1.0$, Bobrov (1970) finds a satisfactory fit for $p_V = 1.1$–1.5 and phase integral $q = 0.5$–0.7. Cook *et al.* (1973) give $p_V = 1.1$, having assumed $q = 0.57$ and $\tau = 1.0$. Lumme (1970) obtains $p_V = 0.8$, $q = 1.1$, and $\tau = 1.25$, but these results have been criticized by Hämeen-Anttila and Pykkö (1972), who suggest that a layer of uniform particles cannot reproduce the photometric behavior of the B ring. Price (1973) discussed the interpretation of data on the combined rings (A and B), but his results are not readily compared with the analyses of the B ring alone. From this brief list, it is apparent that, while most work has tended toward lunar-type phase integrals and geometric albedos of about unity, much remains to be done in defining the range of model parameters that is consistent with the photometric properties of the rings.

A fundamental property of the rings that we have not yet discussed is their physical thickness. The critical observations needed to determine the thickness can be made only when $B = 0.0$, and only during the passages of the Earth through the ring plane

in late 1966 were the required data obtained, by Focas and Dollfus (1969) at the Pic-du-Midi 107-cm telescope and by Kiladze (1969) at the Abastumani 70-cm telescope. These observations have been discussed in detail by Bobrov (1972). The data consist of photographic photometry of the ring ansae as a function of B near the time that $B=0.0$. It is expected that, for plane-parallel rings, there will be two sources of brightness: (1) the edge, which should have a constant surface brightness corresponding to $\tau=\infty$, and (2) the surface of the ring, which should have constant surface brightness for a given B' (excepting, of course, that on either side of $B=0$ we see different faces of the ring) but a projected area that is proportional to B. The observations are consistent with the expectation, showing a linear variation of total brightness with B, so that an estimate can be made of the minimum brightness, which is due to the edge alone. Unfortunately, the two sets of observations, while internally consistent, yield values of this residual brightness that differ by a factor of 5, and the corresponding estimates of thickness of the rings differ by a like amount. It is extremely unfortunate that the data obtained by other observers either have not been reduced yet or have proved inadequate to resolve this inconsistency. Bobrov (1972) shows by a straightforward analysis that the thickness of the ring (assumed homogeneous and cylindrical) is ~ 2.8 km from the French data and ~ 0.6 km from the Georgian. These thicknesses can be considered as upper limits, since they assume a perfectly plane-parallel surface, but Brobov also shows that the photometry of the unilluminated side of the rings by itself implies a thickness of about 3 km. Hence, the true thickness is very unlikely to be less than ~ 2 km, a conclusion that supports the result obtained by Focas and Dollfus.

The dimensions of the rings given in Table XIV, a thickness of 2 km, and a volume density of $\sim 10^{-3}$ lead to a total volume of particles of $\sim 3 \times 10^{22}$ cm^3; if the density of the particles is near unity, the mass of the rings is then $\sim 3 \times 10^{22}$ g. This mass is a factor of 100 less than the minimum mass calculated by Franklin *et al.* (1971) from dynamical considerations involving the position of the Cassini division. Since the ring can hardly be much thicker than 2 km, this larger mass requires $D \geqslant 10^{-1}$, a conclusion clearly inconsistent with the classical model.

To summarize the classical model of the B ring: (1) the ring particles have characteristic sizes in the range between a few centimeters and a few tens of meters. (2) The particles are distributed with a volume density $10^{-3} < D < 10^{-2}$. (3) The visual optical depth and the geometric albedo are both near unity. (4) The physical thickness of the rings is ~ 2 km, implying a total mass of $\sim 3 \times 10^{22}$ g. This picture has been challenged on the grounds that a monolayer is a dynamically preferred configuration and that it does not explain the recently observed wavelength dependence of the opposition surge or the position of the Cassini division, which suggests a much greater mass. In the following sections we will consider how other types of astrophysical observations influence our conception of the physical nature of the rings.

9.3. Spectrophotometry and Chemical Composition

The high albedo of the rings and the high cosmic abundance and low vapor pressure

of H_2O ice have suggested to many investigators that this substance is likely to be present on the surface of the particles. Bobrov (1970) discusses early infrared observations by Kuiper, Moroz, and Shnyrev that appeared to support this suggestion, although the data were insufficient to establish a definitive identification.

Employing much higher spectral resolution, Kuiper *et al.* (1970) at the University of Arizona obtained spectra of the rings between 1 and 4 μm in November 1969 that showed several absorption bands that were not present in spectra of ordinary H_2O ice near 0°C. They attributed these features to NH_3 and erroneously identified this material as the dominant constituent of the rings. However, Pilcher *et al.* (1970) at MIT compared the Arizona data with laboratory spectra obtained by Kieffer (1970) of both NH_3 ice and H_2O ice at temperatures more appropriate to that of the rings and concluded that low-temperature H_2O ice provides a much better match to the spectrum. This conclusion was subsequently verified by Kuiper *et al.* Although no additional infrared spectra of the rings have been published, the identification of H_2O ice as the dominant constituent of the rings seems secure.

The strengths of the absorption features in the infrared reflection spectrum of H_2O ice vary with both temperature and microstructure. Pollack *et al.* (1973b) have presented a theoretical study of the effects of size on the spectrum for spherical ice particles. From a comparison with the spectrum by Kuiper *et al.* (1970), they conclude that the characteristic size of a scattering center in the rings is ~ 30 μm. This dimension refers, presumably, to the scale of surface roughness rather than to the radius of a typical ring particle.

Spectrophotometry of the rings between 0.3 and 1.05 μm by Lebofsky *et al.* (1970) shows that there is a smooth, steep drop in albedo at wavelengths shorter than 0.6 μm, similar to that seen on the high-albedo satellites of Jupiter and Saturn. Higher resolution scans between 0.30 and 0.44 μm by Barker and Trafton (1973) confirm the low ultraviolet albedo and show no evidence for spectral structure over this wavelength range. As we have mentioned previously, this absorption in the blue and ultraviolet cannot be due to unaltered H_2O ice. Lebofsky *et al.* suggest that either the surface might be silicate dust with only a very thin coating of frost, or the frost itself might be altered by irradiation (cf. Lebofsky 1972, 1973). In view of the similarity of the ultraviolet spectra of the rings and of other ice-covered satellites, we tend to favor a process that involves a natural darkening of the frost rather than one that requires the admixture of an additional material.

9.4. Infrared temperatures

The first measurement of thermal radiation from the rings was made in 1968 and 1969 by Allen and Murdock (1971), who found a brightness temperature for the combined A and B rings of 83 ± 3 K at a wavelength of 13 μm. Previously, Low had set an upper limit of 60 K at 20 μm in 1965, when the Earth was near the ring plane (Aumann *et al.* 1969). In 1972 and 1973, with the rings nearly wide open with respect to the Earth, Murphy (1973) measured a temperature for the B ring of 94 ± 2 K at 20 μm, and Morrison (1974) found 96 ± 3 K at 20 μm and 91 ± 3 K at 11 μm. Taken together,

these observations indicate that the infrared brightness temperature of the rings has varied over the past eight years, and that by 1973 the temperature had reached a surprisingly large value for material of high albedo.

No detailed modeling has, so far as we know, been applied to the problem of calculating the temperature of the rings as a function of tilt. For a monolayer, one can compute the equilibrium temperature much as one would for an isolated satellite, except that account must be taken of partial shadowing and obscuration by adjacent particles, particularly at small tilt angles (Murphy, 1973). In the classical models, however, it is necessary to consider the scattering of both sunlight and infrared thermal radiation within the rings and to establish the degree of anisotropy of the thermal radiation from each particle (cf. Aumann and Kieffer, 1973). While an anisotropy index is easy to define for a particular model of an individual ring particle, it is not simply derived for a system of particles of finite optical depth such as the rings.

If the brightness temperature of the B ring is as high as 95 K at a tilt of $B' = 26°$, limits are imposed on both the bolometric Bond albedo (A_{bol}) and the anisotropy index. The maximum subsolar temperature of an isolated particle at the distance of Saturn from the Sun is given by Equation (6) in Section 7. The equilibrium temperature for an isothermal particle is 0.71 times this value; thus, such a particle, even if $A_{\text{bol}} = 0$, can have a maximum brightness temperature of only 90 K. If the particles are not isothermal but are heated only on the side facing the Earth, then the observed brightness temperature of ~ 95 K sets an extreme upper limit on A_{bol} of 0.6.

In a ring consisting of many small particles, an optically thick ring might behave thermally rather like a continuous, partially transparent slab. The incident flux per unit area would vary as $\sin|B'|$ and the brightness temperature would be given by

$$T_B = T_o \sin^{1/4}|B'|, \tag{7}$$

where from the observed temperatures $T_o \simeq 110$ K. This curve is consistent with the observed time variation of infrared brightness, but in the absence of any detection of the ring at values of $B' \leqslant 16°$, the relationship is not well defined observationally. The maximum albedo corresponding to $T_o = 110$ K is $A_{\text{bol}} \simeq 0.2$, a value probably below the lower limit permitted by the visible brightness. It therefore appears the maximum infrared flux cannot be radiated normal to the rings, but must be peaked toward the Sun and Earth. It is clear that more detailed and realistic models for the thermal behavior of the rings are needed.

The ring particles pass through the shadow of Saturn once each orbit, and measurements of their change in temperature at the time of eclipse could provide information on the thermal properties of the particles. Because the maximum phase angle of Saturn is 6°, it has not been possible to measure the temperature of the particles during eclipse, and the only relevant data are a measurement by Morrison (1974) of the 20-μm brightness temperature of the rings 5″ beyond re-emergence from eclipse. He found that the temperature at this point, averaged over a five arcsec beam, was 2.0 ± 0.5 K lower than at the equivalent position before eclipse. Aumann and Kieffer (1973) have modeled the eclipse cooling and reheating of the ring particles and shown

that the temperature at this point is sensitive to the size of the particles, which must according to these observations be either less than 500 μm or more than 2 cm in radius. Since the smaller range of size would suggest lifetimes that are short in comparison to the age of the solar system, Morrison (1974) interprets his observations as indicating that a characteristic particle radius must be greater than 2 cm.

9.5. Microwave radiometry and radar

Until very recently, radio telescopes have lacked the angular resolution necessary to distinguish radiation from the rings from that received from the disk of Saturn. Two techniques are, however, available to set some limits on the ring component from low-resolution radiometry. The first is to observe with the same equipment over a period of several years, during which the apparent solid angle of the rings will vary as the value of B changes; the varying component of the flux can then be assigned to the rings. The second technique is to look for any excess in integrated radiation over that expected from the disk alone, based on either a model atmosphere for Saturn or on the assumption that the ratio of the flux from Saturn to that from Jupiter is independent of wavelength.

Observations of Saturn from 1965 through 1969 ($0<B<17°$) at a wavelength of 3.3 mm by Epstein *et al.* (1970) show no systematic variation with B, suggesting an upper limit to the brightness temperature of the rings in 1969 of about 20K at this wavelength. Epstein and his collaborators have continued these observations, but no post-1969 data have been published.

From an analysis of the millimeter-wave spectrum of Saturn, Wrixon and Welch (1970) concluded that none of the observations published in the 1960's indicated a detection of the rings at these wavelengths. More recently, Janssen (1973) has critically reviewed the observations at wavelengths between 1 mm and 2 cm, normalizing the Saturn temperatures to values obtained with the same equipment for Jupiter, to search for evidence of radiation from the rings. With the one exception of an observation at 1.4 mm (Rather *et al.*, 1973) he finds that these microwave data are all consistent with the hypothesis that the rings do not exist. At 1.4 mm, Rather *et al.* find a flux density that corresponds to a brightness temperature for Saturn that is 45 ± 15K larger than the value they observe for Jupiter. Since both the model atmospheres and the observations at longer millimeter wavelengths suggest that Saturn should have a temperature ~ 0.95 that of Jupiter, they attribute the excess to the rings; correcting for solid angle factors at the time of the observation (in 1973), they obtain a 1.4-mm brightness temperature for the combined A and B rings of 35 ± 15K.

Stringent upper limits to the brightness of the rings at longer radio wavelengths have been set from interferometric measurements, in which the rings can be resolved from the planet. Berge and Read (1968), observing when the Earth was near the ring plane, set an upper limit of ~ 10K at a wavelength of 10 cm. From observations made in 1970 and 1971 at a wavelength of 21 cm, Briggs (1973) and Berge and Muhleman (1973) set upper limits of 6 and 10K, respectively, to the brightness temperature of the rings. These 21-cm observations also establish another effect that may be

relevant to a study of the rings. Both Briggs and Berge and Muhleman find that the equatorial diameter of the microwave-emitting disk of Saturn is 2–3% greater than that of the visible disk. This apparent increase near the equator is most likely due to a low brightness near the poles, which in turn may be a result of the obscuration of one pole by an optically thick, cold ring. If this interpretation should turn out to be correct, the rings are not just invisible at microwave frequencies, they are both cold and of substantial optical thickness.

The non-detection of the rings at radio wavelengths has frequently been attributed to their small opacity, which might be a result of their composition (H_2O ice has a low microwave opacity) or size (particles smaller than the wavelength have small cross sections). The successful detection of a radar return from the rings in January 1973 therefore came as a great surprise. Goldstein and Morris (1973), observing at a wavelength of 12.6 cm with the JPL Goldstone 64-m radar telescope, measured a backscattering cross section of approx 60% of the projected geometrical cross section of the combined areas of rings A and B, which is about a factor of 10 greater than would be expected for even large opaque ring particles.

Goldstein and Morris propose that the particles are much larger than the wavelength and that the high reflectivity is a consequence of the backscattering gain (up to 8/3) that can be achieved in reflection from a rough Lambertian sphere. However, observations of other solar system objects indicate that radar reflections of more than 10% are very uncommon, making it difficult, even with this degree of backscattering gain, to understand how an overall reflectivity of 60% for the rings can be obtained. Further, opaque particles much larger than 10 cm in diameter appear to be completely incompatible with the very low microwave thermal emission from the rings discussed above.

The high radar reflectivity and low microwave emissivity of the rings pose important constraints upon any model of the size, composition and distribution of the ring particles. The fact that the particles are able to interact strongly with radar at microwave frequencies but apparently do not emit thermal radiation at wavelengths between 2 mm and 21 cm creates a paradox that will be discussed more fully in the next section.

9.6. Recent models

An important goal of a modern model for the rings of Saturn must be not only to explain the photometric behavior of the rings, but also to account for the low effective emissivity and high reflectivity of the rings at microwave frequencies. The reason these microwave properties are so paradoxical is that the usual Fresnel laws governing the interaction of microwave radiation with a dielectric surface predict that the emissivity should be high and the reflectivity low – exactly opposite to the situation for the rings. Two models have been proposed to deal with this situation.

In the first, Pollack *et al.* (1973b) propose to seek a solution not in the properties of a single particle but in the cloud of particles suggested by the classical models for the rings. The particles must have high single-scattering albedos at the radar frequency, a situation that can apply only for a restricted range of sizes less than the

wavelength of the radar. In order to obtain the observed radar reflectivity, Pollack *et al.* conclude that a single-scattering albedo for 12.6-cm radiation of greater than 0.9 is required. A Mie-scattering computation shows that this microwave albedo can be obtained for ice spheres with radius between 1 and 15 cm. The low 21-cm emissivity implied by the interferometric radiometry implies a still higher single-particle albedo, ~ 0.99, which in turn requires that the radius of an ice particle be about 2–3 cm. Finally, the apparent detection of thermal radiation from the rings at 1.4 mm suggests that the radius be about 1 cm or less. Similar calculations by these authors for silicate spheres do not yield any size that is compatible with both radar and the 21-cm radiometry.

We have seen previously that lower limits of ~ 3 cm and ~ 2 cm, respectively, were suggested for the particle radius based on consideration of lifetime against orbital decay and of the rate of heating after eclipse. These values, plus the three size ranges suggested by Pollack *et al.* as consistent with the microwave data, have only marginal overlap, at a radius of ~ 2 cm. While it is disturbing that there is so little leeway for a substantial range in particle sizes, this model does appear to be basically consistent with the wide variety of data relating to particle size and composition.

An alternative model suggested by Pettengill and Hagfors (1974) seeks to explain the high radar cross section by scattering within large spherical particles. It is well established that backscattering gains of a factor of 100 can be achieved from smooth transparent spheres that are larger than the radar wavelength, and Pettengill and Hagfors note that H_2O ice has the appropriate dielectric properties for this mechanism to apply at 12.5 cm. Because the potential gain is so much greater than that required to match the observations, only a small fraction of the particles need to be involved, or alternatively it may be that sufficient gain can be invoked from this mechanism even if the particles differ significantly from the smooth spheres considered in the calculations. In their model, the low microwave emissivity is a result of the high transparency of the particles, the point being that the backscattering gain is very sharply peaked, whereas the interaction of the particles with microwave radiation is weak when averaged over all directions.

An important additional datum on the microwave properties of the rings, suggested originally by Pollack (private communication, 1973), could be obtained if an occultation of a discrete radio source were observed. The attenuation would provide a direct measurement of the *total* scattering cross section, while the radar measures the *backscatter* cross section of the rings. Knowledge of both of these parameters would be useful for distinguishing among the models proposed for the ring particles.

9.7. Summary

Although visual and photometric studies of the rings of Saturn have been made for many decades, it is only very recently that a wealth of new data, including photoelectric photometry, spectrophotometry, infrared and microwave radiometry, and radar observations, has become available. Not unexpectedly, this new information has not been fully assimilated, and no models exist that are entirely consistent with

the data. However, it seems clear that present evidence indicates that the ring particles are composed of H_2O ice and favors some variant of the classical models in which the particles are widely distributed and at least part of the opposition surge is due to Seeliger shadowing. The low microwave brightness apparently restricts the mean particle diameter to a value less than a few meters, while several lines of evidence suggest that most particles have a diameter of a centimeter or more.

10. Other Satellites

10.1. Amalthea and the outer satellites of Jupiter

Our only information on the physical characteristics of Amalthea (J5) and the outer satellites of Jupiter is contained in measurements or estimates of brightness. Amalthea is too close to Jupiter to permit high-precision photometry, and J8 through J12 are too faint to be observed except in the largest telescopes. Table V lists the magnitudes of these satellites taken from Harris (1961). The given magnitude of Amalthea is based on visual estimates by the discoverer, Barnard, and there is some evidence that it varies, with the leading hemisphere brighter. For J6, Barnard estimated that the visual magnitude was 13.7, but Andersson and Burkhead (1970) have reported a mean opposition magnitude of $V=14.7$ and a value of $B-V=0.55\pm0.05$ based on two nights of observation with a small telescope in which the satellite itself was not visible. Andersson reports (private communication, 1973) that additional observations of J6 in 1972 with larger telescopes confirm the published V magnitude and support the $B-V$ value of $+0.67$ obtained from a reanalysis of the earlier data. Observations on two nights give $U-B\simeq0.5$. The magnitudes of all the other Jovian satellites given in Table 5 were determined by Nicholson from photographic photometry and were converted to V magnitudes on the assumption that the color index is $+0.8$.

Although the origin of satellite systems does not specifically concern us in this paper, we note that in the course of their study of the outer satellite groups of Jupiter, Colombo and Franklin (1971) suggested that J6 through J12 may have resulted from a single asteroidal collision and that the fragments could be rotating rapidly. Rotation would be revealed by light variations, but their measurement requires a very large telescope. If the outer five satellites of Jupiter are as dark as the satellites of Mars, they are of comparable or slightly larger size, and they may be similar to Phobos and Deimos in such characteristics as shape and crater density. With the meager data at hand there is no compelling reason to assume any particular albedo for the outer Jovian satellites; the range of radii listed in Table V for these objects encompasses the likely range of albedos (0.03 to 1.0). However, recent evidence on the albedo of the Martian satellites, the discovery of several very dark asteroids, and the revelation that at least one of the Trojan asteroids is very dark, all give preference to a low albedo for the outer Jovian satellites, and on this basis we computed 'best guess' radii in Table V by choosing an albedo of 0.1.

In this paper we follow the usual convention of refering to the outer satellites only by their numerical designations. However, mythological names have been proposed

for these objects, and for completeness we list the names that, although not officially recognized, are sometimes found in the literature: J6, Hestia; J7, Hera; J8, Poseidon; J9, Hades; J10, Demeter; J11, Pan; and J12, Andrastea.

10.2. Satellites of Uranus and Neptune

The magnitudes of these seven satellites in Table V are taken from the list by Harris (1961). He obtained photoelectric photometry at McDonald Observatory of Titania, Oberon, and Triton, but the magnitudes given for Miranda, Ariel, Umbriel, and Nereid are based on older photographic data, largely by Gehrels. With the exception of Triton, which we discuss below, there is no evidence on the radii of these satellites, and only the maximum and minimum values given in Table V can be assigned. The satellites of Uranus are illustrated in Figure 29.

Kuiper (in Dollfus, 1970) reported a direct measurement of the diameter of Triton with a diskmeter on the Hale 5-m telescope, giving 3770 ± 1300 km, corresponding to an angular diameter of 0.2″, but as we have noted in Section 3.2, measurements of disks this small are subject to systematic errors (in addition to the formal errors) of up to 0.1″. In Dollfus' (1970) review of radius determinations he notes that Kuiper's measured diameter for Triton corresponds to a visual albedo on the order of 0.2.

Harris (1961) describes photometric measurements of Triton made at McDonald Observatory in the 1950's that suggest that Triton's leading side is roughly 0.25 mag. brighter than the trailing side; if this result is correct, it suggests that Triton lacks a substantial atmosphere. Kuiper (1952) suggested on theoretical grounds that Triton may well have a tenuous atmosphere, but his spectroscopic search in the early 1940's revealed no trace of methane or ammonia at low dispersion. Spinrad (1969) used a photometric ratio technique to search for CH_4 on Triton but found none and established an upper limit of 8 m-atm. More recently, T. Z. Martin (private communication, 1973) searched for methane on Triton with 50 Å mm^{-1} dispersion (twice the effective dispersion in Spinrad's study) but finds no trace of the gas. The calculated maximum surface temperature on Triton ($T_{max} = 68\,K$) is above the condensation temperature of pure CH_4 but well below the condensation temperature of methane hydrate. The absence of atmospheric CH_4 on Triton may result from the condensation of this molecule in the hydrate compound, in which case the vapor pressure is far too low to permit spectroscopic detection.

Cruikshank (unpublished) failed to detect Triton in the 20-μm radiometric band in January, 1973, but set an upper limit to the flux density of 1×10^{-18} W cm^{-2} μm^{-1} averaged over the band. This result does not put any useful restraints on the albedo and radius, however, since a flux density this high would require either a satellite more than 5000 km in radius or a brightness temperature substantially higher than would be expected for equilibrium with the insolation.

Although Triton is generally classed with the Galilean satellites, Titan, and the Moon as one of the large satellites in the solar system, and occasionally authors have even treated it as if its radius, mass, and density were known, we are forced to conclude that none of these parameters is sufficiently well defined to establish even that

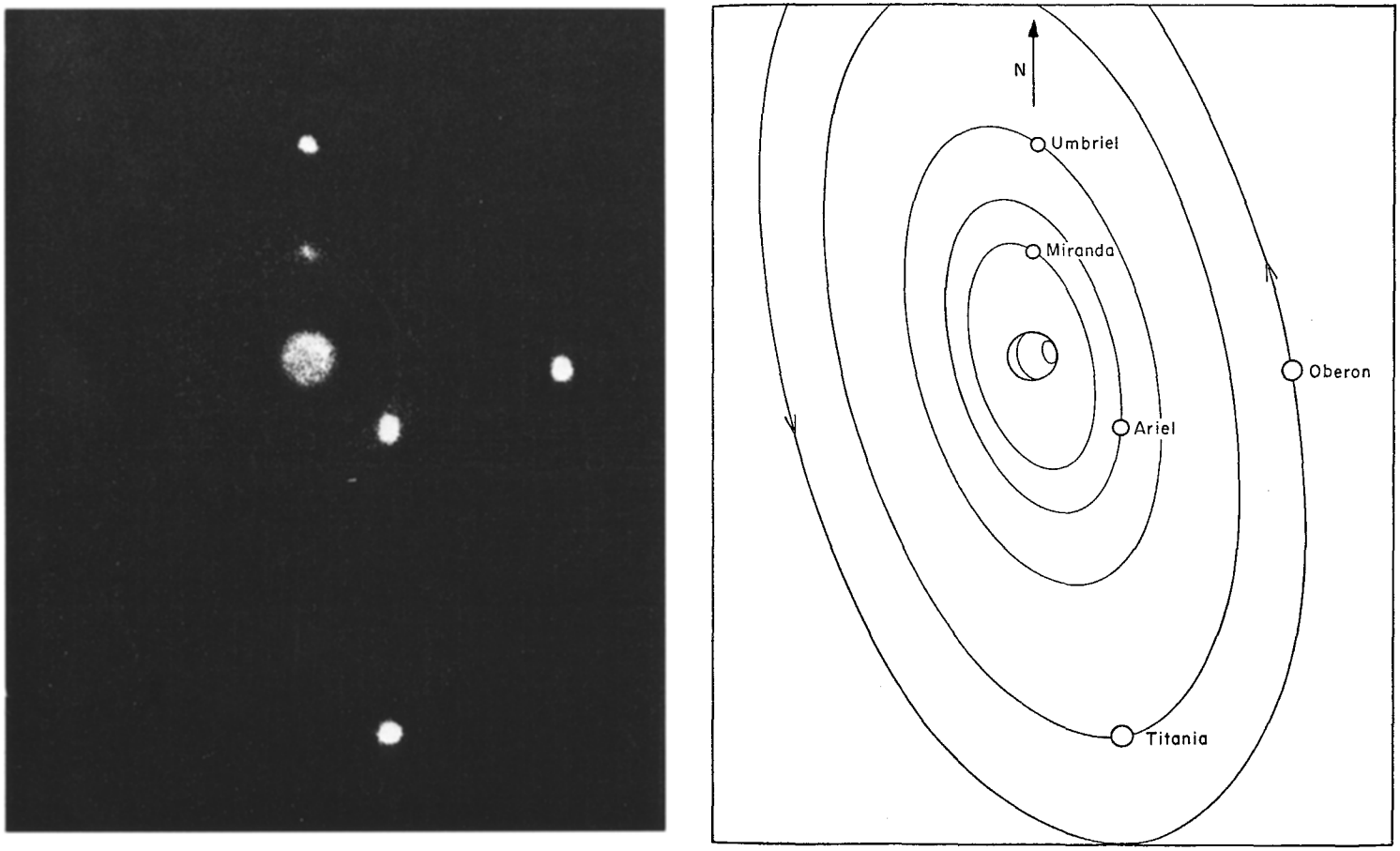

Fig. 29. Uranus and its system of satellites in a composite of two photographs of different exposure, both made with a filter centered on the strong methane absorption band at 0.887 μm. The glare around the planet is consequently diminished. Motion of Miranda and Ariel during the exposure elongated their images. In the key diagram all satellite orbits are shown as foreshortened coplanar circles, although the orbit of Miranda has been recently shown to be an ellipse inclined to the equator of Uranus (Whitaker and Greenberg, 1973). From Sinton (1972).

Triton is larger than, say, the four brightest satellites of Uranus. Only on the basis of its brightness ($V(1, 0) = -1.2$) can it be considered, in our present state of ignorance, as notably different from the other satellites of Uranus and Neptune.

Acknowledgments

This review could not have been written without the active and generous cooperation of dozens of our colleagues. We received more than 50 reprints of papers in advance of publication; we have profited greatly by discussions and correspondence over the year during which this paper was in preparation; and we are especially grateful to the authors who supplied us with prints of their figures for inclusion in this paper. While it is obvious that we cannot thank all of these colleagues by name, we express special gratitude to O. L. Hansen, D. M. Hunten, R. E. Murphy, G. H. Pettengill, J. B. Pollack, W. M. Sinton, and J. Veverka for useful discussions, and we particularly thank T. V. Johnson, D. L. Matson, N. D. Morrison, and C. B. Pilcher for detailed criticism of an earlier draft of the manuscript. A part of DPC's contribution to this paper was made while he was at the Sternberg Astronomical Institute, Moscow, on an exchange visit under the sponsorship of the U.S. National Academy of Sciences. This research was supported in part by NASA Grant NGL 12-001-057.

References

Allen, D. A.: 1971, in T. Gehrels (ed.), *Physical Studies of Minor Planets*, NASA SP-267, p. 41.
Allen D. A. and Murdock, T. L.: 1971, *Icarus* **14**, 1.
Anders, E.: 1971, *Ann. Rev. Astron. Astrophys.* **9**, 1.
Anderson, J. D., Null, G. W., and Wong, S. K.: 1974, *Science* **183**, 322.
Andersson, L.: 1972, *Bull. Am. Astron. Soc.* **4**, 313.
Andersson, L. and Burkhead, M. S.: 1970, *Astron. J.* **75**, 743.
Aumann, H. H., and Kieffer, H. H.: 1973, *Astrophys. J.* **186**, 305.
Aumann, H. H., Gillespie, C. M., Jr., and Low, F. J.: 1969, *Astrophys. J. Letters* **157**, L69.
Axel, L.: 1972, *Astrophys. J.* **173**, 451.
Bailey, J. M.: 1971, *Science* **173**, 812.
Barker, E. S. and Trafton, L. M.: 1973, *Icarus* **20**, 444.
Bartholdi, P. and Owen, F.: 1972, *Astron. J.* **77**, 60.
Berge, G. L. and Muhleman, D. O.: 1973, *Astrophys. J.* **185**, 373.
Berge, G. L. and Read, R. B.: 1968, *Astrophys. J.* **152**, 755.
Binder, A. B. and Cruikshank, D. P.: 1964, *Icarus* **3**, 299.
Binder, A. B. and Cruikshank, D. P.: 1966a, *Icarus* **5**, 7.
Binder, A. B. and Cruikshank, D. P.: 1966b, *Astrophys. J.* **144**, 1240.
Blanco, C. and Catalano, S.: 1971, *Astron. Astrophys.* **14**, 43.
Bobrov, M. S.: 1970, in A. Dollfus (ed.), *Surfaces and Interiors of Planets and Satellites*, Academic Press, New York, p. 377.
Bobrov, M. S.: 1972, *Astron. Zh.* **49**, 427; transl. in *Soviet Astron. – AJ* **16**, 348 (1972).
Bowell, E. and Zellner, B.: 1973, in T. Gehrels (ed.), *Planets, Stars and Nebulae Studied with Photopolarimetry*, University of Arizona, Tucson, in press
Briggs, F. H.: 1973, *Astrophys. J.* **182**, 999.
Brinkmann, R. T.: 1973, *Icarus* **19**, 15.
Brinkmann, R. T. and Millis, R. L.: 1973, *Sky Telesc.* **45**, 93.
Brouwer, D. and Clemence, G. M.: 1961, in G. P. Kuiper and B. M. Middelhurst (eds.), *Planets and Satellites*, University of Chicago, Chicago, p. 31.

Brown, R. A.: 1974 in A. Woszczyk and C. Iwaniszewska (eds.), 'Exploration of the Planetary System', *IAU Symp.* **65**, in press.
Burns, J.: 1972, *Rev. Geophys. Space Phys.* **19**, 463.
Caldwell, J., Larach, D. R., and Danielson, R. E.: 1973, *Bull. Am. Astron. Soc.* **5**, 305.
Cameron, A. G. W.: 1973, *Space Sci. Rev.* **14**, 383.
Carlson, R. W., Bhattacharyya, J. C., Smith, B. A., Johnson, T. V., Hidayat, B., Smith, S. A., Taylor, G. E., O'Leary, B. T., and Brinkmann, R. T.: 1973, *Science* **182**, 53.
Cess, R. and Owen, T.: 1973, *Nature* **245**, 272.
Clarke, A. C.: 1968, *2001: A Space Odyssey*, Signet Books, New York.
Colombo, G. and Franklin, F. A.: 1971, *Icarus* **15**, 186.
Cook, A. F. and Franklin, F. A.: 1970, *Icarus* **13**, 282.
Cook, A. F., Franklin, F. A., and Palluconi, F. D.: 1973, *Icarus* **18**, 317.
Coupinot, G.: 1973, *Icarus* **19**, 212.
Cruikshank, D. P. and Morrison, D.: 1972, *Sky Telesc.* **44**, 83.
Cruikshank, D. P. and Murphy, R. E.: 1973, *Icarus* **20**, 7.
Danielson, R. E. and Tomasko, M. G.: 1971, *Bull. Am. Astron. Soc.* **3**, 243; see also unsigned article in *Sky Telesc.* **42**, 10.
Danielson, R. E., Caldwell, J. J., and Larach, D. R.: 1973, *Icarus* **20**, 437.
Dermott, S. F.: 1970, *Monthly Notices Roy. Astron. Soc.* **149**, 35.
Dermott, S. F.: 1972, *Icarus* **17**, 223.
Dollfus, A.: 1961, in G. P. Kuiper and B. M. Middlehurst (eds.), *Planets and Satellites*, University of Chicago, Chicago, p. 534.
Dollfus, A.: 1967, *Sky Telesc.* **34**, 136; see also IAU Circular No. 1995.
Dollfus, A.: 1970, in A. Dollfus (ed.), *Surface and Interiors of Planets and Satellites*, Academic Press, New York, p. 46.
Dollfus, A.: 1971, in T. Gehrels (ed.), *Physical Studies of Minor Planets*, NASA SP-267, p. 95.
Dollfus, A. and Murray, J. B.: 1974, in A. Woszczyk and C. Iwaniszewska (eds.), 'Exploration of the Planetary System', *IAU Symp.* **65**, in press.
Duncombe, R. L., Seidelmann, P. K., and Klepczynski, E. J.: 1973a, *Ann. Rev. Astron. Astrophys.* **11**, 135.
Duncombe, R. L., Klepczynski, W. J., and Seidelmann, P. K.: 1973b, in A. G. W. Cameron, (ed.) *Fundamentals of Cosmic Physics*, in press.
Epstein, E. E., Dworetsky, M. M., Montgomery, J. W., Fogarty, W. G., and Schorn, R. A.: 1970, *Icarus* **13**, 276.
Fallon, F. W. and Murphy, R. E.: 1971, *Icarus* **15**, 492.
Ferrin, I. R.: 1974, *Icarus* **22**, in press.
Fink, U., Dekkers, N. H., and Larson, H. P.: 1973, *Astrophys. J. Letters* **179**, L155.
Focas, J. H. and Dollfus, A.: 1969, *Astron. Astrophys.* **2**, 251.
Franklin, F. A., Colombo, G., and Cook, A. F.: 1971, *Icarus* **15**, 80.
Franz, O. and Millis, R.: 1970, *Icarus* **14**, 13.
Franz, O. G. and Millis, R. L.: 1973, *Bull. Am. Astron. Soc.* **5**, 304.
Franz, O., Millis, R., and Pettauer, T. V.: 1969, *Bull. Am. Astron. Soc.* **1**, 344.
Gillett, F. C., Forrest, W. J., and Merrill, K. M.: 1973, *Astrophys. J. Letters* **184**, L93.
Gillett, F. C., Merrill, K. M., and Stein, W. A.: 1970, *Astrophys. Letters* **6**, 247.
Goldreich, P. and Lynden-Bell, D.: 1969, *Astrophys. J.* **156**, 59.
Goldreich, P. and Soter, S.: 1966, *Icarus* **5**, 375.
Goldstein, R. M. and Morris, G.: 1973, *Icarus* **20**, 260.
Gondolatsch, F.: 1965, in K. H. Hellwege and H. H. Voigt (eds.), *Landolt- Börnstein Tables, New Series*, Springer-Verlag, Berlin, Vol. 1, p. 150.
Gradie, J. and Zellner, B.: 1973, *Bull. Am. Astron. Soc.* **5**, 404.
Green, T. F., Shorthill, R. W., and Smith, D. W.: 1973, *Bull. Am. Astron. Soc.* **5**, 306.
Gromova, L. V., Moroz, V. I., and Cruikshank, D. P.: 1970, *Astron. Circular (U.S.S.R.)*, No. 569, p. 6 (in Russian).
Gross, S. H.: 1973, *Bull. Am. Astron. Soc.* **5**, 305.
Guérin, P.: 1970, *Sky Telesc.* **40**, 88.
Guérin, P.: 1973, *Icarus* **19**, 202.
Hämeen-Antilla, K. A. and Pykkö, S.: 1972, *Astron. Astrophys.* **19**, 235.

Hansen, O. L.: 1972, 'Thermal Radiation from the Galilean Satellites Measured at 10 and 20 Microns', Ph.D. Thesis, California Institute of Technology, Pasadena.
Hansen, O. L.: 1973, *Icarus* **18**, 237.
Hansen, O. L.: 1974, *Astrophys. J. Letters* **187**, in press.
Harris, D. L.: 1961, in G. P. Kuiper and B. M. Middlehurst (eds.), *Planets and Satellites*, University of Chicago, Chicago, p. 272.
Hunten, D. M.: 1967, *Space Sci. Rev.* **6**, 493.
Hunten, D. M.: 1971, *Space Sci. Rev.* **12**, 539.
Hunten, D. M.: 1972, *Comm. Astrophys. Space Phys.* **4**, 149.
Hunten, D. M.: 1973, *J. Atmospheric Sci.* **30**, 726.
Irvine, W. M. and Lane, A. P.: 1973, *Icarus* **18**, 171.
Janssen, M.: 1973, 'Short Wavelength Radio Observations of Saturn's Rings', presented at JPL/NASA Workshop on the Rings of Saturn, Pasadena, Aug. 1973.
Johnson, H. L.: 1965, *Comm. Lunar Planetary Lab.* **3**, 73.
Johnson, T. V.: 1969, 'Albedo and Spectral Reflectivity of the Galilean Satellites of Jupiter', Ph.D. Thesis, California Institute of Technology, Pasadena.
Johnson, T. V.: 1971, *Icarus* **14**, 94.
Johnson, T. V. and McCord, T. B.: 1970, *Icarus* **13**, 37.
Johnson, T. V. and McCord, T. B.: 1971, *Astrophys. J.* **169**, 589.
Johnson, T. V. and McGetchin, T. R.: 1973, *Icarus* **18**, 612.
Joyce, R. R., Knacke, R. F., and Owen T.: 1973, *Astrophys. J. Letters* **183**, L31.
Judge, D. L. and Carlson, R. W.: 1974, *Science* **183**, 318.
Katterfeld, G. N. and Nesterovich, E. I.: 1971, *Modern Geol.* **2**, 41.
Kemp, J. C. and Murphy, R. E.: 1973, *Astrophys. J.* **186**, 679.
KenKnight, C. E.: 1972, *Astrophys. J. Letters* **176**, L43.
Khare, B. N. and Sagan, C.: 1973, *Icarus* **20**, 311.
Kieffer, H.: 1970, *J. Geophys. Res.* **75**, 501.
Kiladze, R. I.: 1969, *Byull. Abastuman. Astrofiz. Obs.* **37** (in Russian).
Kliore, A., Cain, D. L., Fjeldbo, G., Seidel, B. L., and Rasool, S. I.: 1974, *Science* **183**, 323.
Kovalevsky, J.: 1970, in A. Dollfus (ed.), *Surfaces and Interiors of Planets and Satellites*, Academic Press, New York, p. 2.
Kuiper, G. P.: 1944, *Astrophys. J.* **100**, 378.
Kuiper, G. P.: 1951, *Proc. Nat. Acad. Sci.* **37**, 717.
Kuiper, G. P.: 1952, in G. P. Kuiper (ed.), *The Atmospheres of the Earth and Planets*, University of Chicago, p. 306.
Kuiper, G. P.: 1956, in A. Beer (ed.), *Vistas in Astronomy* **2**, Pergamon Press, New York, p. 1631.
Kuiper, G. P.: 1957, *Astron. J.* **62**, 245.
Kuiper, G. P.: 1961, in G. P. Kuiper and B. M. Middlehurst (eds.), *Planets and Satellites*, University of Chicago, Chicago, p. 575.
Kuiper, G. P.: 1965, in K. H. Hellwege and H. H. Voigt (eds.), *Landolt-Börnstein Tables, New Series*, Springer-Verlag, Berlin, Vol. **1**, p. 166.
Kuiper, G. P.: 1972, *Comm. Lunar Planetary Lab.* **9**, 199.
Kuiper, G. P.: 1973, *Sky Telesc.* **46**, 228 (unsigned news note).
Kuiper, G. P., Cruikshank, D. P., and Fink, U.: 1970, *Sky Telesc.* **39**, 14 (with correction in *Sky Telesc.* **39**, 80.)
Kuzmin, A. D. and Losovsky, B. Ya.: 1973, *Icarus* **18**, 222.
Lane, A. P. and Irvine, W. M.: 1973, *Astron. J.* **78**, 267.
Lebofsky, L. A.: 1972, *Bull. Am. Astron. Soc.* **4**, 362.
Lebofsky, L. A.: 1973, *Bull. Am. Astron. Soc.* **5**, 307.
Lebofsky, L. A., Johnson, T. V., and McCord, T. B.: 1970, *Icarus* **13**, 226.
Lee, T.: 1972, *Comm. Lunar Planetary Lab.* **9**, 179.
Leovy, C. B. and Pollack, J. B.: 1973, *Icarus* **19**, 195.
Lewis, J. S.: 1971a, *Science* **172**, 1127.
Lewis, J. S.: 1971b, *Icarus* **15**, 174.
Lewis, J. S.: 1972, *Icarus* **16**, 241.
Lewis, J. S.: 1973, *Space Sci. Rev.* **14**, 401.
Lewis, J. S. and Prinn, R. G.: 173, *Comm. Astrophys. Space Phys.* **5**, 1.

Low, F. J.: 1965, *Bull. Lowell Obs.* **5**, 184.
Lumme, K.: 1970, *Astrophys. Space Sci.* **8**, 90.
Matson, D. L.: 1971, in T. Gehrels (ed.), *Pysical Studies of Minor Planets*, NASA SP-267, p. 45.
McCord, T. B., Johnson T. V., and Elias, J. H.: 1971, *Astrophys. J.* **65**, 413.
McDonough, T. R. and Brice, N. M.: 1973a, *Nature* **242**, 513.
McDonough, T. R. and Brice, N. M.: 1973b, *Icarus* 20, 136.
McElroy, M. B., Yung, Y. L., and Brown, R. A.: 1974, 'Sodium Emission from Io: Implications', *Astrophys. J. Letters*, in press.
McGovern, W. E.: 1971, in C. Sagan, T. C. Owen, and H. J. Smith (eds.), *Planetary Atmospheres*, D. Reidel Publ. Co., Dordrecht, p. 394.
Millis, R. L.: 1973, *Icarus* **18**, 247.
Minton, R. B.: 1973, *Comm. Lunar Planetary Lab.* **10**, 35.
Moroz, V. I.: 1965, *Astron. Zh.* **42**, 1287; transl. in *Soviet Astron – AJ* **9**, 999 (1966).
Moroz, V. I.: 1967, *Physics of Planets*, Nauka Press, Moscow (translated in NASA TTF-515), p. 473.
Morrison, D.: 1973a, *Icarus* **19**, 1.
Morrison, D.: 1973b, *Comm. Astrophys. Space Phys.* **5**, 51.
Morrison, D.: 1973c, *Bull. Astron. Soc.* **5**, 404.
Morrison, D.: 1974, *Icarus*, in press.
Morrison, D. and Cruikshank, D. P.: 1973, *Icarus* **18**, 224.
Morrison, D., Cruikshank, D. P., Murphy, R. E., Martin, T. Z., Beery, J. G., and Shipley, J. P.: 1971, *Astrophys. J. Letters* **167**, L107.
Morrison, D., Cruikshank, D. P., and Murphy, R. E.: 1972, *Astrophys. J. Letters* **173**, L143.
Morrison, D., Morrison, N. D., and Lazarewicz, A.: 1974, 'Four-Color Photometry of the Galilean Satellites', submitted to *Icarus*.
Münch, G.: 1973, *Bull. Am. Astron. Soc.* **5**, 305.
Murphy, R. E.: 1973, *Astrophys. J. Letters* **181**, L87.
Murphy, R. E. and Aksnes, K.: 1973, *Nature* **244**, 559.
Murphy, R. E., Cruikshank, D. P., and Morrison, D.: 1972, *Astrophys. J. Letters* **177**, L97.
Murray, B. C., Wildey, R. L., and Westphal, J. A.: 1964a, *Astrophys. J.* **139**, 986.
Murray, B. C., Westphal, J. A., and Wildey, R. L.: 1964b, *Astrophys. J.* **141**, 1590.
Newburn, R. L., Jr., and Gulkis, S.: 1973, *Space Sci. Rev.* **3**, 179.
Noland, M., Veverka, J., and Pollack, J. B.: 1973, *Icarus* **20**, 490.
Noland, M., Veverka, J., Morrison, D., Cruikshank, D. P., Lazarewicz, A., Elliot, J., Goguen, J., and Burns, J.: 1974, 'Six-Color Photometry of Iapetus, Titan, Rhea, Dione and Tethys', submitted to *Icarus*.
O'Leary, B. T.: 1972, *Science* **175**, 1108.
O'Leary, B. T. and Miner, E. D.: 1973, *Icarus* **20**, 18.
O'Leary, B. T. and Van Flandern, T. C.: 1972, *Icarus* **17**, 209.
O'Leary, B. T. and Veverka, J. A.: 1971, *Icarus* **14**, 265.
Öpik, E. J.: 1963, *Geophys. J. Roy. Astron. Soc.* **7**, 490.
Owen, T. C.: 1965, *Science* **149**, 974.
Owen, F. N. and Lazor, F. J.: 1973, *Icarus* **19**, 30.
Pascu, D.: 1973, *Astron. J.* **78**, 794.
Pettengill, G. H. and Hagfors, T.: 1974, *Icarus*, **21**, in press.
Pilcher, C. B., Chapman, C. R., Lebofsky, L. A., and Kieffer, H. H.: 1970, *Science* **167**, 1372.
Pilcher, C. B., Ridgeway, S. T., and McCord, T. B.: 1972, *Science* **178**, 1087.
Pollack, J. B.: 1973, *Icarus* **19**, 43.
Pollack, J. B., Veverka, J., Noland, M., Sagan, C., Hartmann, W. K., Duxbury, T. C., Born, G. H., Milton, D. J., and Smith, B. A.: 1972, *Icarus* **17**, 394.
Pollack, J. B., Veverka, J., Noland, M., Sagan, C., Duxbury, T. C., Acton, C. H., Jr., Born, G. H., Hartmann, W. K., and Smith, B. A.: 1973a, *J. Geophys. Res.* **78**, 4313.
Pollack, J. B., Summers, A., and Baldwin, B.: 1973b, *Icarus* **20**, 263.
Porter, J. G.: 1960, *J. Brit. Astron. Assoc.* **70**, 33.
Price, M. J.: 1973, *Astron. J.* **78**, 113.
Price, M. J. and Hall, J. S.: 1971, *Icarus* **14**, 3.
Rather, J. D. G., Ulich, B. L., and Ade, P. A. R.: 1974, 'Brightness Temperature Measurements of Saturn, Jupiter, Mars and Venus at 1 mm Wavelength', submitted to *Icarus*.

Sagan, C.: 1971, *Space Sci. Rev.* **11**, 827.
Sagan, C.: 1973, *Icarus* **18**, 649.
Sinton, W. M.: 1972, *Sky Telesc.* **44**, 304.
Sinton, W. M.: 1973, *Icarus* **20**, 284.
Smith, B. A.: 1970, *Science* **168**, 828.
Smith, B. A. and Smith, S. A.: 1972, *Icarus* **17**, 218.
Soter, S.: 1973, *CRSR* 462, Cornell University.
Spinrad, H.: 1969, *Publ. Astron. Soc. Pacific* **81**, 895.
Stebbins, J.: 1927, *Lick Obs. Bull.* **13**, 1.
Stebbins, J. and Jacobsen, T. S.: 1928, *Lick Obs. Bull.* **13**, 180.
Taylor, G. E.: 1972, *Icarus* **17**, 202.
Texereau, J.: 1967, *Sky Telesc.* **23**, 226.
Thomas, J. R.: 1972, *EOS* **53**, 1090.
Trafton, L.: 1972a, *Astrophys. J.* **175**, 285.
Trafton, L.: 1972b, *Astrophys. J.* **175**, 295.
Trafton, L.: 1974, *Icarus* **21**, in press.
Veverka, J.: 1971a, in T. Gehrels (ed.), *Physical Studies of Minor Planets*, NASA SP-267, p. 79.
Veverka, J.: 1971b, *Icarus* **14**, 355.
Veverka, J.: 1973, *Icarus* **18**, 657.
Veverka, J. and Noland, M.: 1973, *Icarus* **19**, 230.
Wamsteker, W.: 1972, *Comm. Lunar Planetary Lab.* **9**, 171.
Watson, K., Murray, B. C., and Brown, H.: 1963, *Icarus* **1**, 317.
Webster, D. L., Alksne, A. Y., and Whitten, R. C.: 1972, *Astrophys. J.* **174**, 685.
Whitaker, E. A. and Greenberg, R. J.: 1973, *Comm. Lunar Planetary Lab.* **10**, 70.
Widorn, Th.: 1952, *Mitt. Univ.-Sternw. Wien* **5**, 1929.
Wrixon, G. T. and Welch, W. J.: 1970, *Icarus* **13**, 163.
Younkin, R. L.: 1974, *Icarus* **21**, in press.
Zellner, B.: 1972a, *Astrophys. J. Letters* **174**, L107.
Zellner, B.: 1972b, *Astron. J.* **77**, 183.
Zellner, B.: 1973, *Icarus* **18**, 661.
Zellner, B. and Copen, R. C.: 1974, 'Minor Planets and Related Objects. XVI. Satellites of Mars', *Astron. J.*, in press.